Research on a digital twin system on farm work utilizing agricultural machinery

(農業機械作業のデジタルツインシステムに関する研究)

2025

Hokkaido University, Graduate School of Agriculture,

Frontiers in Production Sciences Doctor Course

Yu Yue

Research on a digital twin system on farm work utilizing agricultural machinery

BY

Yu Yue

Dissertation

Submitted to Department of Environmental Resources in the Graduate School of Agriculture

Hokkaido University, Sapporo, Japan, 060-8589 in partial fulfillment of the requirements for the degree of

Doctor of Philosophy

2025

TABLE OF CONTENTS

LIST OF FIGURES

LIST OF FIGURES

LIST OF FIGURES

LIST OF FIGURES

LIST OF TABLES

LIST OF TABLES

LIST OF SYMBOLS

LIST OF SYMBOLS

Symbol	Description	Unit
l	The distance between front wheel and rear wheel	m
l_f	The distance between the center of the front wheel and the center of mass	m
l_r	The distance between the center of the rear wheel and the center of mass	m
w	The distance between left wheel and right wheel	m
δ	Steering angle to the real tractor or the virtual tractor	deg
δ_{left}	Steering angle of the left virtual wheel	deg
δ_{right}	Steering angle of the right virtual wheel	deg
T	Torque of the virtual wheels	N
v	The overall tractor velocity	m/s
v_{target}	The target velocity set for the tractor	m/s
d_e	Lateral error of the steering controller	m
θ_e	Heading error of the steering controller	deg
L	Look ahead distance of steering controller	m
x, y	Accurate tractor position information in cyber space	m
x_{sim}, y_{sim}	Tractor position output from GNSS simulator	m
δ_r	Simulated real steering angle	deg

Symbol	Description	Unit
δ_c	Steering command from the steering controller	deg
r_d	Turning radius in cyber space	m
r_p	Turning radius in physical space	m
δ_d	Steering angles in cyber space	deg
δ_p	Steering angles in physical space	deg
P_x, P_y	The relative coordinates of the zigzag path point once the starting point is assumed to be $(0,0)$	m
A	Amplitude of the zigzag path	/
ω	Frequency of the zigzag path	/
α_f	Side-slip angle of the front tire	deg
α_{f_0}	The maximum value of the side-slip angle α_f during the linear part	deg
α_r	Side-slip angle of the rear tire	deg
α_{r_0}	The maximum value of the side-slip angle α_r during the linear part	deg
k_f	The slope of the linear part of front tire model	/
k_r	The slope of the linear part of rear tire model	/
v_x	The vertical velocity of the tractor body	m/s
v_y	The longitudinal velocity of the tractor body	m/s
μ_f	Side friction stiffness of the front tire	/
μ_r	Side friction stiffness of the rear tire	/

LIST OF SYMBOLS

Symbol	Description	Unit
φ	Heading angle of the tractor	deg
r	Angular velocity of the tractor body	deg/s
v_{row}	The target velocity of the tractor of current row in a formation	m/s
d_{row}	The distance between the current tractor and the adjacent tractor in the previous row	m

LIST OF ABBREVIATIONS

LIST OF ABBREVIATIONS

Legend	Description
DT	Digital Twin
IoT	Internet of Things
NCGPC	Non-linear Continuous-time Generalized Predictive Control
API	Application Programming Interface
GNSS	Global Navigation Satellite System
IMU	Inertial Measurement Unit
ECU	Electronic Control Unit
RTK-GNSS	Real Time Kinematic- global navigation satellite system
TCP	Transmission Control Protocol
UTM	Universal Transverse Mercator
CoM	Center of Mass

CHAPTER 1. INTRODUCTION

1.1 Research Background

1.1.1. Issues related with robot tractor

In response to the shortage of agricultural labor due to an aging population, robotized agricultural machinery such as unmanned tractors, has been developed and plays an important role in reducing dependence on humans during agricultural production. Well-known agricultural machinery companies such as *John Deree* and *Kubota* have already launched commercial tractors equipped with automatic navigation functions, which means tracking planed navigation paths automatically. These robot tractors significantly improve agricultural productivity.

However, several issues related with development and applications of robot tractors raise concerns. During the development of robot tractors, including algorithm optimization and hardware validation, field experiments are usually required. These field experiments have a large demand of economic cost, time and materials. Besides, excessive field experiments would cause damage to arable land, due to air pollution from exhaust gas and tread pressure generated by repeated experiments of heavy machines. Considering that the algorithm and hardware system of the robot tractor are not stable in the early stage of development, potential safety problems may happen as well, such as tractor accidents. For applications of the developed robot tractors, work schedule optimization is always a difficult problem to solve. A typical way for work schedule optimization is iterating several possible solutions through field pre-validation tests, but this solution will encounter the same problems as the field experiment mentioned above. Additionally, testing and operation of the robot tractor will be greatly limited by weather. For example, conducting tractor tests can be very dangerous at dark night or in foggy weather when visibility is low.

The above problems affect efficiency and feasibility of robot tractors in terms of both development and application. To mitigate the negative impact from these issues, a new system should be proposed to replace excessive field experiments, providing a more sustainable way with lower cost and absolute safety.

1.1.2. Conceptualization of agricultural digital twins

Owing to the issues of field experiments related with robot tractors, this study considers conducting research on robot tractors in cyber space. Traditional ways of conducting cyber experiment for agricultural machinery mainly rely on commercialized simulation software such as MATLAB. However, these kinds of software can only simulate simplified situations by simple control logic and is not well visualized (Zhou et al., 2015).

In addition to commercialized simulation software, several cases have also been reported in which industrial robot simulation platforms were used for agricultural field (Iqbal et al., 2020; Yu et al., 2023). However, it’s still difficult to smoothly use the simulation results to analyze real conditions since industrial-level simulation environments are specifically designed for factories and do not take the details of agricultural environments into account. For example, large side-slip caused by wet soil and posture change caused by tough road condition are always missing in the industrial-level simulation, which is completely not accurate enough for agricultural robot tractors.

Currently, applications in cyber spaces have become a popular topic in industry, and various development platforms for building virtual environments such as Unity and Unreal 4 provide technical support for conducting real tasks in cyber space through simulation. The use of cyber technologies can help support both the stability and efficiency of dynamic calculation, and the visualization of applied control methodology (Mouratiadou et al., 2023). As one of the emerging concepts of applications in cyber space, the digital twin concept is very close to the expected effect of this study. A digital twin (DT) is a virtual model of a physical object or system that replicates the object's structure and behavior. Characterized by seamless integration of physical and cyber spaces, DT technology is increasingly recognized by both academia and industry (Tao et al., 2019). So far, applications of DT have emerged in various fields, including manufacturing, healthcare, and education (Xu et al., 2024). The main benefits of DT application include reduced production times and costs, simplified integration of heterogeneous technologies, creating safer working environments, and establishing more environmentally sustainable operations (Pylianidis et al., 2021). With these advantages, DT can serve as an advanced digitization platform for agriculture, since it can easily transcend agricultural time cycles and spatial limitations without any air pollution or potential damage to the soil and crops (Escribà-Gelonch et al., 2024; Nie et al., 2022).

1.2 Current Research Status

1.2.1. Digital twin research in agriculture

The influence of DT technology in agriculture is expanding, and many researchers have begun to establish DT applications at various levels within the field of agriculture (Wang, 2024). Among them, crop and vegetation digitization has become the most prominent area of focus (Purcell and Neubauer, 2023). These studies usually combine Internet of Things (IoT) technology to monitor and evaluate the condition of field crops in real time (Alves et al., 2019; Zhang et al., 2023) while also building DT models to predict crop yields or optimize operation plans (Mitsanis et al., 2024; Zohdi, 2024). In addition to crops, livestock systems have also been explored as DT targets in agriculture. For example, a DT of the control system of a swine housing facility can be created in cyber space, enabling analysis of various factors to improve control strategies aimed at reducing energy use or increasing production (Jeong et al., 2023; Jo et al., 2019).

However, most DT adoptions in the agricultural domain remain in their early stages, revealing a knowledge gap in fully implementing DTs within agricultural systems (Arulmozhi et al., 2024). One key reason for this is the difficulty of accurately modeling living organisms, such as animals and plants, which remain central to agricultural production. Compared with applications for plants and livestock, DT development for agricultural equipment is more feasible. DTs of agricultural machinery can accurately monitor the operating status of real agricultural machinery or optimize operations in cyber space. Owing to the successful cases of DT technology in the industrial and manufacturing fields, agricultural machinery shows the potential to be accurately digitized as well. Kim et al. (2022) established a full-scale soil–tool–machine coupling model based on the coupling of DEM (discrete element method) and MBD (multibody dynamics) to predict draft force according to tillage depth during tillage operation. Yin et al. (2024) introduced a lightweight network-based approach to construct a DT system for a combine harvester. This virtual system could precisely predict fuel consumption under full-load conditions. Guo et al. (2024) analyzed the characteristics of the online optimization problem for adjustable settings in agricultural machinery and developed a DT system to search for the optimal set of parameter settings.

The above-mentioned research mainly focuses on the accurate digitization of detailed agricultural operation issues, while another important issue remains: how to accurately replicate the movement of agricultural machinery. For many specific agricultural operations, machinery movement conditions such as trajectory, largely determine operation quality in tasks such as tilling, transplanting, and harvesting.

1.2.2. Accurate modeling of agricultural vehicle

In order to accurately replicate the movement of agricultural machinery, such as tractors, it is important to establish an accurate agricultural vehicle model. However, so far, constructing highly precise, realistically performing dynamic models for agricultural vehicles in cyber space remains a challenge (López-Castñneda et al., 2022). Unlike urban roads, the ground supporting the movement of agricultural vehicles is mainly composed of soil, which can be easily deformed. The hardness of soil is related to various factors, such as the soil type, moisture, and salinity (Natsis et al., 2008), and soil conditions have large spatial heterogeneity, resulting in a wide range of road condition changes for agricultural vehicles (Iwasaki et al., 2020). Therefore, the simple kinematic models applied to road-legal vehicles cannot be satisfactorily used to estimate vehicle conditions in an agricultural setting (Ospina and Noguchi, 2018). Especially under field environments with soil, agricultural vehicles are very likely to slip while moving, and traditional kinematic model are completely inadequate in estimating the state of agricultural vehicles in such scenarios.

To enhance the accuracy of state estimation and automatic control for agricultural vehicles, many scholars recommend the use of side-slip models. The most common method of describing side-slip is by using a linearization model (Snider, 2011). The basic idea is to combine a kinematic bicycle model with a tire model (Pacejka and Bakker, 1992), and linearize the entire state update equation. The linearization model assumes that both the slip angle and steering angle are very small, and extracts only the linear component of the tire model (Xu et al., 2022). To further reduce the control error caused by side-slip, Li et al. (2020) proposed a predictive lateral control method to stabilize a highly automated vehicle at the tire-road friction limits, which means the tire condition is always within the linear portion. This linearization model shows better accuracy compared with classic dynamic models since the friction limits of both the front and rear tires are utilized to define an enveloped stable zone. However, the linearized model is originally utilized for automobiles to estimate the side-slip angle caused by the slight tire deformation occurred on paved roads. When agricultural vehicles are moving in the field, especially on wet soil, the tires and the ground are prone to have relative lateral movement, and the side-slip angle at this time is much larger than the applicable range of traditional linear model. Therefore, when the peculiarities of the agricultural environment are more prominent, such as the soil becoming wetter and softer, the accuracy of the linear model will be significantly lower.

Considering the limitations of the linearization model, non-linear dynamic models for agricultural vehicles have also been studied. Ospina and Noguchi (2016) applied the least squares method to the experimental data collected by RTK-GPS and IMU, in order to obtain mathematical expressions that account for the non-linearities of the dynamic model. Krid et al. (2017) presented a new approach to solving a tracking path problem by applying non-linear continuous-time generalized predictive control (NCGPC), which considers the lateral slip of the tires. Their use of NCGPC achieved good control accuracy and robustness upon changes to the state of the robot vehicle. Singh (2019) improved Pacejka's Magic Formula expressions for the tire cornering stiffness and peak grip level. Due to the extensions of the tire model, the vehicle side-slip angle can be estimated during both steady state and transient maneuvers. Watanabe and Sakai (2020) constructed a non-linear model based on Coulomb's classic theory of friction in order to simulate bouncing and sliding. Their simulation results showed that bouncing and sliding occur on steep terrain, resulting in steering instability. Han et al. (2023) investigated the influence law between the longitudinal slip, lateral slip, and deflection slip, to establish a parametrically modified wheel-soil model. According to validation tests conducted using MATLAB/Simulink and CarSim software, the lateral slope variation has the most significant impact on the side-slip angle and lateral slip rate.

Although numerous studies have attempted to estimate the side-slip of agricultural vehicles by using non-linear dynamic models, most of these have relied heavily on highly parameterized non-linear fittings, which are also quite challenging to extend for general use under smart management systems in cyber space. Thus, it is essential to develop a non-linear model that can accurately describe a wide range of environmental conditions, and at the same time has simple parameters for tuning, to be practically promoted to large platform applications for various agricultural environments in cyber space. This means an ideal non-linear model in DT system should strike an optimal balance between accuracy, wide environmental applicability, and parameter simplicity.

1.2.3. Potential applications based on digital twin system

Finally, potential applications based on digital twin systems in agricultural are investigated. One important application of digital twin systems is to support development of new agricultural machinery. The use of simulation technologies to validate or pre-validate a designed vehicle in cyber space is a safe, efficient, and low-cost alternative to real-world experiments (Geng et al., 2017; Zhang et al., 2019; Lin et al., 2024). Based on cyber-physical strategies, Aliev et al. (2018) used the software program Star CCM+ to perform numerical modeling for mechanical and technological processes that are used in the agricultural industry. The results that they obtained indicate a broad range of uses for numerical modeling in theoretical research concerning agricultural-industry mechanical and technological processes. Cyber technologies to support agricultural vehicle validation have also been developed. Agricultural equipment can be reverse-engineered to obtain a CAD (computer-aided design) copy or digital twin, and the desired equipment can then be simulated and optimized virtually (Cazan et al., 2023). Cyber application can also serve as evaluation tool. The influence and fine-tuning of precision agriculture operations logic can be evaluated by existing simulation systems or by designing new ones, in comparisons of scenarios and setups (Cutini et al., 2023). Although the above-cited studies examined the use of cyber-physical simulation technology in the development of agricultural equipment, most of them were limited to macro-technologies or concepts. More specific and clear application cases need to be verified.

Besides, cyber applications could also be used to manage agricultural vehicles. For example, a discrete-event digital model of grain transportation was developed to evaluate how truck and driver resource constraints impact material flow efficiency, resource utilization, and system throughput (Turner et al., 2019). Based on digital twin system on farm work related with agricultural machinery, it is possible to make work schedule optimization in cyber space with high efficiency and low cost.

1.3 Research Objectives

According to the analysis of current research status, accurately replicating the movement of agricultural machinery is a key issue to be solved in DT system. Therefore, this study aims to establish a DT for a specific agricultural tractor so that both the virtual and real tractors can perform very similar moving conditions under exactly the same automatic steering controller. In this way, the operation state of the real tractor can be replicated in cyber space simply by introducing the control strategy and work schedule from the real environment.

Additionally, the particularities of the agricultural environment need to be taken into account. Especially under extreme agricultural environment such as moving on wet soil, side-slip is more likely to occur between the agricultural vehicle tires and the soil ground, causing a large error compared with basic linear tractor model. To address this issue, a non-linear tractor model, which could simulate side-slip should be proposed and applied in the DT system to make the simulation more practical and adaptive to various agricultural environments. Besides, during the operation simulation of the proposed DT system, errors caused by dynamic environmental changes may continue to accumulate. Thus, for remote controlling and monitoring, an online communication subsystem should be developed to synchronize the virtual tractor and real tractor during a long period of operation.

Finally, to investigate the abilities of the proposed DT system in practical tasks related with agricultural machinery, two types of validations for potential applications should be conducted in cyber space: (1) For robot tractor, and (2) For agricultural operation. For robot tractor, the proposed DT system is supposed to be utilized to explore the optimal design of different combinations of tire parameters and center of mass positions. For agricultural operation, pre-validation examples should be given to show the potential of the proposed DT system in work schedule optimizations for both tractor numbers and operation strategies.

1.4 Organization of Thesis

The thesis is organized as follows:

Chapter 1 introduces the research background, current research status and objectives. It first discusses the issues of robot tractor field experiments and the conceptualization of agricultural digital twin systems, then summaries the current research progress. Finally, research objectives are given according to the above-mentioned analysis.

Chapter 2 presents the framework of the proposed digital twin system, describing the research materials, digitalization methodology and overall architecture. The proposed system includes 3D terrain model reconstruction, basic tractor model establishment, GNSS error simulation, steering system simulation and tire interaction simulation, to replicate the real tractor moving condition as much as possible.

Chapter 3 describes the experimental validation tests of the proposed digital twin system. Three types of field experiments: step response test, zigzag test and real navigation test, were conducted to compare with the results between cyber space and physical space.

Chapter 4 presents a non-linear tractor model applied in the proposed digital twin system, to enhance the practicality under extreme agricultural environment such as muddy field that are prone to cause large side-slips.

Chapter 5 presents an online communication system for cyber-physical synchronization during a long period of operation. This system is supposed to eliminate the accumulating real-time errors between virtual tractor and real tractor due to dynamic environmental changes.

Chapter 6 discusses about the potential applications of the proposed digital twin system. Application examples of new agricultural robot development and agricultural work schedule optimization are conducted in cyber space, respectively.

Chapter 7 summarizes this study's main contributions and future work.

CHAPTER 2. FRAMEWORK OF THE PROPOSED DIGITAL TWIN SOLUTION

2.1 Research Materials

This section provides an overview of the materials utilized in this research, including development tool and environment, which means the software to create the cyber environment together with scripts usages, and the real tractor and real field in physical space which serve as the prototype of the proposed DT system to be projected into cyber space.

2.1.1. Development tool and environment – Cyber space

The tool utilized in this study to develop DT system is the Unity built-in physics engine, which is called PhysX. Originally, Unity is a cross-platform game development tool developed by *Unity Technologies*®. The built-in game engine also supports rigid body physics calculation, ensuring that the rigid body objects can be correctly accelerated and respond to collisions, gravity, and various other forces. Thus, in this study, the game engine is used as a development tool, to develop simulation programs for agricultural vehicles with physical feedback. Compared with existing commercial vehicle simulation software, Unity has the following advantages for use in secondary development:

(1) High flexibility:

Traditional simulation software is always very limited in functionality. Users can mainly change the parameters or adjust different modules. However, using the Unity built-in physics engine to develop vehicle model simulation programs allows for lower-level customization. This means not only that the agricultural environment details can be included, but also that the macro- structural design for the vehicle or the internal calculation principles and parameters can be customized.

(2) Strong portability:

Due to the cross-platform feature of Unity, the developed agricultural vehicle simulation model can be ported to many different operating systems stably. Moreover, due to Unity’s rich application interfaces and scalability, the developed vehicle model can collaborate with many different projects through a network pipeline.

Unity's physics engine is provided in the form of a C# library. 3D models or objects can be defined as basic components in the physics engine. By calling the physics engine's Application Programming interface (API) in programmed C# scripts, state information such as the global/local position and posture of the component in each frame can be obtained. At the same time, control input, such as torque and force, could be assigned to the components through API, or directly change a certain component’s position and posture by modifying the state value. Between the current frame and the next frame, the state of each component would be updated by the physics engine according to current state and control. In the programmed vehicle model, the raw data of vehicle state information are position and posture information directly obtained by physics engine’s API.

In this research, all the parts of a tractor 3D model were first designed in Blender (Version 3.3), and then imported into Unity (Version 2021.3.35f1) in the form of an OBJ file. All the algorithms related to the vehicle dynamic model were programmed using C# scripts in Visual Studio (Version 2019). The 3D models of tractor parts and the corresponding C# scripts were then integrated in Unity to realize the physical effects and relative movements of different parts. As for the hardware specifications, a desktop PC was used to run the developed project. The CPU was the Intel i9-14900kf, and the GPU was the NVIDIA RTX 6000 Ada Generation with a memory of 48 GB. Fig. 2.1 shows the 3D model of the virtual tractor imported into Unity environment. This 3D model of the virtual tractor will move under the C# control script of the proposed DT system, to simulate the driving process of real tractors.

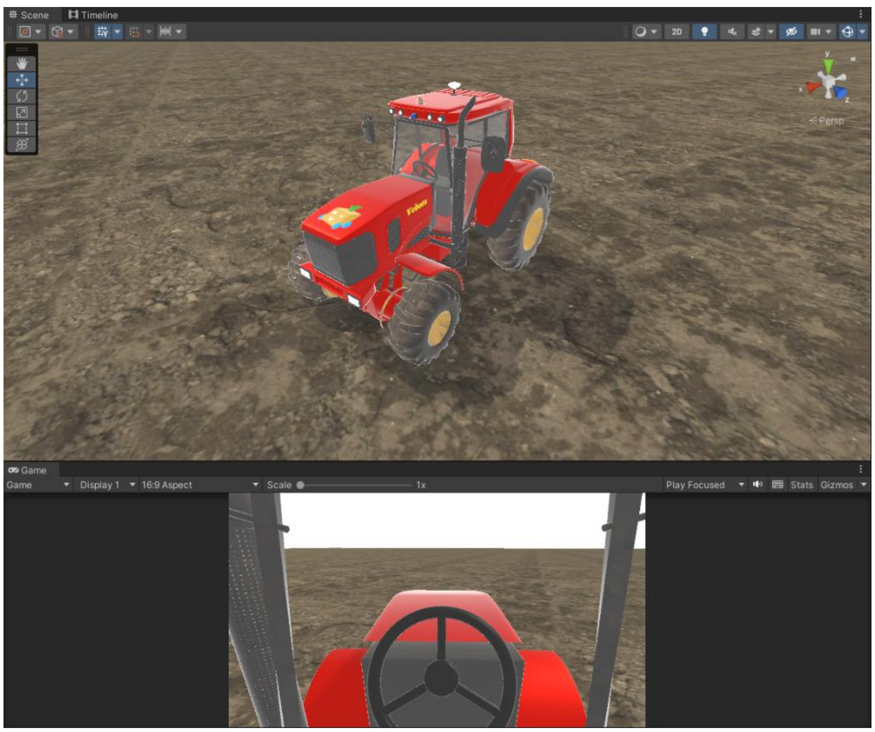

Fig. 2.1. 3D model of the virtual tractor in Unity environment

2.1.2. Tractor prototype and real field – Physical space

The tractor selected as the prototype of the DT system is Yanmar EG 105 Wheeled-type Tractor, as shown in Fig 2.2. This tractor has already been modified as a robot tractor with automatic navigation system. Based on the position and posture data from global navigation satellite system (GNSS) and Inertial Measurement Unit (IMU), navigation system will calculate desired steering angles at a certain frequency, to control the tractor to follow a target navigation path. Additionally, the specifications of Yanmar EG105 are shown in Table 2.1.

Fig. 2.2. Yanmar EG105 Wheeled-type Tractor

Table 2.1. Parameter specifications of Yanmar EG105

Parameters	Value
Full length	4.26 m
Full width	2.04 m
Maximum height	2.735 m
Weight	3850 kg
The distance between left wheel and right wheel (w)	1.46 ~ 1.83 m
The distance between front and rear wheel (l)	2.4 m
The radius of the front wheel	0.48 m
The radius of the rear wheel	0.74 m

As for field in physical space, this research involves two real fields for digitalization in cyber space and verification experiments: Hokkaido University experimental farm (Hokudai Field) and paddy field at Iwamizawa-city, Hokkaido prefecture (Iwaimizawa Field).

2.2 Preliminary Digitalization

Preliminary digitization includes (1) digitization of farm terrain, (2) digitization of basic tractor model (3) reproduction of vehicle controller. Through preliminary digitization, the terrain, the basic parameters and control methods of the tractor model in physical space can be reproduced in cyber space, realizing preliminary digitization of the proposed DT solution.

2.2.1. Digitalization of field terrain

The agricultural environment is complex and changeable. Unlike automobiles, tractors usually do not move on flat roads, but on the undulating soil surface. Changes of terrain can greatly affect the moving state of the tractor. Therefore, if we want to propose a high-precision DT solution, the influence of terrain should be introduced into the cyber space as much as possible. To collect terrain data of these two fields in physical space, DJI 350 RTK Drone together with Zenmuse P1 camera was utilized to survey. The resolution of the image set captured by the Zenmuse P1 was 8192*5460, and all images were then imported into the DJI terra software for Aerotriangulation. To improve the accuracy of Aerotriangulation, 20 landmarks were evenly placed in the fields and their GNSS locations were manually measured for feature point matching. Finally, based on the result of Aerotriangulation, 3D models of the surveyed fields could be reconstructed using DJI Terra software and imported into cyber space (an environment created by Unity software), as shown in Fig. 2.3. Additionally, since the terrain data collected by the drone is equipped with GNSS position information, GNSS coordinates can be calibrated to the reconstructed 3D model as well. In this way, the navigation plan in physical space, such as navigation guidance paths (a point set of GNSS coordinates), could be easily imported into the cyber space.

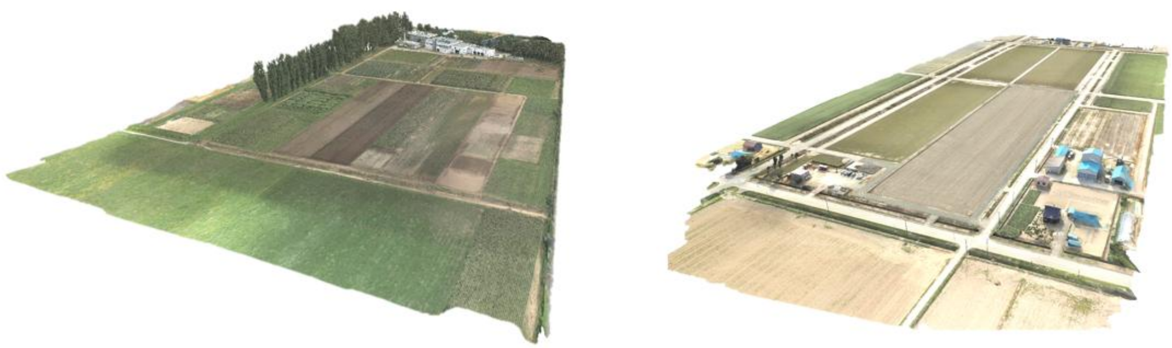

(a) Hokudai field **(b) Iwamizawa field**

Fig. 2.3. Reconstructed 3D models of two real fields in cyber space

2.2.2. Digitalization of basic tractor model

Firstly, physical specifications of the basic tractor model should be defined based on a real tractor phototype in cyber space. In this research, Yanmar EG 105 Wheeled Tractor is selected as the phototype and Table 2.2 shows all specifications values of the constructed virtual tractor model, which is designed based on the specifications of the real tractor. All key parameter specifications of the virtual tractor model and real tractor are identical. Based on these specifications, a 3D model of virtual tractor was constructed in Blender software and then imported into cyber space (Unity environment).

Table 2.2. Parameter specifications of the virtual tractor

Parameters	Virtual tractor
Mass of the tractor body	3850 kg
The distance between front wheel and rear wheel (l)	2.4 m
The distance between left wheel and right wheel (w)	1.8 m
The radius of the front wheel	0.48 m
The radius of the rear wheel	0.74 m

Then, the tractor 3D model should be controlled to move in cyber space. To achieve this, the 3D tractor model should be defined as an Object in Unity system first. Next, collision detection components provided by Unity engine could be utilized to reproduce the movement of the tractor body and wheels. This basic tractor model construction methodology is shown in Fig. 2.4. The tractor body of the 3D tractor model is attached by a Box collider, while four virtual wheels are attached by four wheel colliders, correspondingly. The detailed simulation logic of the constructed tractor model will be explained in Section 4.2.2, together with the non-linear lateral force estimation method.

In this research, the control input could be expressed as: $C = [\delta, T]^{\mathrm{T}}$, where δ represents the steering angle of the virtual front wheels, and T represents the torque of the virtual wheels. Control input could be assigned to wheel colliders through API provided by Unity physics engine. Between the current frame and the next frame, the state of each component, including wheel collider and box collider, would be updated by the physics engine according to current state and control.

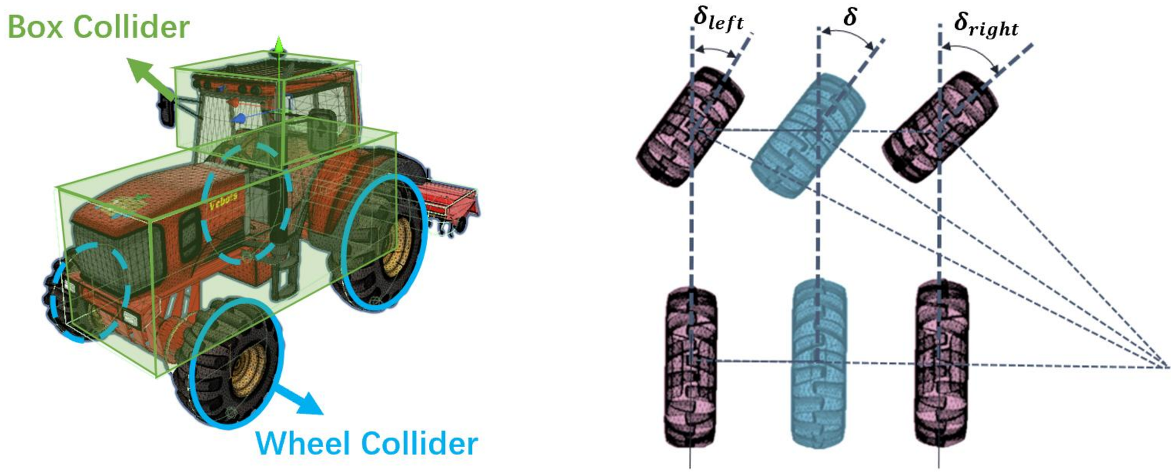

(a) Collider components configuration **(b) Steering input distribution**

Fig. 2.4. Construction of the basic tractor model in cyber space

The steering input distribution diagram is shown in Fig. 2.4 (b). In order to stabilize the tractor, the left and right front wheels always have different steering angles during the turning, which is called the Ackermann steering principle (Zhang et al., 2022). Assume the steering angle from steering controller is δ, then the steering angle of the left virtual wheel δ_{left} and the right virtual wheel δ_{right} based on Ackermann geometry can be expressed as

$$\delta_{left} = \tan^{-1}\left(\frac{l}{\frac{w}{2}+\frac{l}{\tan\delta}}\right) \tag{2.1}$$

$$\delta_{right} = \tan^{-1}\left(\frac{l}{\frac{l}{\tan\delta}-\frac{w}{2}}\right) \tag{2.2}$$

where w represents the distance between the left wheel and right wheel.

2.2.3. Reproduction of vehicle controller

As explained in section 2.2.2, the control input could be expressed as: $C = [\delta, T]^{\mathrm{T}}$ where δ represents the steering angle of the virtual front wheels, and T represents the torque of the virtual wheels. Therefore, the vehicle controller includes two sub-controllers: "Velocity controller" and "Steering controller", to control the longitudinal and lateral motion of the tractor.

For the velocity control, in physical space, the target velocity is input to the Electronic Control Unit (ECU) of the tractor, and then the tractor mechanical transmission system and engine speed controller adjusts the current velocity to the target velocity. Since most agricultural machinery operations maintain a constant speed in pursuit of quality, during the automatic navigation process, the target velocity kept unchanged. Therefore, in this research, a PID velocity controller is designed for calculating the torque T of the tractor model to maintain a fixed target velocity.

$$T = K_p e(t) + K_i \int e(t)\, dt + K_d \frac{de(t)}{dt}, \;\; e(t) = v(t) - v_{target} \tag{2.3}$$

Where, $v(t)$ represents the overall vehicle velocity at time t, v_{target} represents the target velocity set for the vehicle, and K_p, K_i, K_d represent the proportional coefficient, integral coefficient and differential coefficient, respectively. In this study, according to the optimal tuning results from virtual experiment, the values of the three coefficients are as follows:

$$K_p = 1.5\, N \cdot s, \;\; K_i = 0.9\, N, \;\; K_d = 6\, N \cdot s^2 \tag{2.4}$$

As for the steering controller, this is the core of the automatic navigation system when doing agricultural operations. When following different navigation paths or applied for different tractors, the steering controller often needs to be fine-tuned to find the optimal control strategies to ensure the quality of agricultural operations. This can be considered as an external variable of the proposed DT system. Exploring optimal control strategies through iteration in cyber space is also one of the important applications of DT systems. Thus, in this study, verifying the error between the virtual tractor and the real tractor under the same steering controller is crucial for verifying the feasibility and application potential of the proposed DT solution. We reproduced exactly the same steering controller of the real tractor in cyber space. This steering controller (Kise et al., 2001) can be expressed as:

$$\delta = \alpha_1 * d_e + \alpha_2 * \theta_e \tag{2.5}$$

where d_e represents the lateral error, which means the projected distance of the vehicle's position to the target path, θ_e represents the heading error, which means the angle between the desired heading and the vehicle heading angle. The desired heading is defined as: the direction of the line from the vehicle position to a target point on the target path. This target point is obtained by passing a distance L along the target path from the vehicle projection point on the path. L is called lookahead distance and is set as $5\ m$. α_1 is set to be $30\ °/m$ and α_2 is set to be 0.8 for all validation tests for both real tractor and virtual tractor. Besides, the frequency of the steering control is 10 Hz, which is also consistent with the condition in physical space.

2.3. Detailed Digitalization for Tractor Characteristic

2.3.1. GNSS error simulator

In physical space, GNSS error is very important for automatic systems since reliable positioning is a prerequisite for the accurate operations of agriculture machinery (Li et al., 2021). In recent years, Real Time Kinematic- global navigation satellite system (RTK-GNSS) has become a popular choice to provide position information with centimeter-level accuracy. However, considering that automatic navigation system for agricultural vehicles can also reach centimeter-level accuracy, even utilizing RTK-GNSS, the positioning error cannot be ignored. To take this issue into account in our proposed DT system, an RTK-GNSS error simulator was established.

The real tractor has been retrofitted with an automatic navigation system, including a Trimble RTK-GNSS with an antenna located on the tractor roof. Considering that data with a fixed GNSS signal cannot be obtained stably in the initial stage, remove the beginning part of this data set and keep the following position data with the amount of 8000. Since the minimum scale of this RTK-GNSS is 1mm, many data points actually have the same 2D coordinates. The number of occurrences of data points at each coordinate position is counted and displayed in the form of a color bar. In this way, the error distribution of GNSS signals could be observed.

Algorithm 1

Input: (x, y) – *Actual virtual tractor position*
$\mathcal{M}$ - *Error distribution table*

Output: (x_{sim}, y_{sim}) - *Virtual tractor position with GNSS error simulation*

Begin

Import the error distribution table $\mathcal{M}$, *get the maximum row number* i_{max}
Generate a random number σ *from* (0,8000]
Initialize $m_{right} = i_{max}, m_{left} = -1$
While $m_{left} + 1 < m_{right}$ **Do**
  $m_{pos} = (m_{right} + m_{left})/2$
  If $\sigma > a_{m_{pos}}$ *and* $\sigma \leq b_{m_{pos}}$ **Then**
    $x_{sim} = x + (\Delta x_{m_{pos}} - 16) * 0.001, y_{sim} = y + (\Delta y_{m_{pos}} - 16) * 0.001$
    Break
  Else If $\sigma < a_{m_{pos}}$
    $m_{right} = m_{pos},$
  Else If $\sigma = a_{m_{pos}}$
    $m_{pos} = m_{pos} - 1$
      $x_{sim} = x + (\Delta x_{m_{pos}} - 16) * 0.001, y_{sim} = y + (\Delta y_{m_{pos}} - 16) * 0.001$
    Break
  Else If $\sigma > b_{m_{pos}}$
    $m_{left} = m_{pos}$
  End If
End While

End

To establish the GNSS error simulator, first, the collected data points are distributed into square grids that represent spatial units of 1mm*1mm. In this way, the collected data points can be categorized using grids without precision lost. According to the range of collected data points, the size of the error distribution matrix is defined as 32*32. Then, count the number of data points that appear in each square grid and record the row and column coordinates of the square. Sort the square grid coordinates from small to large according to the number of data points. Finally, these grid coordinate information together with the number of data points are made into an error distribution table $\mathcal{M}$. For each row i of the table, the record information format is: $[\Delta x_i, \Delta y_i, a_i, b_i]$. Where $(\Delta x_i, \Delta y_i)$ represents the matrix coordinate of the square grid, (a_i, b_i) means the number interval of data points. $(b_i - a_i)$ equals the number of data points appeared in this grid. The number interval starts from 0 and is superimposed to the total amount of the data, 8000, therefore, $a_i = b_{i-1}$, $a_o = 0$ and $b_{i-max} = 8000$.

Based on this error distribution table, the error probability distribution of RTK-GNSS can be introduced into the simulator. The weighted average coordinates of the collected data points are located in the square grid (16,16) and this position is regarded as the actual position. That is to say, in the Unity cyber space, once the tractor position information (x, y) is obtained, this position data is located as the center point of the error distribution matrix (16,16). Then, generate a random integer number σ from $(0{,}8000]$, and find row i which makes $\sigma \in (a_i, b_i]$ in the error distribution table through binary search. The detailed searching procedures are shown in Algorithm 1. Finally, the output position of the GNSS error simulator (x_{sim}, y_{sim}) is calculated as:

$$x_{sim} = x + (\Delta x_i - 16) * 0.001 \tag{2.6}$$

$$y_{sim} = y + (\Delta y_i - 16) * 0.001 \tag{2.7}$$

To validate the effectiveness of the proposed GNSS error simulator, the output simulation results from the simulator were compared with the collected static position data in physical space, as shown in Fig. 2.5. It is clear that the distribution of the simulated GNSS position data points are similar to that of the collected static position data.

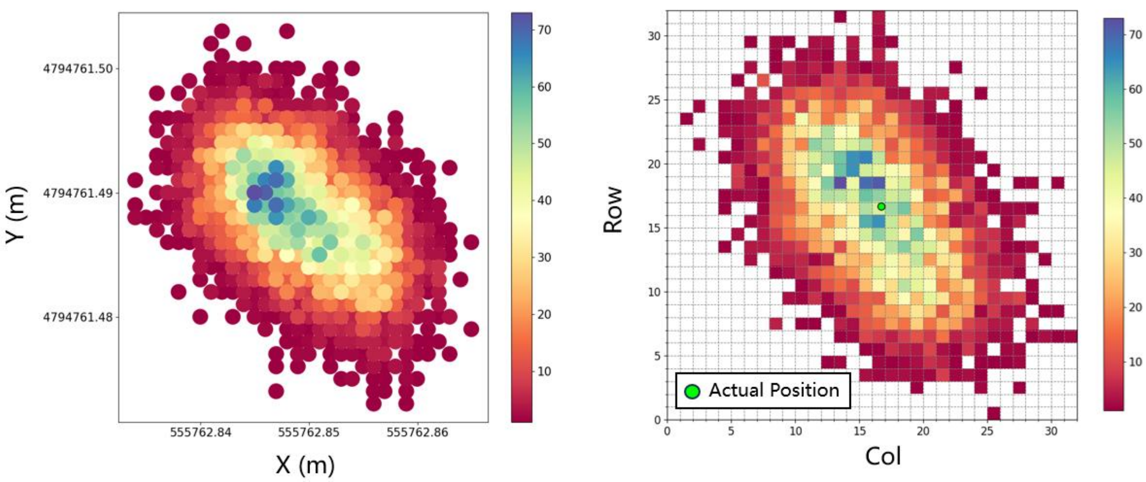

(a)Static position data collected by RTK-GNSS (b) GNSS simulator result

Fig. 2.5. Comparison between the collected static position data and the output results from the proposed GNSS error simulator

2.3.2. Steering system simulator

The simulated position information output by the GNSS error simulator can be used to obtain a steering command δ_c through calculation by the steering controller. However, in reality, after the steering controller inputs the steering command to the tractor's ECU, the steering system will adjust the wheels to the desired position gradually based on the input command. This process will not be finished instantly because the slip angle which then generates lateral tire force should be developed first and so that it takes time for the tire to be steered. And the hardware capability and the steering control design will also dominate this steering lag (Zardin et al., 2018). Therefore, to build a high-precision DT system of the tractor, a simulator considering a nonlinear dynamic steering behavior including the dead-time and the delay-time must be built for reproducing the real steering system.

In the automotive field, a traditional method is to use a first-order delay system to describe the process of steering angle formation (Xu et al., 2021). However, this method encounters a problem when simulating the steering system of a tractor, that is, the steering system of a tractor usually responds slowly and is easily limited by the maximum steering speed that the mechanical system can achieve. Additionally, compared with automobiles, the steering systems of many tractors are not precise enough and have control dead times. According to the above characteristics of tractors, a steering system simulator is proposed:

$$\delta_r(t) = \begin{cases} \delta_r(t-\Delta t) & |\delta_c(t) - \delta_r(t-\Delta t)| < 0.1^{\circ} \\ \delta_r(t-\Delta t) * \left(1 - \frac{\Delta t}{\tau}\right) + \frac{\Delta t * \delta_c(t) * s}{\tau} & \frac{0}{0} 0.1^{\circ} \leq |\delta_c(t) - \delta_r(t-\Delta t)| < 5^{\circ} \\ \delta_r(t-\Delta t) + \Delta t * k * \frac{(\delta_r(t) - \delta_r(t-\Delta t))}{|\delta_r(t) - \delta_r(t-\Delta t)|} & \frac{0}{0} 5^{\circ} \leq |\delta_c(t) - \delta_r(t-\Delta t)| \end{cases} \quad (2.8)$$

Where $\delta_r(t)$ represents current simulated real steering angle. $\delta_r(t-\Delta t)$ represents the simulated real steering angle of last frame. Δt represents the time interval of the current frame and last frame and $\Delta t = \frac{1}{60} s$ since the updating frequency of Unity physical engine is set to be 60 Hz. $\delta_c(t)$ represents the current steering command from the steering controller. s, τ are coefficients of a first-order differential equation, and s is set to be 1 while τ is set to be 0.1

based on trial and error tests. k is the linear steering changing speed coefficient and it is set to be 16.

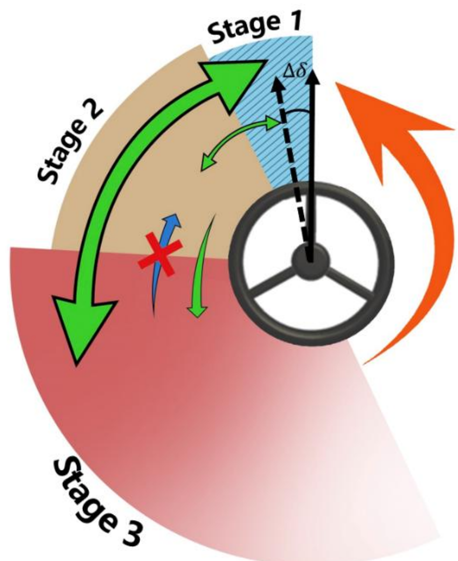

Fig. 2.6. Illustration of the 3 stages in steering system simulator

According to the absolute difference between current steering command $\delta_c(t)$ and the last simulated real steering angle $\delta_r(t-\Delta t)$, the steering system simulator is divided into 3 stages nonlinearly, as shown in Fig. 2.6. For stage 1, when $|\delta_c(t)-\delta_r(t-\Delta t)|<0.1^\circ$, the simulated steering angle will keep unchanged to simulate the dead time behavior of tractor's steering system. For stage 2, when $\frac{0}{0}0.1^\circ \leq |\delta_c(t)-\delta_r(t-\Delta t)|<5^\circ$, the first-order differential equation is utilized to express the relation between the simulated real steering $\delta_r(t)$ and the steering command $\delta_c(t)$. At this time, $\delta_r(t)$ will lag slightly behind $\delta_c(t)$, but is able to track continuously. For stage 3, when $|\delta_c(t)-\delta_r(t-\Delta t)|\geq 5^\circ$, it means that the instantaneous change in the steering command $\delta_c(t)$ is too large. At this time, the steering system usually loses its tight tracking ability and can only change the simulated steering angle

$\delta_r(t)$ at a limited linear change speed. Besides, according to the experimental tests, once entering state 3, self-locking phenomenon would occur and stage 3 would not directly transition to stage 2, but can only be unlocked by stage 1. Therefore, in this simulator, state 1 and state 2, state 1 and state 3 can be transitioned in both directions, but state 2 can only be transitioned to state 3 while stage 3 cannot be transitioned to stage 2. Between stage 2 and stage 3, the transition of the steering system behavior is more like a hysteresis loop, which means the transition paths in different directions are different.

2.3.3. Tire interaction simulator-turning radius correction

After obtaining the simulated real steering angle output by the steering system simulator, this steering angle should be input into the tractor model to control the tractor to move. However, although a basic tractor model has been established during the preliminary digitization, this tractor model is not accurate enough to reproduce the motion of the tractor in physical space. An intuitive phenomenon is that when the virtual tractor model and the real tractor receive the same steering angle input, their turning radius are obviously different. There are many reasons explained for this phenomenon. However, according to previous research, one of the most important issues is that the complex interaction between the tire and the ground caused large difference between the turning radius of real tractor and theoretical tractor model (Ospina and Noguchi, 2016). Since tractors operate in farm fields most of the time, soft soil can easily cause relative slip between the tires and the ground, thus affecting the turning radius. Besides, in order to increase stability, the front wheels of some tractors are designed to deliberately change the roll angle when turning. Therefore, there is a big gap of steering behavior between tractor in physical space and the theoretical tractor model. In addition, due to the mechanical structure of the steering system, the left and right turning radius of the tractor are not symmetrical when the left and right steering angles are the same.

The interaction between the tire and the ground is a very complex and highly dynamic process, and it is obviously very difficult to accurately model this process through physical principles. Thus, in this study, we aim to appropriately fuzzy some complex dynamic interaction parameters, focus only on the control input and output of the model, build a relatively accurate end-to-end relationship, and achieve fully offline DT with acceptable accuracy. Additionally, considering that when the range of dynamic interaction parameters varies too much, the fuzzy end-to-end relationship may fail. Therefore, the ground conditions are classified and different tire interaction relationships are established to deal with different ground conditions. In this way, the proposed DT solution can be applicable to different terrains, and its feasibility also enhanced.

In this study, we constructed tire interaction relationship for two typical ground types: paved ground and soft soil ground. First, the real tractor was controlled to move on the target ground surface at steering angles of ±5°, ±10°, ±15°, ±20°, ±25°, ±30°, and ±35°, and the trajectory circle was recorded. Then, based on the first trajectory circle, calculate the radius of the trajectory circle as the turning radius of the corresponding steering angle. At the same time, the constructed virtual tractor was also controlled under same steering inputs, and with an added set of ±40° in cyber space. Generally, the properties of soil such as soil hardness are considered to be a main factor to influence the interaction conditions between ground and tractor tires(Goodin and Priddy, 2016). To provide a reference for the target soft soil ground condition for this study, 12 soil spots within the experimental field were sampled and the measured soil property parameters are shown in Table 2.3.

Table 2.3. Soil properties of 12 spots within the experimental field

Statistics	Bulk Density (kg/cm^3)	Cone Index (kPa)
Maximum	1.46	931.6
Minimum	1.23	215.7
Average	1.32	581.9
Standard Deviation	0.07	241.5

Based on the calculated turning radius under different steering angles, the relationship between turning radius (r_d represents turning radius in cyber space, r_p represents turning radius in physical space) and steering angle (δ_d represents steering angles in cyber space, δ_p represents steering angles in physical space) is fitted through power formula, as shown in Fig. 2.7. For both asphalt ground and soil ground in the physical space, the turning radius under the same left and right steering input is slightly different, and the tractor's left-turning ability is slightly weaker than its right-turning ability. In the cyber space, since the basic tractor model is an ideal model, its left-right steering ability is always symmetrical. Additionally, the R-squared values of all the power fitted equations are greater than 0.99, which proves that power relationship can well explain the potential correlation of the collected turning radius and corresponding steering angles.

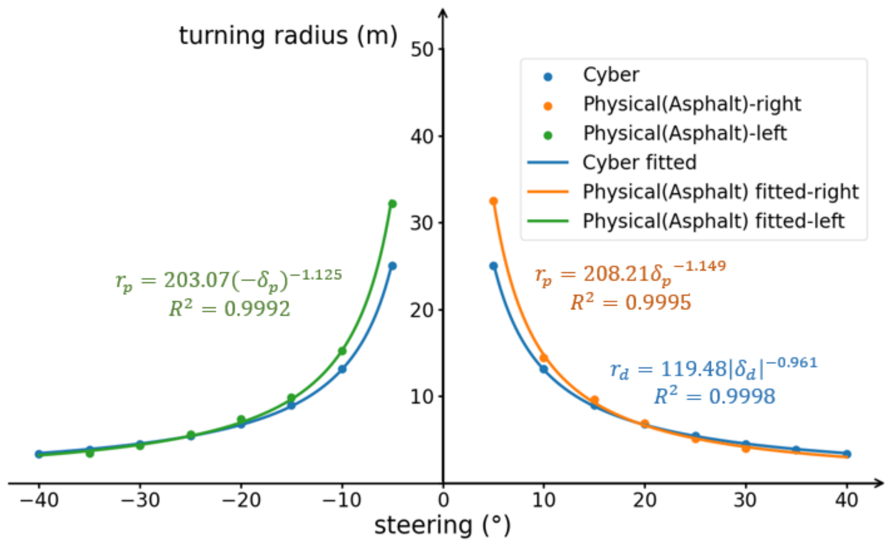

(a) Fitted relationship for cyber space and physical space on asphalt ground

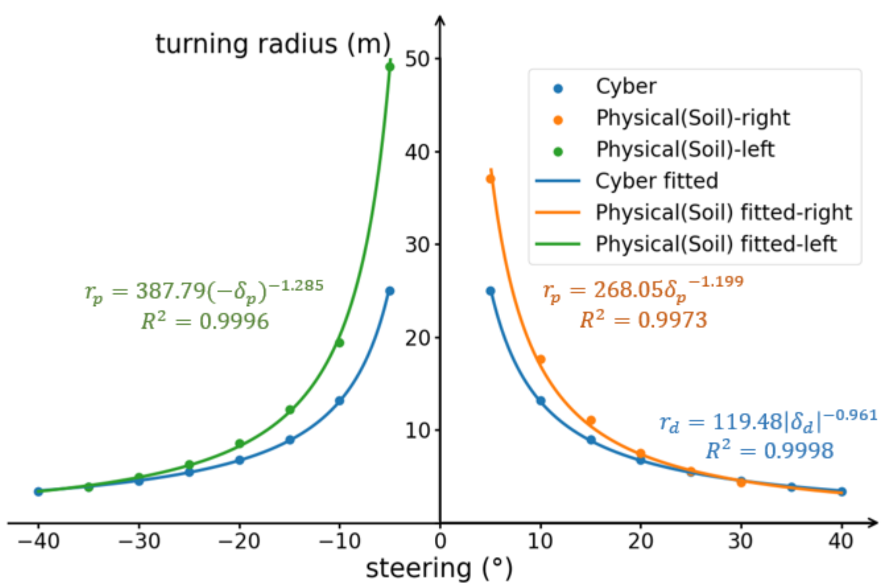

(b) Fitted relationship for cyber space and physical space on soil ground

Fig. 2.7. The fitted relationship between turning radius and steering angle

Finally, with the same turning radius output, calculate the relationship between input steering angles from physical space and cyber space, the steering correction formula can be obtained.

For asphalt ground:

$$\delta_d = \begin{cases} (0.5738437 * {\delta_p}^{1.149})^{1.04058} & \delta_p \geq 0 \\ -(0.5883685 * \left|\delta_p\right|^{1.125})^{1.04058} & \delta_p < 0 \end{cases} \tag{2.9}$$

For soil ground:

$$\delta_d = \begin{cases} (0.4457377 * {\delta_p}^{1.199})^{1.04058} & \delta_p \geq 0 \\ -(0.3081049 * \left|\delta_p\right|^{1.285})^{1.04058} & \delta_p < 0 \end{cases} \tag{2.10}$$

Through this steering correction formula, complex interactions of tires are simply introduced into the tractor model. The simulated real steering angle δ_r output by the steering system simulator can be regarded as δ_p, then it should be converted into δ_d through the correction formula and input into the basic tractor model, so that the behavior of the real tractor can be reproduced more accurately in the cyber space.

2.4. Summary of the Overall Architecture

In summary, a DT solution for agricultural machinery has been proposed to reproduce the motion state of a specific tractor in this study. The overall technology architecture of the proposed DT solution is shown in Fig. 2.8. The preliminary digitization of the terrain and the tractor are conducted first, which can also be regarded as the preparation work of this study. To achieve this, utilize drone to collect data of farms that need to be operated in physical space, then generate point cloud files of farm terrain based on 3D reconstruction technology and import them into cyber space. Then, Yanmar EG105 wheeled-type tractor is taken as an example to establish a virtual tractor in cyber space, including the key parameters and specifications of the basic tractor model and the exactly same controller as in physical space. Besides, in order to achieve better visualization effects, Unity software was utilized to construct the cyber space for our proposed DT solution. At this point, the basic model reproduction of the tractor and the terrain in cyber space has been completed.

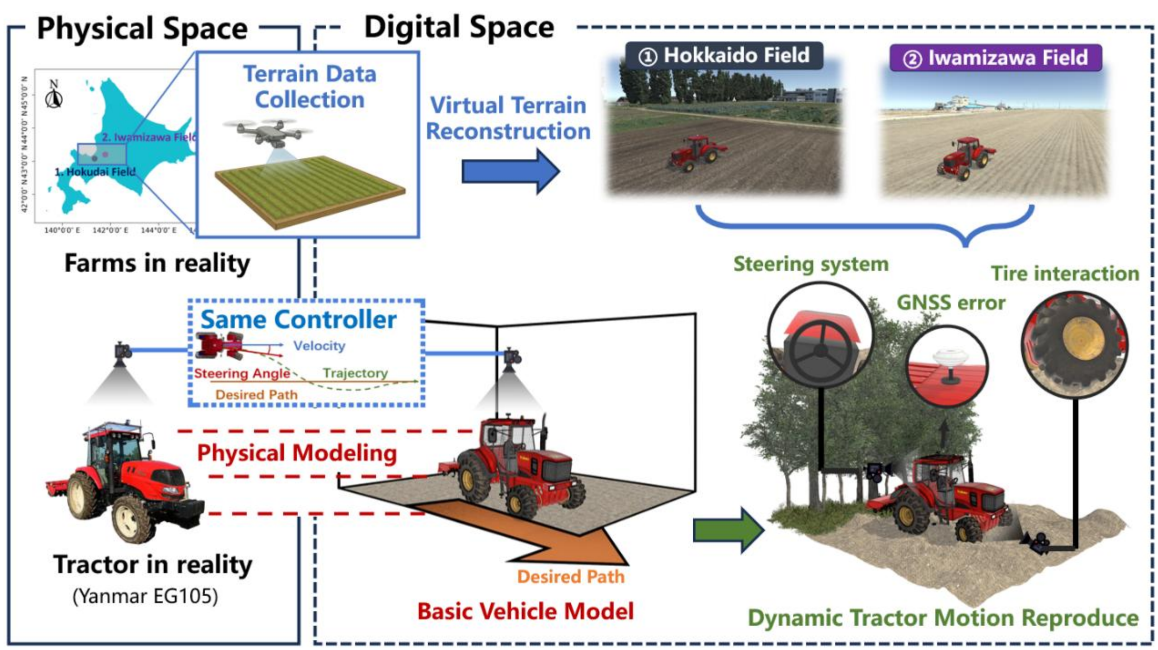

Fig. 2.8. Technology architecture of the proposed DT solution

After the basic tractor model of real tractor, together with the terrain 3D model was imported into cyber space, sub-systems, which could reflect detailed tractor motion characteristics, were developed to realize the proposed DT solution. These sub-systems include GNSS error simulator, steering system simulator and tire interaction simulator, to achieve accurate dynamic motion reproduce of the target real tractor.

Finally, the control chart of the proposed DT solution is shown in Fig. 2.9. The inputs of this system are target velocity and target path, and the steering controller is set up the same as in physical space. The output of this system is the simulated tractor's motion. Through this system, by simply importing the target path, target velocity, and controller settings of the tractor in physical space, the motion state of this tractor can be accurately reproduced in cyber space.

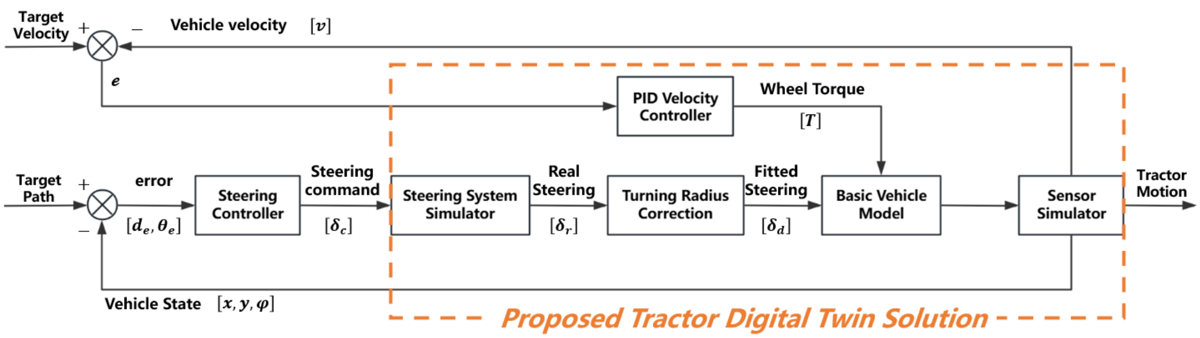

Fig. 2.9. Control chart of the proposed DT solution

CHAPTER 3. EXPERIMENTAL VALIDATION TESTS FOR THE PROPOSED DIGTITAL TWIN SOLUTION

3.1. Introduction

To validate the feasibility and accuracy of the proposed DT solution, field experiments were conducted to compare with the results in the cyber space of DT system. Considering that the proposed DT system is used to reproduce the motion state of the tractor during agricultural operation and could support for optimizing the operation plan in the cyber space, the verification experiment should include the difficulties and key points of the tractor operation as much as possible. Therefore, three types of experiments were conducted for verification: step response test, zigzag test and real navigation test.

3.2. Step Response Test

Generally, most of the field agricultural operations involve agricultural machinery moving along a straight path between crop rows at a fixed speed, working with implements to complete agricultural operation. A common scenario is that when switching from current path to the next path (for example, through headland turning), there is a high possibility to cause a significant initial navigation error. In the process of eliminating this initial navigation error, different tractor models or control algorithms will lead to significantly different trajectories, thus affecting the operation quality. As a DT system, if this process can be accurately reproduced in the cyber space under the same steering controller as in the physical space, it will be of great significance for work schedule optimization and control strategy optimization.

To specifically test the performance of the proposed DT system in the above scenario and verify the difference between it and the real tractor in physical space under the same controller, a step response experiment was designed. Considering that the terrain of agricultural environment is highly variable, we made two turning radius correction formulas for asphalt ground and soil ground as expressed by Eq. (2.9) and Eq. (2.10). Therefore, the step response experiments were conducted on two different types of ground to validate the turning radius correction formula as well. One experiment site is located at the experimental field of Hokkaido University, to represent the soil ground, while another site located at the parking lot near the experimental field, to represent the asphalt ground. In order to observe the motion performance of the tractor under a step offset in the experiment, the step response test is designed shown in Fig. 8. During the test, as the look ahead target point of steering controller moves, the tractor will first turn in the direction of the step offset change of the target path, then briefly return to the front direction, and finally continue to move toward the second path to eliminate navigation errors. There are mainly two advantages of this experimental design: (1) This design can accurately control the step offset value to validate the performance of the tractor under different navigation errors. If only one path is used for testing with a certain set initial navigation error, it is very difficult to manually drive the tractor to the designed position every time in physical space. (2) This experimental design will cause the tractor to turn towards the step offset direction twice. Compared with the design of a single path with a fixed initial error, this is more complex and can better verify the difference between the proposed DT system and the tractor in physical space. Finally, since the reconstructed 3D terrain model in the cyber space has been calibrated with GNSS information, the experimental navigation paths in the physical space can be directly imported into the cyber space. The cyber space and the physical space share exactly the same navigation paths, navigation settings and navigation control algorithms.

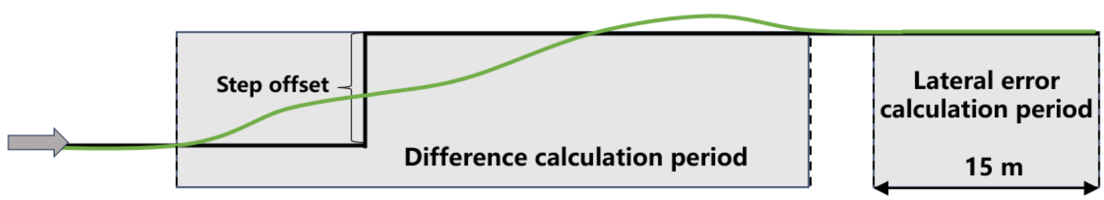

Fig. 3.1. Illustration of step response experiment design and error indicators calculation range

In this test, there are mainly two error indicators to evaluate the DT system performance, the first one is the trajectory difference between the DT system and real tractor. The calculation range is from the time when the tractor starts turning to the time when the tractor converges to the second path. The calculation method is to traverse each trajectory point of the DT system and calculate the shortest distances to the real tractor trajectory to make a difference error set. The second error indicator is the lateral error d_e on steady state after the tractor converges to the second path. The calculation range is unified to the last 15m of the second path.

3.2.1. Validation for asphalt ground

Considering that asphalt ground is flat and can provide greater lateral force than soil, the tires are less likely to slip so that the tractor's trajectories are easier to reproduce in cyber space. Therefore, the step response experiments for asphalt ground were also used as trial and error tests to optimize the parameters for the steering system simulator explained in Eq. (8). Fig. 3.2 shows the trajectory results of the proposed DT system and physical space in the validation tests with a step offset of 100 cm, and the tractor target velocity is fixed at 5 km/h.

In Fig. 9, a flowchart presents how the proposed steering simulator affects the trajectory change by a comparison with DT solution before the proposed steering simulator applied. The average and maximum trajectory difference during the offset turning part is 2.0 cm and 6.5 cm respectively, which validate the high accuracy of the proposed DT system for simulating tractor motions in physical space.

However, as shown in Fig. 3.2, when the steering simulator is not applied in the DT system, the trajectory of the virtual tractor deviates significantly from the trajectory of physical especially during the turning part. In order to investigate the cause of this significant difference, the trajectories of the DT system before and after the steering simulator applied are compared during the step offset turning part. Additionally, as a reference, the values of the simulated real steering angle δ_r are visualized on the trajectories through color. From the different color change conditions, it is obvious that DT system without steering simulator applied, output a large steering angle at an earlier stage compared with that of DT system when steering simulator is applied. This is because the process of steering angle formation is missing without steering simulator, so that the steering command is directly converted into mechanical output, which responds faster than the real situation, resulting in different trajectories. In contrast, the proposed steering system simulator could simulate the process of the steering angle formation, performed like a steering signal delay.

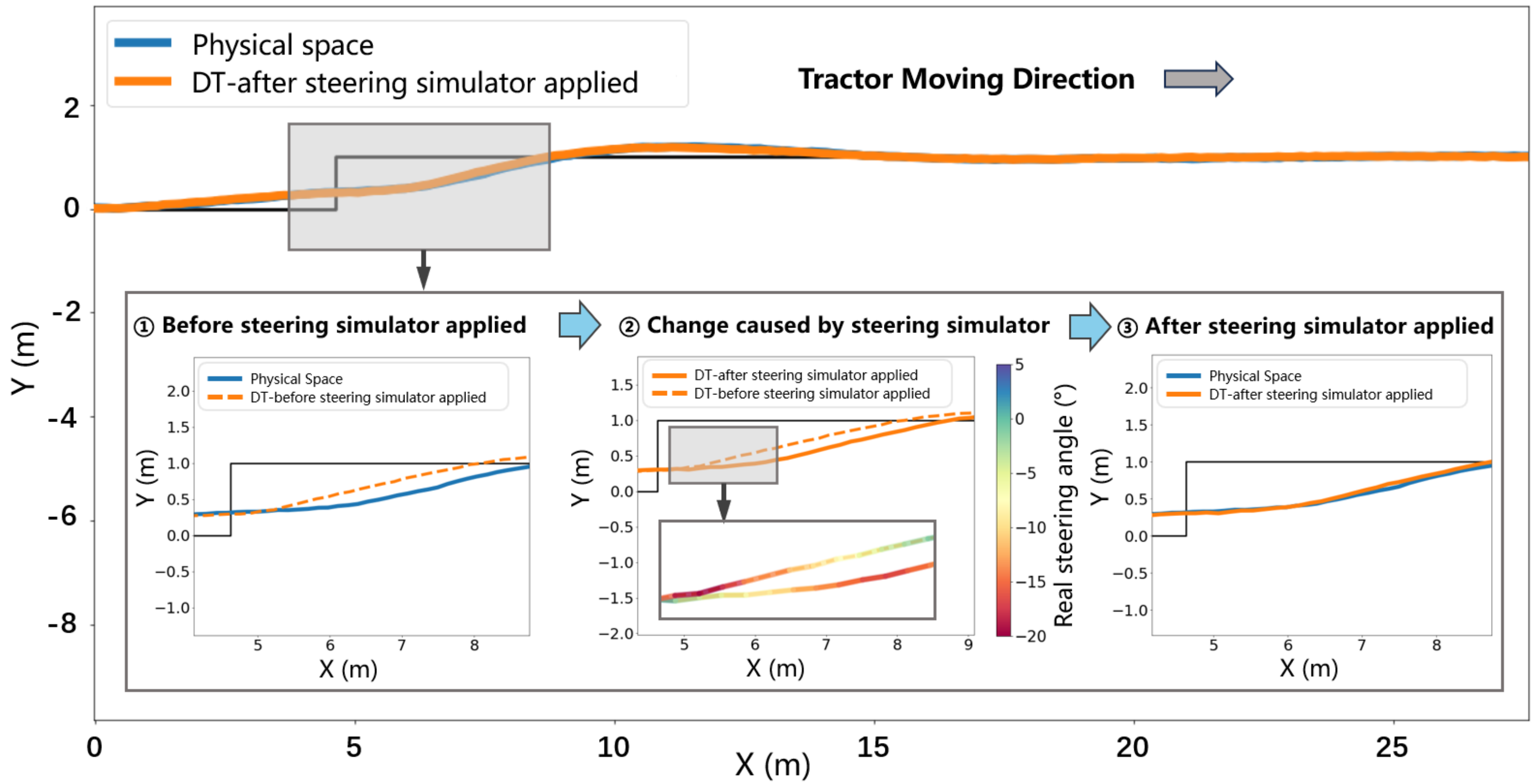

Fig. 3.2. Trajectory results of the proposed DT system and physical space on asphalt ground

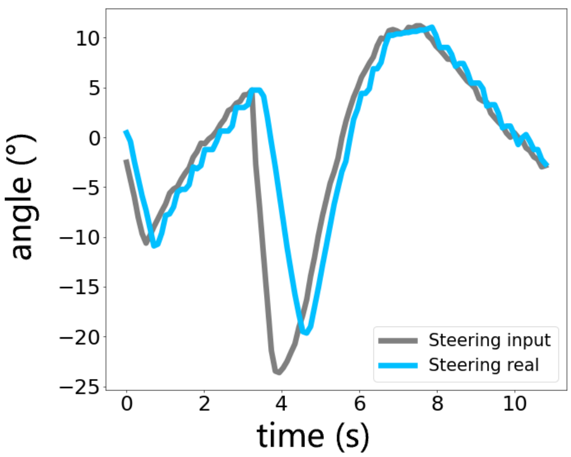

(a) Physical space

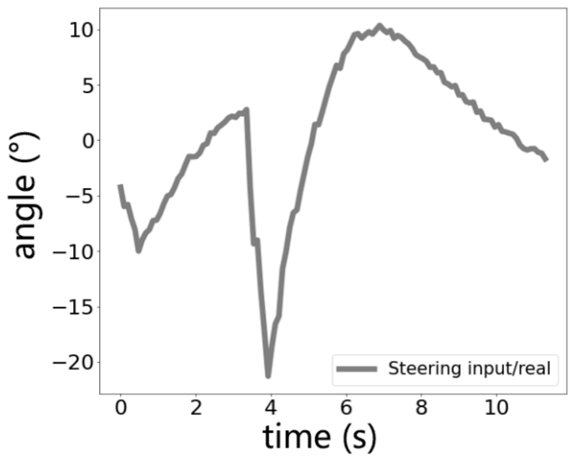

(b) DT-before steering simulator applied

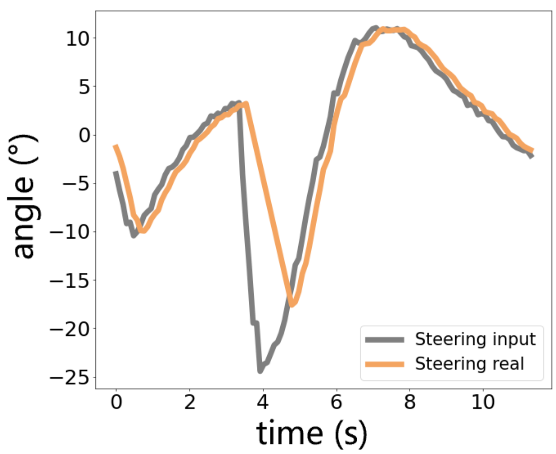

(c) DT-after steering simulator applied

Fig. 3.3. Change of steering input and simulated real steering

For more accurate comparison between physical space, DT systems that before and after steering simulator is applied, the time series of steering input and simulated real steering angles change are shown in Fig. 3.3. Although the tendencies of all steering angle changes are similar, the steering angle output by the DT system without a steering system simulator has the fastest respond, with a significant difference from the physical space. For both physical space and DT with steering simulator, the mechanical real steering angle has a clear delay compared to the steering input. Specifically, when the steering input changes too fast, the mechanical system may fail to tightly follow and would be limited by a maximum linear change speed. During this part the gap between the input steering and real steering is continuously increasing, which would cause a big trajectory difference if steering system is not precisely simulated. Besides, the steering simulator parameters are optimized through the minimization of trajectory difference between DT and physical space. Although the trajectory difference has already been validated to be quite small for asphalt ground with centimeter level, the slope of the maximum linear change part is a little different between the proposed DT system and physical space. This may be caused by the limitations of data sensing. In this study, the mechanical real steering angles for each time stamp in physical space were obtained by the feedback from tractor's ECU. The possibility of error from ECU to the actual steering position also exists.

Additionally, for asphalt ground, step response experiments with different step offsets and velocity were also conducted to further evaluate the performance of the proposed DT system of reproducing real tractor's behavior. The experimental results of different step offset and velocity are shown in Table 3.1. As can be seen from Table 3.1, the trajectory difference will increase slightly as the target velocity increases. This is because as the vehicle velocity increases, the side-slip angles of tires are more likely to increase, which will cause a larger fluctuation range of the actual side stiffness of the tire interacting with the ground, thereby increasing the difference between DT and physical space. Besides, as the setting step offset increases, the trajectory difference will also increase. According to the steering controller, the input steering angle during the turning part will increase as the step offset increases. Similar to velocity, an increase of the steering angle will lead to a larger side-slip angle and thereby cause a larger fluctuation range of the actual side stiffness of the tire.

Finally, it can be concluded that when the step offset is within -150 cm, even the maximum trajectory differences between DT and physical space are within 10cm for both speed of 3 km/h and 5 km/h. Considering that most commercial field automatic navigation systems can only track straight navigation paths with centimeter-level accuracy, the proposed DT system has already achieved a very high accuracy for asphalt ground.

3.2.2. Validation for soil ground

The step response experiments were also conducted for soil ground, with different step offsets and target velocities. Additionally, in this experiment, the proposed DT system with a traditional steering simulator (Xu et al., 2021) which only utilizes a first-order delay system to simulate steering behavior, has also been tested and compared for the validation of the proposed steering simulator. All trajectory differences result of step response experiments conducted for soil ground are shown in Table 3.2.

Table 3.1. Trajectory difference in step response experiments for asphalt ground (cm)

Step offset setting (cm)		-200	-150	-100	-50	50	100	150	200
3 km/h	Maximum	8.4	8.7	7.3	8.3	6.3	6.6	8.4	9.2
	Average	3.7	3.4	3.3	2.6	2.6	3.1	4.5	3.3
5 km/h	Maximum	12.6	7.8	8.7	5.0	9.2	6.5	6.4	11.5
	Average	5.0	3.9	2.9	1.6	2.9	2.0	1.8	3.8

Table 3.2. Trajectory difference in step response experiments for soil ground (cm)

Step offset setting (cm)			-200	-150	-100	-50	50	100	150	200
DT with the proposed steering simulator	3 km/h	Maximum	24.0	10.7	7.5	9.4	8.9	9.1	14.5	14.6
		Average	11.6	5.0	2.8	3.3	3.8	3.8	7.1	5.2
	5 km/h	Maximum	39.8	10.8	7.0	7.4	9.5	8.1	14.9	21.6
		Average	16.4	5.4	2.8	2.5	4.3	2.6	4.5	7.4
DT using traditional steering simulator	3 km/h	Maximum	37.5	20.7	10.3	11.1	9.1	15.7	22.7	23.6
		Average	13.9	8.7	4.9	5.7	4.0	5.4	8.9	8.6
	5 km /h	Maximum	50.3	33.7	19.9	9.7	13.0	23.4	41.8	44.9
		Average	23.0	12.3	5.7	3.7	6.3	7.4	12.2	14.6

From Table 3.2, it is clear that for different step offsets and different target velocities, the performances of the DT system with proposed steering simulator are all way better than that of the traditional steering simulator. When the step offset is smaller than 100 cm, even the maximum trajectory difference of the DT system with proposed steering simulator is lower than 10 cm, proving the effectiveness and advantages of the proposed method. Normally, compared with asphalt ground, soil ground would cause larger trajectory differences, due to larger side-slip angles caused by a larger fluctuation range of the terrain. Besides, the accuracy differences between results from 3 km/h test and 5 km/h test, and the accuracy differences between different step offsets have all increased. As we have analyzed before, the underlying reason why different step offsets and different target velocities could affect the accuracy of the DT system is that these factors will influence the fluctuation range of the instantaneous slip angle. Compared with asphalt ground, the terrain fluctuation of soil is larger. This will increase the fluctuation of the cornering stiffness coefficient between soil and tire, which finally leads to a greater fluctuation of the instantaneous slip angle of the tire. According to the above discussion, although factors such as step offset, target velocity and terrain will amplify the fluctuation range of dynamic parameters in DT system and thus affect the accuracy. This kind of amplification effect can be effectively mitigated by attempting to reproduce the tractor characteristic as much as possible, such as using the proposed steering system. This point has been proved by the superiority of the proposed DT system over the traditional solution in terms of trajectory differences. Additionally, another way to deal with the large fluctuation range of dynamic parameters is that more precisely classified database of ground-tire interaction models could be established, through more turning radius data collection from different ground.

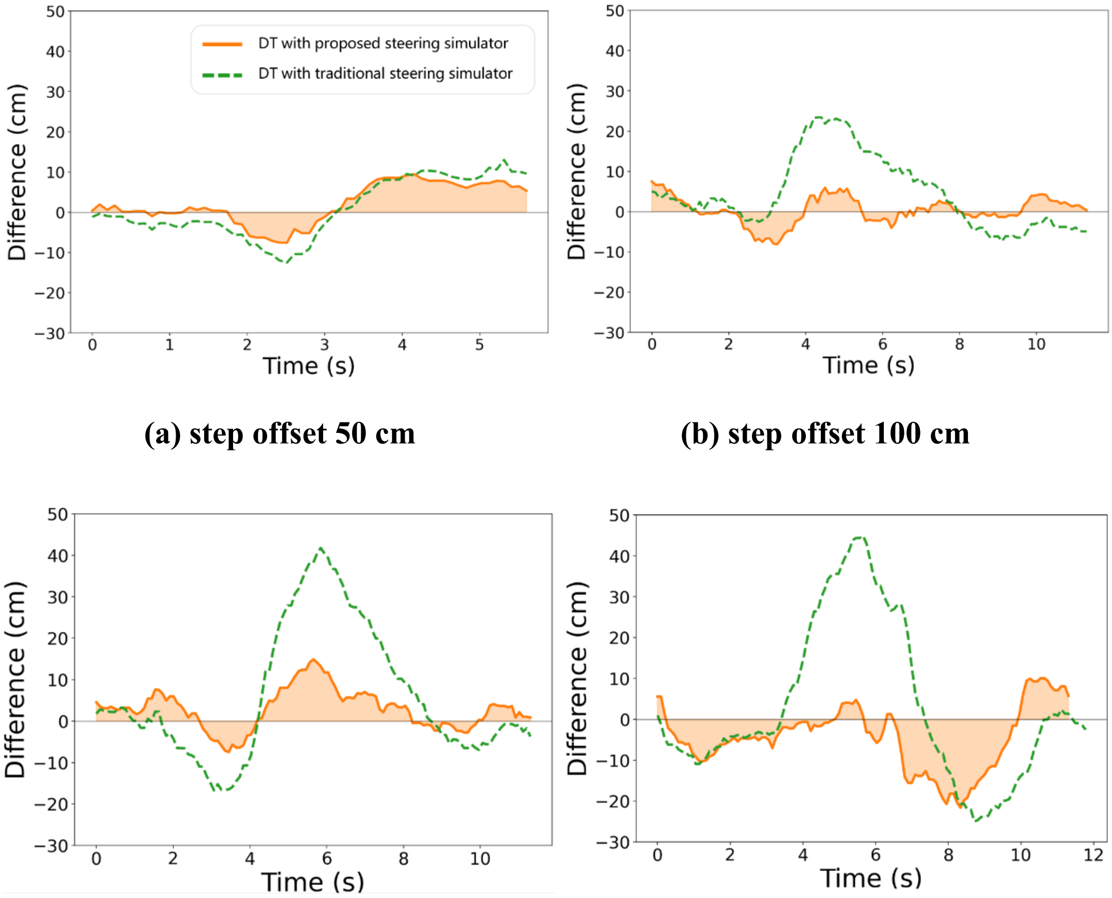

(a) step offset 50 cm

(b) step offset 100 cm

(c) step offset 150 cm

(d) step offset 200 cm

Fig. 3.4. Time series of trajectory difference change during offset turning

To provide a more detailed comparison, 4 examples of the time series of the trajectory difference change during the turning part of step offset 50 cm, 100 cm, 150 cm and 200 cm are shown in Fig. 3.4. When the step offset is 50 cm, the performances of the proposed steering simulator and the traditional steering simulator are very close, but as the step offset increases, the gap between the two steering simulator becomes more and more obvious. This may be because when the step offset is 50cm, the steering angle command input by the steering controller also changes slowly, and the proposed steering simulator keeps transitioning between stage 1 and stage 2. The traditional steering simulator is equivalent to stage 2 only, so the performances of the two simulators are very close under this condition. The simulation of the dead time behavior (stage 1) may be the reason why the proposed steering simulator has a slight advantage. However, when the step offset increases to more than 100 cm, the steering angle command may change dramatically, causing the proposed simulator to enter stage 3, which is completely incapable of being simulated by the traditional simulator, resulting in a large gap between the two trajectories. Besides, according to Fig. 3.4, as the step offset increases, the time required for the tractor to converge to the second path also increases. When the target velocity remains unchanged, a longer moving time means a longer moving distance, and the possibility of side-slip due to terrain fluctuations will also increase. This is also an explanation for the positive correlation between offset and trajectory difference based on the time series analysis.

To further validate the effectiveness of transitioning stages in the proposed steering simulator, a detailed comparison between DT with proposed simulator and with traditional simulator is shown in Fig. 3.5. Obviously, the trajectory of DT with proposed steering simulator is much closer to that of physical space. From the zoom in part of Fig. 3.5 (a), it can be concluded that the formation of difference in trajectories between the proposed steering simulator and traditional simulator is mainly due to the maximum limited steering changing speed (stage 3) At the beginning of this part, the trajectories of both two steering simulator are very close, and at this time the proposed simulator is transitioning between dead time behavior (stage 1) and first-order delay system (stage 2). However, when the steering command input suddenly increases, the proposed steering simulator enters stage 3 and changes very slow, while the simulated real steering of traditional simulator changes very fast, resulting in a clear divergence between the two trajectories. According to Fig. 3.5 (b) and (c), the steering command input for both steering simulators show similar tendency, but the simulated real steering angles are very different, especially during 0.3s to 1.5s, which is also the time of stage 3. Although the traditional simulator also exhibits relatively large differences from the steering input during this period, the tracking speed of the first-order delay system is still too fast, far exceeding the maximum linear steering speed demonstrated by the steering system in physical space.

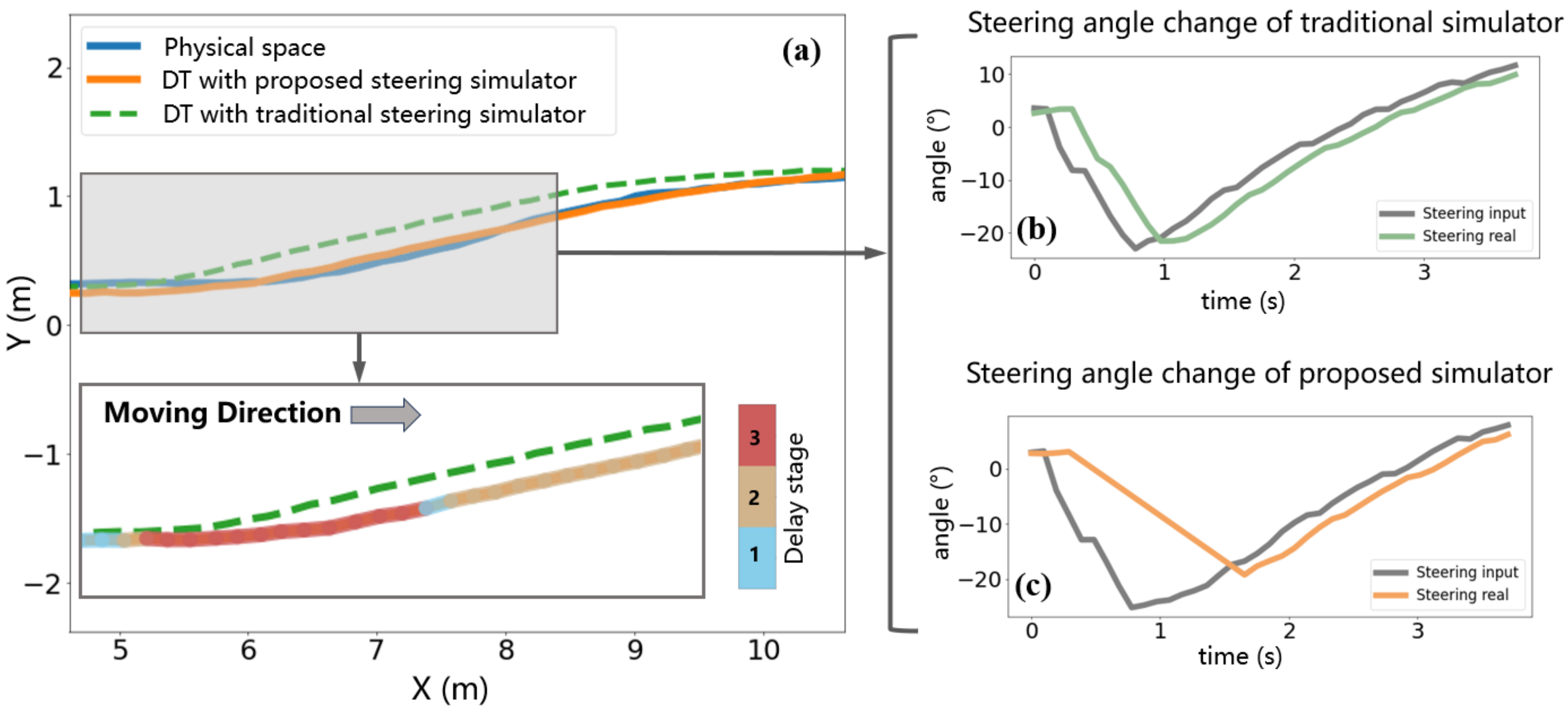

Fig. 3.5. Experimental results comparison between DT with proposed steering simulator and DT with traditional simulator on soil ground. (a) Trajectory with stage visualization (b) steering angle change of traditional simulator (c) steering angle change of proposed simulator

Additionally, this comparison also validates the necessity of the hysteresis loop designed between stage 3 and stage 2, to simulate the steering system behavior of physical space. The tracking ability of the first-order delay system (stage 2), which is the traditional steering simulation method, is quite strong. Therefore, when the difference between simulated real steering and input steering is smaller than 5°, if the proposed simulator transition from stage 3 to stage 2 directly, the simulated real steering angle could quickly catch up with the steering command input, lead to a small downward broken line. This is inconsistent with the steering angle change tendency in physical space.

Finally, the average lateral error calculated in the last 15 m of the second straight path for physical space, DT with proposed steering simulator and DT with traditional steering simulator, are presented in Table 3.3. Most values of average lateral errors are between 2 cm and 5 cm, maintaining a satisfactory accuracy. Besides, the difference between the proposed steering simulator and traditional simulator is also limited since the steering angle commands for straight path navigation after convergence are also quite small and change smoothly. The only notable phenomenon is that as the step offset increases, the average lateral error in the physical space decreases. This may be because with repeated navigation tests, the tire marks on the soil surface form grooves, which provide greater lateral force to the tires, keeping the tractor body stable. Such dynamic terrain changes currently difficult to achieve in DT systems, which is considered as a limitation.

Normally, in real agricultural production, under the control of a reliable automatic navigation solution, when a tractor switches from one path to the next, the initial offset error should not exceed 1.0 m. Because the space between crop rows provided for a tractor to pass through is usually very limited, if the initial offset error is too large, it means that the tractor is going to damage the crops. Therefore, considering the application under steering controllers for real productions, the current DT solution can maintain centimeter-level accuracy in both asphalt ground and soil ground, demonstrating significant superiority over traditional solutions.

Table 3.3. Average lateral error for physical space, DT with proposed steering simulator and DT with traditional steering simulator (cm)

Offset setting (cm)		-200	-150	-100	-50	50	100	150	200
Physical space	3 km /h	2.5	2.4	2.7	2.5	3.4	3.0	2.0	1.8
	5 km/h	1.5	2.2	2.3	2.4	3.6	3.1	2.1	1.5
DT-proposed simulator	3 km /h	3.3	3.2	3.1	3.6	3.8	4.3	3.4	3.8
	5 km/h	3.6	2.9	2.5	2.7	4.0	4.2	3.0	5.6
DT-traditional simulator	3 km /h	3.9	3.1	3.1	3.2	3.7	4.0	3.9	3.9
	5 km/h	5.1	3.2	2.5	3.3	4.3	3.9	4.6	4.4

3.3. Zigzag Test

In the step response test, the DT system with proposed steering simulator was verified to provide higher accuracy compared to the traditional steering simulator when the steering angle changes greatly. In order to further explore the performance differences between the proposed steering simulator and the traditional simulator when the steering angle is constantly changing, zigzag tests was conducted on soil ground as well. Instead of two straight paths with step offset, both virtual tractor and real tractor will track a trigonometric path. The shape and size of the path can be expressed as:

$$P_y = A * \sin(\omega P_x) \tag{3.1}$$

Where (P_x, P_y) represents the relative coordinates of the points from this path once the starting point is assumed to be $(0,0)$. A is the amplitude of the navigation path and $A = 5$, ω is the frequency of the path and the value is $1/5$, $1/4$ and $1/3$. The larger ω is, the larger the curvature of the path is, and the easier it is to produce a large steering command change.

Fig. 3.6 (a) shows the average trajectory difference results for different trigonometric path frequency. The color bands represent the interval range of standard deviation. It is obvious that the proposed steering system simulator is significantly ahead of the traditional simulator in both average trajectory difference and standard deviation fluctuation. As the path frequency increases, the steering command changes more dramatically, which is more likely to cause the trajectory difference to increase. However, compared with the traditional simulator, the trajectory difference of the proposed steering simulator increases significantly more slowly as the path frequency increases. This conclusion is consistent with the comparison result in the step response tests when the steering command is relatively large.

To further investigate the performance of the proposed steering simulator and traditional simulator, the comparison of trajectory results of path frequency $1/3$ is shown in Fig 3.6. (b). Because in this case, the trajectory difference is most likely to increase, and the gap between the two methods is the largest at this time among all the tests. From the trajectory result, the proposed steering simulator is very close to the trajectory of the real tractor, while the trajectory of the conventional simulator has a significant gap with both when turning. As discussed before, this is because the steering angle in traditional simulators changes too fast and therefore cannot simulate the maximum steering change speed limit of the real steering system. Here, we would like to explore in more depth the reasons why the trajectory of DT system with proposed steering simulator differs from that of real tractor. To this end, we zoom in the trajectory result at the initial stage of the turning part, which is from ① to ② shown in Fig. 3.6 (c). Additionally, the simulated steering angles are visualized through a color bar. According to the steering color, at position ①, the steering angles of both real tractor and virtual tractor are the same. However, even so, there is still a slight trajectory difference between the virtual tractor and the real tractor at this moment. This small difference may be caused by a small side-slip or terrain change. Since the tractor is going to turn from position ①, the steering angle increases rapidly to the maximum value, and the difference between the trajectories of the virtual tractor and the real tractor becomes larger and larger.

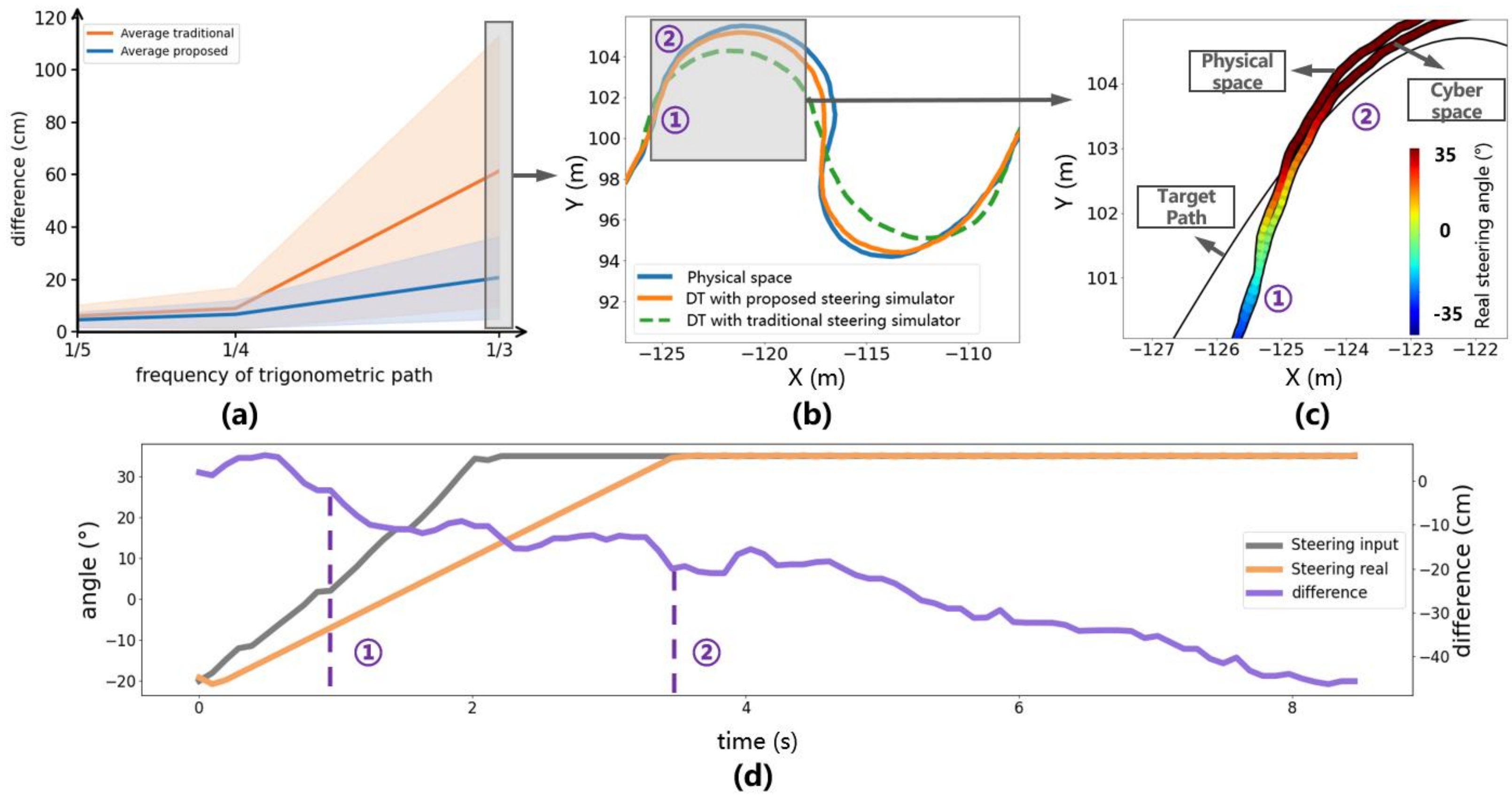

Fig. 3.6. Zigzag test results on soil ground (a) trajectory difference results for different trigonometric path frequency (b) comparison of trajectory results (c) trajectory with steering angle visualization (d) steering angle change and trajectory difference change of the proposed simulator

To verify the reason of this accumulating trajectory difference, steering angle change and trajectory difference change of the proposed simulator are investigated and shown in Fig.3.6 (d). According to the change of the steering angle, it is obvious that the proposed steering simulator has entered stage 3 and once reached the maximum steering angle it remained unchanged. This process can be regarded as open-loop control and is very long. Open-loop control can easily amplify error disturb and cause errors to accumulate quickly, so this could be regarded as one possible reason accounts for the increasing absolute value of the trajectory difference. Besides, when the steering angle is very large, once the ground conditions change slightly (such as become a little wetter), there may be a non-linear relationship between the lateral force of the tire and the side-slip angle, which may lead to a side-slip. Under this condition, the correction formula for turning radius may fail.

In summary, the proposed DT system is verified to have two limitations: (1) Errors would accumulate quickly when controlled in open loop (2) The correction formula for turning radius may fail when non-linear side-slip occurs.

3.4. Real Navigation Test

Although the feasibility of the proposed DT solution has been verified from a detailed perspective in the step response experiment, it is still necessary to further verify the simulation capability of the proposed solution for large-scale agricultural operation in physical space. Therefore, a real navigation plan was conducted in a real field located in Iwamizawa City, Hokkaido, serve as a practical agricultural operation scenario.

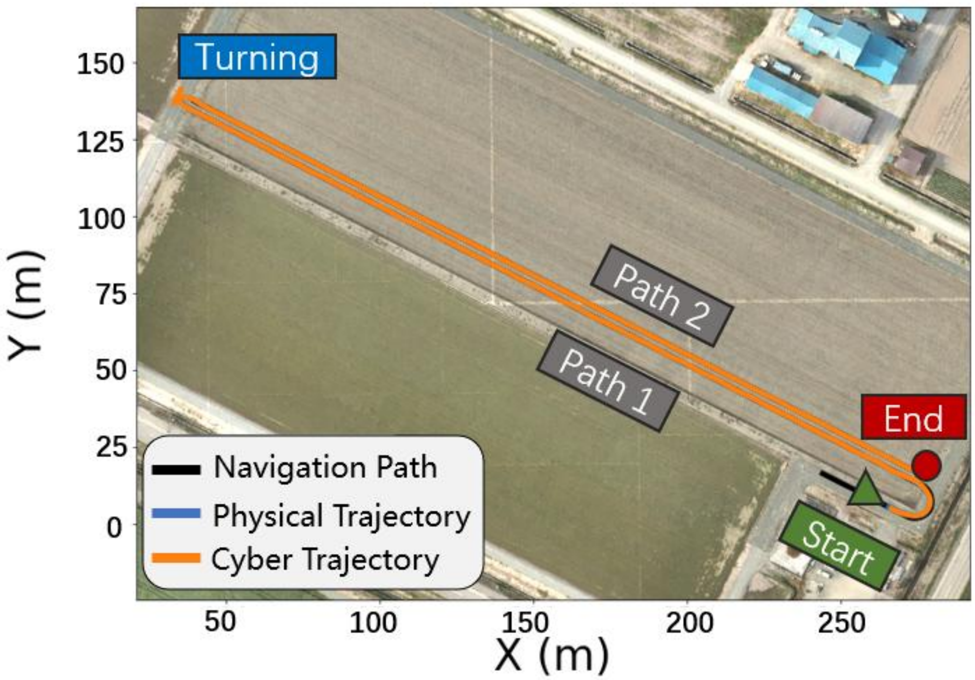

(a) Real navigation plan and trajectory results

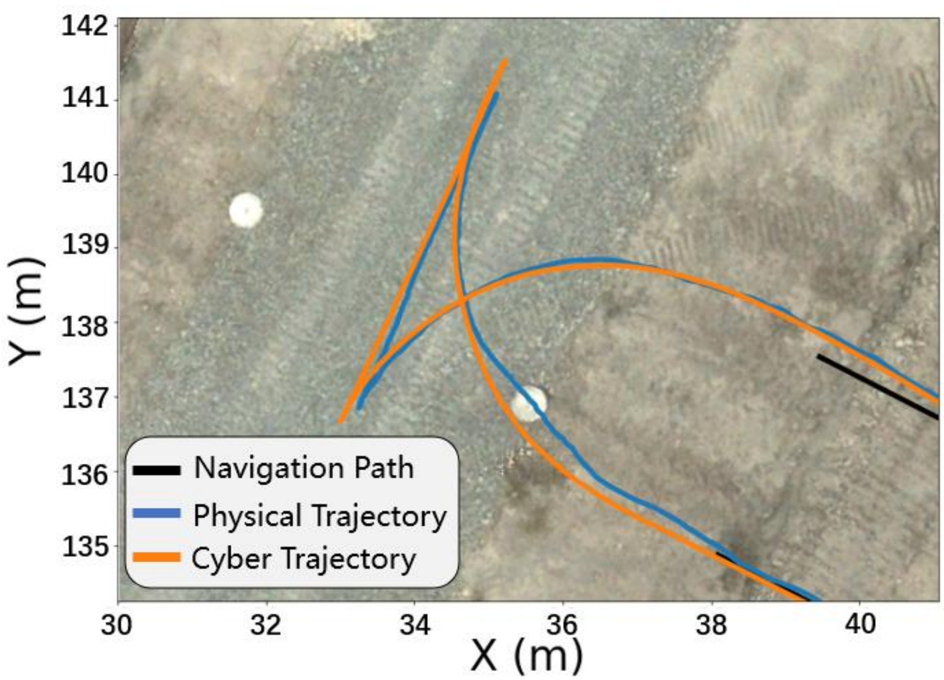

(b) Trajectory results of headland turning

Fig. 3.7. Trajectory results of the real navigation plan

In the real navigation plan, the real tractor will start at the entrance of a parking lot near this field, and enter the field after a U-turn. Then, the tractor will follow two straight paths with a fixed target velocity of 5 km/h and a fixed lookahead distance of 5 m. Once reaches the headland of the field, the tractor will perform a switch-back turning instructed by the steering controller. Additionally, exactly the same navigation guidance paths, navigation settings and navigation control algorithm were imported into the cyber space for simulation validation tests. Regarding the terrain change, before the tractor of DT system enters the field (including U-turn) and when doing headland turning, the ground is closer to asphalt ground so that the steering correction is performed using Eq. (9). When the tractor of DT system is following two straight paths within the field, since the ground is soil, the steering correction is performed using Eq. (10).

The trajectory results of the real navigation plan are shown in Fig. 3.7. As presented in Fig. 3.7 (a), The trajectories in the cyber space overlap well with those in the physical space, proving that the proposed DT system can well reproduce the navigation plan in physical space of real production. Fig. 3.7 (b) shows the trajectory results of the headland turning part. Since there is a soil slope at this location, when the tractor climbs the slope and turns at the same time, the soil slope will deform when the tires interact with the slope, causing a large deviation between the tractor trajectory and the ideal arc. However, in the proposed DT system, the terrain cannot perform real-time deformation, so the trajectory of DT system is a relatively ideal and clean arc. Although the difference between DT and physical space during headland turning is worse than that in the step response test, the virtual tractor of the DT system can still successfully complete the headland turning and enter the second path with a very close initial offset error like in physical space.

To conduct quantitative analysis for the real navigation experiment, navigation errors of the two straight paths within the field are summarized and shown in Table 3.4. From the results in the table, the navigation errors in cyber space and physical space are very close, with the average lateral errors difference being 2 cm and 0.4 cm respectively, and the average heading difference being 0.2° and 0.14° respectively. Such results prove that in terms of trajectory accuracy, the proposed DT can reproduce the navigation plan for agricultural production in physical space accurately.

Table 3.4. Navigation error statistics of the two paths during real navigation test

Error type			Physical space	Cyber space
Path 1	Lateral Error	Maximum	13.9 cm	12.9 cm
		Average	3.2 cm	5.2 cm
	Heading Error	Maximum	3.6°	3.8°
		Average	0.79°	1.49°
Path 2	Lateral Error	Maximum	11.7 cm	7.8 cm
		Average	2.7 cm	2.3 cm
	Heading Error	Maximum	2.8°	2.2°
		Average	0.66°	0.52°

Finally, the relationships between projection distance on the navigation path and the time spent are discussed. The projection distance means the distance from the real-time projection point of the tractor on the navigation path to the starting point of this straight path, which is used to evaluate the longitudinal movement accuracy of the tractor. The change of the projection distance during the two straight navigation paths are shown in Fig. 3.8. Overall, the projection distances of the virtual tractor and the real tractor are very close. In order to observe their difference more clearly, at each moment, the projection distance of the virtual tractor is subtracted from the projection distance of the real tractor to obtain a projection distance difference. This projection distance difference will slowly accumulate over time. According to the results from the two paths, the longitudinal error is approximately between 1-1.5m every 120s of moving. The inability to eliminate the longitudinal accumulated error is considered to be one of the limitations of the proposed DT system.

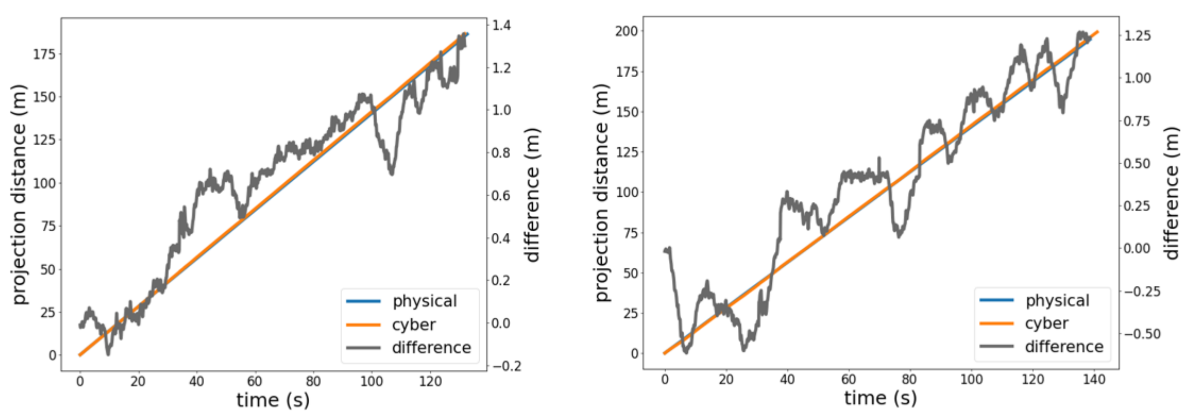

(a) Path 1 **(b) Path 2**

Fig. 3.8. Change of the projection distance during the two straight navigation paths

3.5. Conclusions

To validate the feasibility and accuracy of the proposed DT solution, three types of field experiments: step response test, zigzag test and real navigation test, were conducted to compare with the results between cyber space and physical space. The following advantages have been validated in this chapter through field experiments:

(1) The proposed steering system simulator, which is a sub-system of the proposed DT solution, has been validated to have better ability to precisely simulate a tractor's steering behaviors compared with traditional steering simulation method simply using first-order delay system. This is an important contribution for the effectiveness of the proposed DT solution.

(2) Validation results of both step response test and real navigation test prove the feasibility and effectiveness of the proposed DT solution to reproduce accurate agricultural machinery motion state of an agricultural production plan in cyber space.

Based on the advantages of the above abilities, the proposed DT solution shows strong potential to be further applied in the applications of agricultural machinery feasibility pre-validation, work schedule optimization, and remote farm management. However, the proposed DT system was also verified to have two major limitations: (1) Errors would accumulate quickly when controlled in open loop (2) The correction formula for turning radius may fail when non-linear side-slip occurs.

CHAPTER 4. NON-LINEAR IMPROVEMENT ON THE TRACTOR MODEL FOR SIDE-SLIP SIMULATION

4.1. Introduction

As verified in Chapter 3, one of the limitations of the proposed DT system is that it cannot cope with large side-slips during the operation. Unlike urban roads, the ground supporting the movement of agricultural vehicles is mainly composed of soil, which can be easily deformed. The hardness of soil is related to various factors, such as the soil type, moisture, and salinity, and soil conditions have large spatial heterogeneity, resulting in a wide range of road condition changes for agricultural vehicles.

Although tire interaction simulator mentioned in Chapter 2 is proposed to deal with this issue, When the peculiarities of the agricultural environment are more prominent, such as the soil becoming wetter and softer, the relationship between the tire lateral force and the tire side-slip angle will follow a non-linear tendency, which will cause the tire interaction simulator and basic tractor model to be less accurate. To solve this problem, the basic tractor model is improved to be a non-linear model, to make the simulation more practical to be applied under extreme agricultural environments, such as muddy field that are prone to cause large side-slips.

4.2. Side-slip Vehicle Model Construction

In this section, the model construction methodology of the non-linear model simulating side-slip is explained. The proposal for this non-linear dynamic model includes two steps. First, the lateral force estimation method is built up by combining a simplified non-linear tire model and side-slip angle estimation method. Then, based on the lateral force estimation, a non-linear tractor model is proposed and simulated in cyber space using 3D physics engine.

4.2.1. Lateral force estimation

To analyze the side-slip condition of a wheeled vehicle, the tire lateral force should be estimated first. Fig. 4.1 shows a schematic of the lateral force analysis. First, the side-slip angle is estimated based on a typical bicycle model. The bicycle model assumes that the wheels are always perpendicular to the ground and only move horizontally. The vehicle control in the bicycle model is same as the proposed tractor model mentioned in Chapter 2: $C = [\delta, T]^{\mathrm{T}}$, where δ represents the steering angle of the vehicle, and T represents the torque of the vehicle engine. In addition, the vehicle model proposed in this study is only for field without obvious slopes, and it is assumed that the agricultural vehicle is moving with a fixed target speed and does not have a very high towing load, such as pulling extremely heavy equipment or agricultural implements with great resistance. Under this kind of condition, the variation range of forward velocity can be regarded as relatively small and limited. Thus, only the lateral force and side-slip of the vehicle are considered in the proposed vehicle model.

Fig. 4.1(a) shows a schematic of the bicycle model. For the front wheel, the front side-slip angle α_f can be expressed as

$$\alpha_f = \tan^{-1}\left(\frac{v_y + l_f r}{v_x}\right) - \delta \tag{4.1}$$

where v_x and v_y represent the longitudinal and vertical velocity of the vehicle body, r represents the angular velocity of the vehicle body around the center of mass, and l_f represents the distance between the center of the front wheel and the center of mass.

For the rear wheel, the rear side-slip angle α_r can be expressed as

$$\alpha_r = \tan^{-1}\left(\frac{v_y - l_r r}{v_x}\right) \tag{4.2}$$

where l_r represents the distance between the center of the rear wheel and the center of mass.

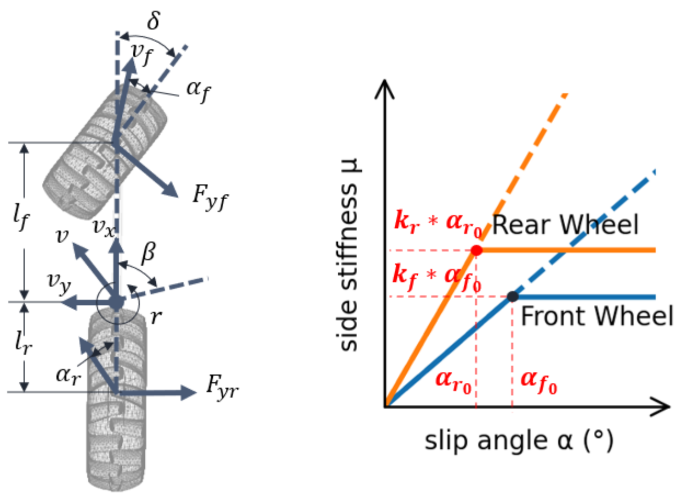

(a) bicycle model **(b) non-linear tire model**

Fig. 4.1. Lateral force estimation for tires

According to Pacejka's Magic Tire model (Pacejka and Bakker, 1992), the relationship between the tire side-slip angle and the lateral force can be expressed by fitted formulas with proper coefficients. In the fitted curve, when the side-slip angle is relatively small, there is a linear relationship between the slip angle and the tire lateral force. As the side-slip angle continues to increase, the growth trend of the lateral force gradually slows down and finally reaches the maximum lateral force value. Typically, the value of the maximum lateral force is determined by the vertical load on the tire and the friction stiffness between the tire and the ground. After that, as the side-slip angle increases, the lateral force will decrease slightly and eventually remain constant. The traditional linear dynamic model (Snider, 2011) only considers the linear part of the relationship between the side-slip angle and lateral force, assuming that the side-slip angle is always very small during vehicle motion. However, in the actual agricultural environment, the side-slip angle is sometimes quite large since there is a wider range of road condition changes compared with paved roads for cars. Therefore, in this study, the complete relationship between slip angle and lateral force is considered even when the side-slip angle is quite large.

Considering that the parameters in Pacejka's Magic Tire model are very complex, it is difficult for researchers or engineers to use that model if they do not have professional evaluation equipment to accurately measure the parameters. In order to make the non-linear tire model more convenient to use in the field of agricultural machinery, and also preserve the non-linear relationship between the side-slip angle and lateral force as much as possible, the non-linear relationship is simplified in this study.

Fig. 4.1 (b) provides a schematic of the non-linear tire model. Assuming that the vehicle body always remains perpendicular to the ground when in motion, the vertical load on each tire also remains unchanged. Therefore, in this model, the lateral friction stiffness μ can be used to represent the lateral force. Before reaching the maximum value of the lateral friction stiffness, the relationship between the slip angle and lateral friction stiffness is linear. After reaching the maximum value, the lateral friction stiffness stays unchanged even if the slip angle continues to increase. Additionally, the front wheels and rear wheels should have different model parameters, since the front wheels of agricultural vehicles usually have different size and weight than the rear wheels.

In the proposed non-linear tire model, for the front tire the relationship between side friction stiffness μ_f and side-slip angle α_f can be expressed as:

$$\mu_f = \xi(\alpha_f) = \begin{cases} k_f * \alpha_f & \alpha_f \le \alpha_{f_0} \\ k_f * \alpha_{f_0} & \alpha_f > \alpha_{f_0} \end{cases} \tag{4.3}$$

where α_{f_0} represents the maximum value of the side-slip angle α_f during the linear part, and k_f represents the slope of the linear curve.

For the rear tire model, the relationship between side stiffness μ_r and side-slip angle α_r can be expressed as:

$$\mu_r = \xi(\alpha_r) = \begin{cases} k_r * \alpha_r & \alpha_r \le \alpha_{r_0} \\ k_r * \alpha_{r_0} & \alpha_r > \alpha_{r_0} \end{cases} \tag{4.4}$$

Similarly, α_{r_0} represents the maximum value of the side-slip angle α_r during the linear part, and k_r represents the slope of the linear curve. In this way, based on the physical parameters and the state condition of the vehicle during movement, the lateral force of the front and rear tires can be estimated at each time stamp.

4.2.2. Simulation framework

During the simulation in Unity virtual space, the physical states of the tractor model, would be updated by the Unity built-in physics engine, which is called PhysX. The virtual 3D vehicle model is defined as a parent object named 'Tractor', with a set of virtual wheels 'WheelControl'. Among them, 'lrc' stands for left rear wheel, 'rrc' stands for right rear wheel, 'rfc' stands for right front wheel, and 'lfc' stands for left front wheel. At each time stamp, the side-slip angle will be estimated according to Eq. (4.1) and (4.2), and then the side stiffness will be calculated according to Eq. (4.3) and (4.4).

The virtual sensing system is responsible for getting state information of the vehicle at each time stamp. Firstly, the global position coordinate of the vehicle (x,y) and the heading angle φ are directly obtained through C# API provided by Unity physics engine. Since the focus of this chapter is to simulate and validate the side-slip behavior mode of the virtual vehicle, artificial sensor noise is not intentionally added to the raw data. Then, to estimate the side-slip angle according to Eq. (4.1) and (4.2), v_x, v_y and r are calculated based on the directly obtained (x,y) and φ. For v_x and v_y, the velocity vector v is first estimated by differentiating vehicle position (x,y) of two adjacent frames, and then the longitudinal and lateral components of v are calculated based on the angle between velocity v and heading angle φ. For angular velocity r, it could be calculated by differentiating vehicle heading angle φ of two adjacent frames as well. Additionally, the simulation frame rate is fixed at 60 Hz, so the time interval between two adjacent frames is 0.0167 s. l_f and l_r are specification parameters of the defined virtual vehicle. δ is an input controlled by navigation algorithm or manually steering. In the programmed vehicle model script, steering angle δ is achieved by directly change the horizontal posture of the wheel colliders through physics engine's API.

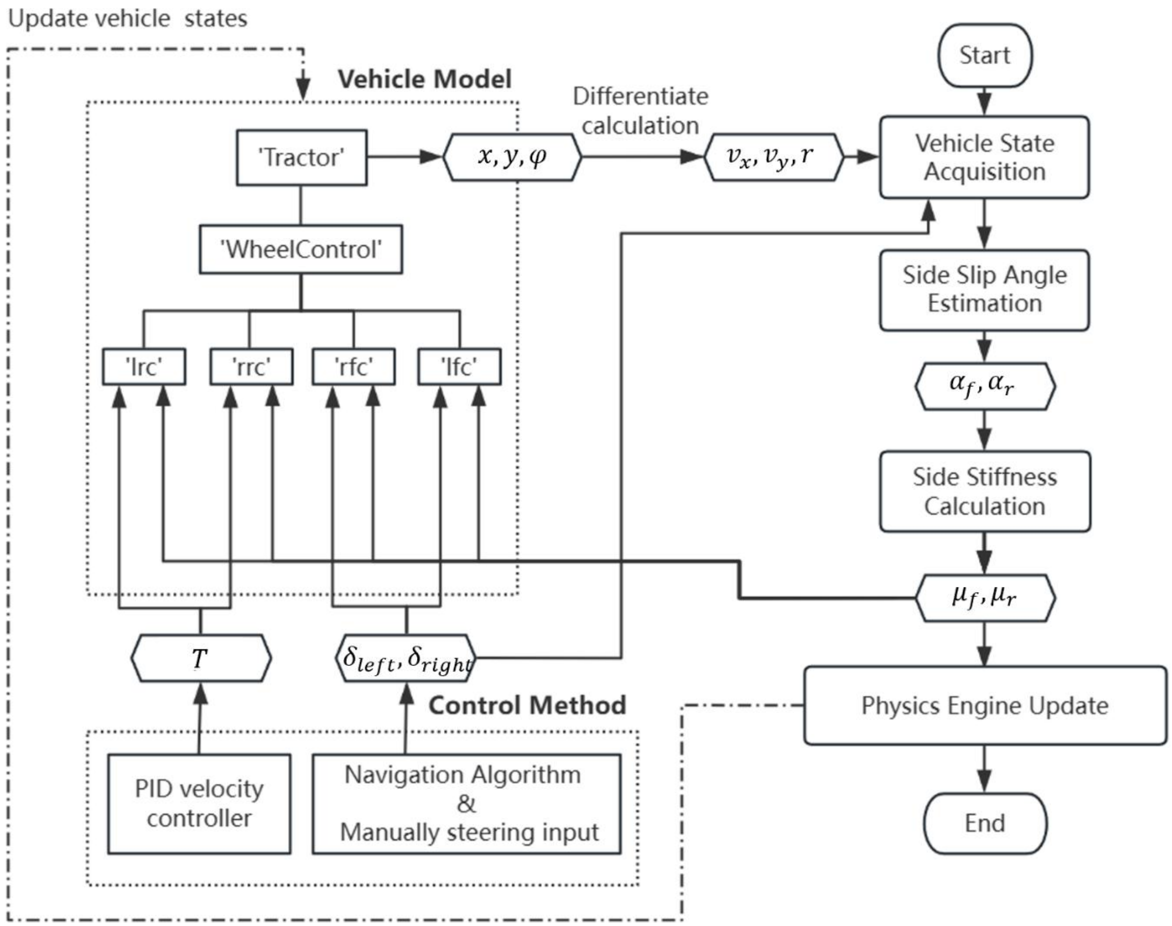

Fig. 4.2. The overall framework of the vehicle model simulation process

After calculations for equations Eq. (4.1) and (4.2), the side stiffness results μ_f and μ_r are given to the front (attached to ‘rfc’ and ‘lfc’) and rear (attached to ‘rrc’ and ‘lrc’) wheel colliders directly through physics engine’s API, respectively. At the same time, the torques of two rear wheels are also calculated based on the PID controller mentioned in Chapter 2, and then input to the corresponding wheel colliders through API, respectively. Finally, according to the constructed non-linear vehicle model in Unity, including all the parameter specifications, the vehicle state will be continuously updated. Regarding the accuracy of the virtual sensing system, the raw state data obtained directly from physics engine’s API can be regarded as absolutely correct without any intentionally added sensor noise. The overall framework of the vehicle model simulation process is shown in Fig. 4.2.

4.3. Pre-validation Tests in Cyber Space

To pre-validate the performance and potential of the proposed non-linear dynamic model, pre-validation experiments were conducted in cyber space. These experiments were also conducted for the kinematic model and traditional linear dynamic model for purposes of comparison, as shown in Fig. 4.3.

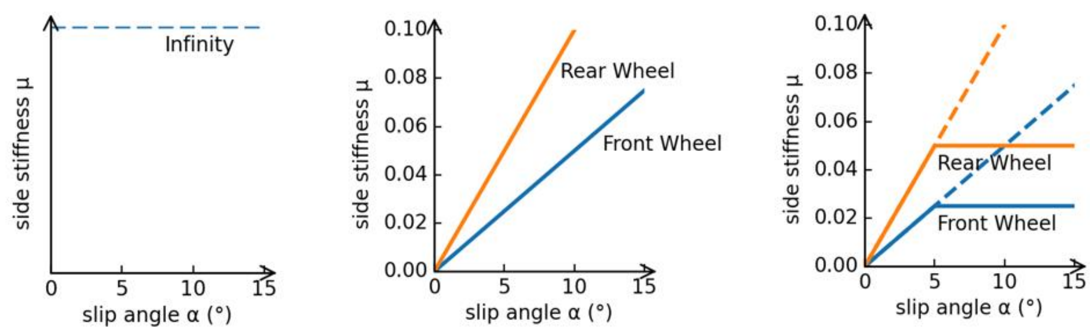

(a) Kinematic model (b) Linear dynamic model (c) Non-linear dynamic model

Fig. 4.3. Vehicle models tested in the pre-validation experiments

The kinematic model can be regarded as being able to provide infinite lateral force to quickly eliminate the instantaneous side-slip angle. Therefore, in the kinematic model the side stiffness is set to a very large constant value and will not be influenced by side-slip angle. The linear model provides the lateral force based on a linear relationship with the side-slip angle. Considering that the rear wheels of agricultural vehicles usually have larger size and weight than the front wheels, the tire model slope of the rear wheels is set to be larger than that of the front wheels. For the linear dynamic model, the relationship between side stiffness and side-slip angle can be expressed as: $(k_f = 0.005,\ k_r = 0.01)$. The non-linear dynamic model has a limitation of the side stiffness value compared with linear model. Fig. 4.3 (c) shows an example of a non-linear model to be tested. The relationship between side stiffness and side-slip angle can be expressed as: $(\alpha_{f0} = 5°, k_f = 0.005, \alpha_{r0} = 5°, k_r = 0.01)$.

4.3.1. Fixed steering tests

To validate the performance of the proposed non-linear model under constant steering angle input, we first conducted fixed steering tests. Three different values of steering angles were input as step signal, which means the steering angle changed from 0° to the expected angle immediately. The input of the steering angles is shown in Fig. 4.4.

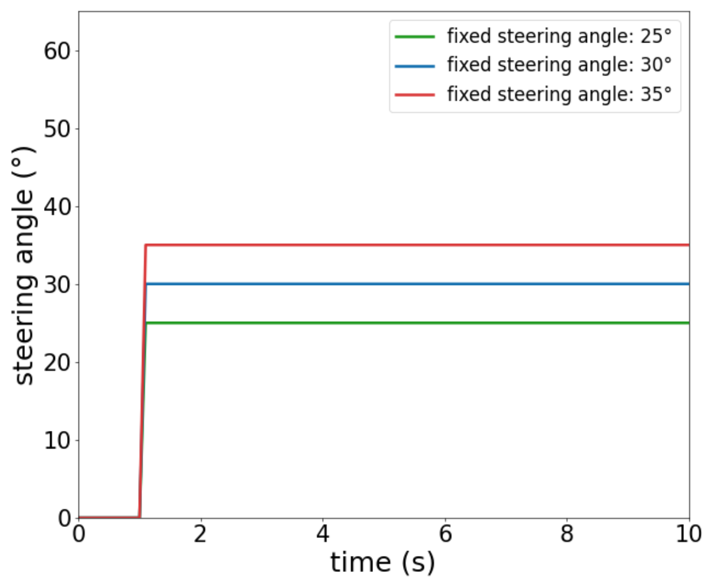

Fig. 4.4. Steering input in fixed steering tests

The trajectory result of the fixed steering tests is shown in Fig. 4.5. It can be seen that the trajectories of both the kinematic model and the linear dynamic model are standard circles, which means the turning radius of these two models is stable under a fixed steering angle input. However, when the steering angle increases to 35°, the trajectory of the non-linear model is no longer a standard circle but a curve with increasing curvature, indicating that the vehicle's turning radius continues to change. The irregular trajectory pattern implies the non-linearity of the proposed non-linear model. This phenomenon is consistent with the tractor oversteer in real space, proving that the proposed non-linear model has the potential to be out-of-control even if the steering angle input is unchanged.

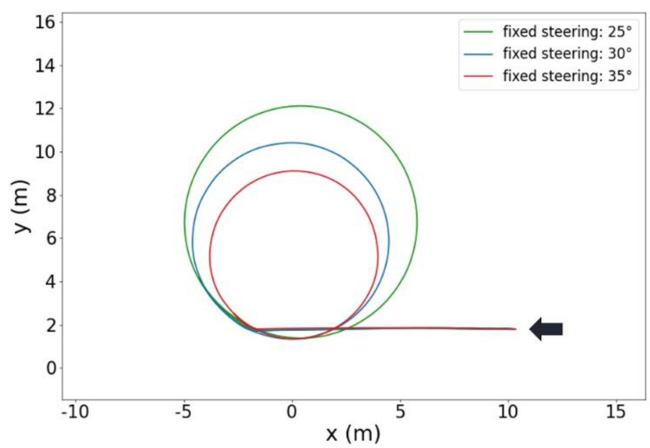

(a) kinematic model

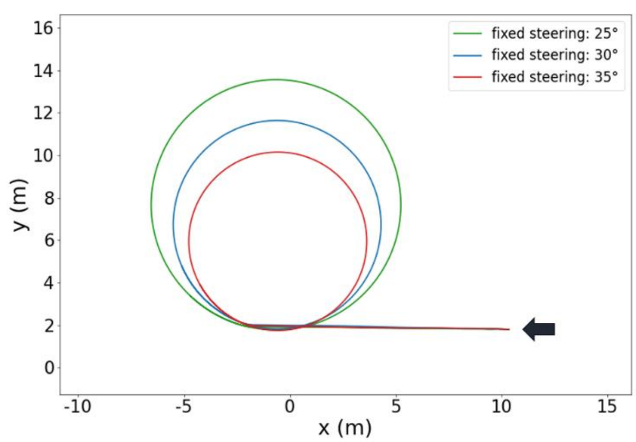

(b) linear dynamic model

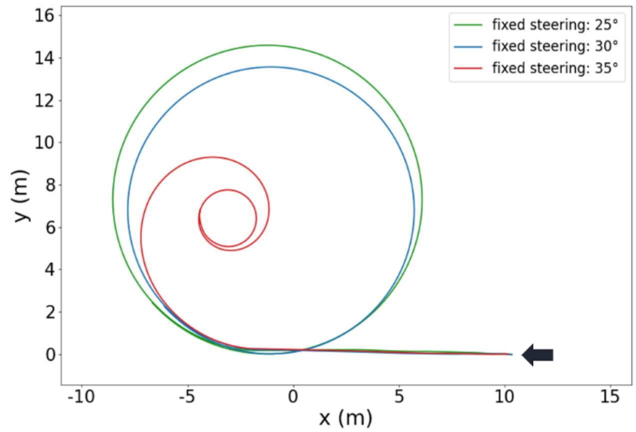

(c) non-linear dynamic model

Fig. 4.5. Trajectory result of the fixed steering tests

Table 4.1 shows the turning radius of each model under different steering angle input. It is evident that as the input steering angle increases, the turning radius decreases for all models, except the oversteer case of the non-linear model. This result is consistent with common sense in real space, and proves the accuracy of the three simulated models and the constructed vehicle model in 3D cyber space. Moreover, under the same steering angle input, the non-linear model has the largest steering radius, followed by the linear model, and the kinematic model has the smallest turning radius. This proves that under the same steering angle input, the non-linear model has the largest side-slip, followed by the linear model, while the kinematic model has almost no side-slip. Finally, it is worth mentioning that the turning radius difference between the non-linear model and the linear model is much larger than the difference between the linear model and the kinematic model, which means that even with the same tire model slope, the effect of the non-linear model will be significantly different from that of the linear model.

Table 4.1. Turning radius of each model under different steering angle input

Steering Input	Kinematic Model	Linear Dynamics Model	Non-linear Dynamics Model
25°	5.36 m	5.89 m	7.30 m
30°	4.53 m	4.92 m	6.79 m
35°	3.88 m	4.19 m	oversteer

To further discuss the unstable condition of oversteer, the side-slip angle change of the non-linear model under 35°fixed steering is investigated and compared with that of linear model, as shown in Fig. 4.6. According to Fig. 4.6 (a), the front slip angle has a sharp increase just after the step steering input and then gradually declines, while the rear slip angle responds to the step steering input more slowly than the front one. Although both front and rear slip angles increase due to the steering input, they are converged within 2s and remain stable since the linear model could continuously increase the lateral force as the slip angle increases. However, according to Fig. 4.6 (b), both front and rear side-slip angles of the non-linear model cannot be converged under 35° fixed steering. After the step steering is input, the initial situation is very similar to that of linear model, the front slip angle increases instantly and then gradually decreases. The difference is that the non-linear model cannot continuously increase the lateral force. When the lateral force reaches the maximum value but is still not enough to stabilize the vehicle body, the rear slip angle continues to increase. Under this condition, the rear slip angle will exceed the front slip angle, and the turning radius of the vehicle decreases rapidly, showing oversteer or even spin. This process proves that the proposed non-linear models can estimates the change of the sideslip angle to simulate unstable vehicle behaviors such as oversteer.

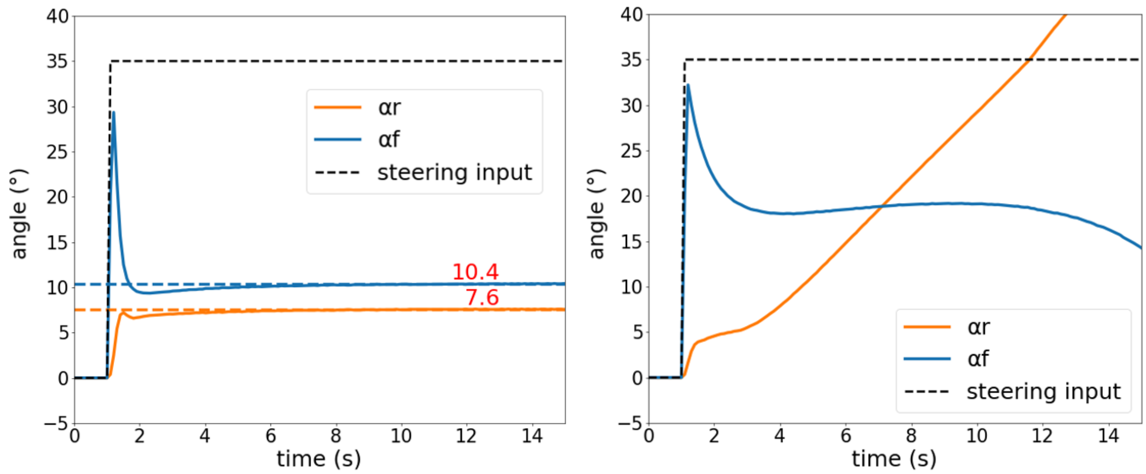

(a) Linear model **(b) Non-linear model (Oversteer)**

Fig. 4.6. Side-slip angle change during 35° fixed steering tests

4.3.2. Continuously changing steering tests

In the previous test, the expected steering angle was input as a fixed step signal. In this test, to further validate the proposed non-linear model performance under changing steering angles, the input is set to vary according to a trigonometric function of a fixed frequency. The time sequence of the input steering angle is shown in Fig. 4.7. To better evaluate the differences between different vehicle models, same as fixed steering tests, the proposed non-linear model with parameters ($\alpha_{f0} = 5°, k_f = 0.005, \alpha_{r0} = 5°, k_r = 0.01$), was tested and compared with the kinematic model and linear dynamic model with parameters ($k_f = 0.005, k_r = 0.01$) .

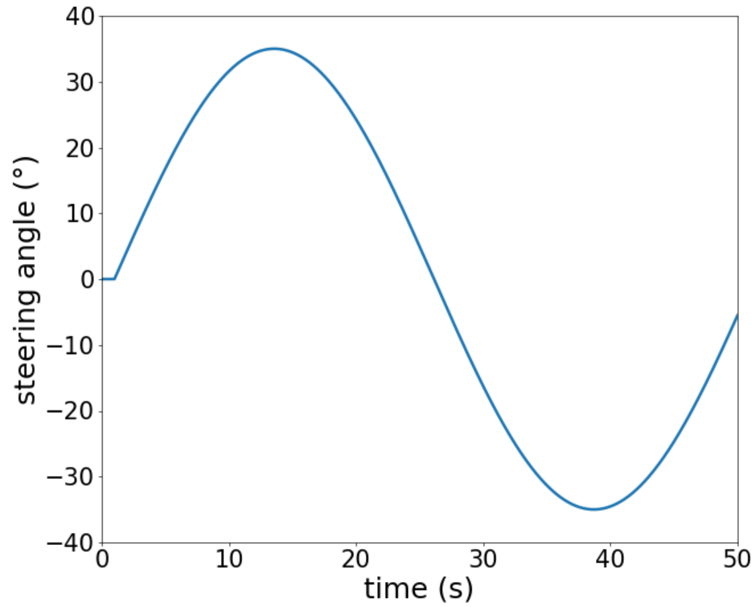

Fig. 4.7. Continuously changing steering input

The trajectory results of three models under continuously changing steering input are shown in Fig. 4.8. It can be estimated that the trajectories of the kinematic model and the linear model share the same geometric patterns, with only the geometric parameters being different. This indicates that the difference in simulation results between the linear model and the kinematic model is only the turning radius caused by stable slip during steering, while the trajectory patterns are always consistent in terms of geometry. However, the trajectory's geometric pattern in the proposed non-linear model shows irregularity, which suggests that the turning radius of the non-linear model is not stable. As the steering angle increases, spin may occur and thereby cause the heading angle to change dramatically, which proves the non-linearity of the proposed model.

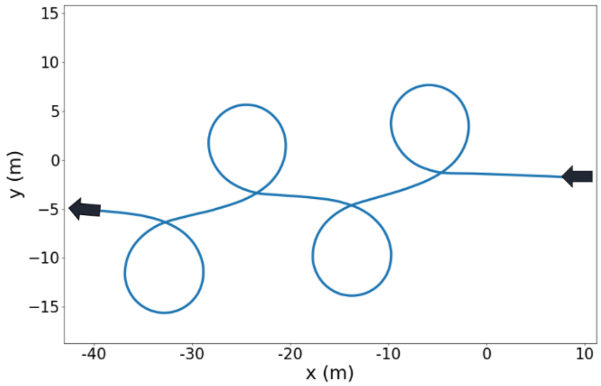

(a) kinematic model

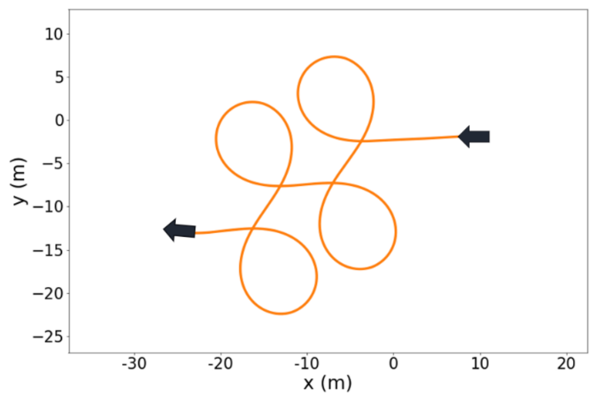

(b) linear dynamic model

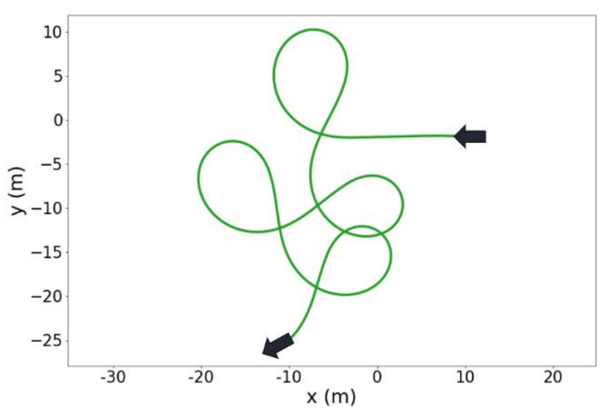

(c) non-linear dynamic model

Fig. 4.8. Trajectory result of the continuously changing steering test

4.4. Validation through Field Experiments

In the previous section, the non-linearity of the proposed model has been pre-validated based on the comparison with traditional models in cyber space. However, the steering inputs follow relatively simple rules, while under real-world conditions the steering angle input may not exhibit such a clear pattern. One common case is that the vehicle is always controlled to follow a desired path manually or automatically. Besides, to better validate the model ability of simulating a real tractor status, comparison with experimental data from a real tractor is necessary. Therefore, in this section the performance of the proposed non-linear model was tested under automatic control to follow a desired path and the test results were also compared with those of real-world field experiments to verify the accuracy and effectiveness of the proposed model. At the same time, the linear model was also tested for comparison to evaluate the features and advantages of the proposed non-linear model, while the kinematic model would not be compared in this section because its ability to simulate real-world trajectories is generally considered inferior to that of the dynamic linear model.

In order to fully validate the effectiveness of the non-linear model under various road conditions, we selected two scenarios that represent two boundary cases for real-world experiments and utilized the proposed model to simulate and reproduce this navigation process in cyber space. The locations for these two scenarios are exactly the same as the soil and asphalt ground validation experiments in Chapter 3. The two real-world experiment scenarios and corresponding simulation scenarios are shown in Fig. 4.9.


(a) Asphalt road **(b) Muddy field**


(c) Asphalt road in cyber space **(d) Muddy field in cyber space**

Fig. 4.9. Real-world field validation experiments on two different grounds

The first experimental scenario is located in the parking lot of Hokkaido University. This area is very flat and paved with asphalt, which is considered as being able to provide very strong lateral force to prevent the tractor from side-slips. Thus, the experiment on asphalt road is to verify the simulation accuracy of the proposed model when the vehicle side-slip is very small and even close to zero. The second scenario is located at the experimental field of Hokkaido University. In contrast to the first scenario, in order to verify the effectiveness of the proposed model in the case of large side-slip, the second experiment was conducted in a muddy field after rain. The tractor used for both experiments was Yanmar EG105 which has already been mentioned in Chapter 2, with all onboard settings identical. The navigation desired path is exactly the same for both experiments, which were trigonometric curves with a half period of 18.8 m and an amplitude of 5 m. Besides, the steering control algorithm (Kise et al., 2001), the vehicle setting speed (fixed at 5 km/h) and parameter of look ahead distance (1.8 m) used in all experiments, including simulation in cyber space, were also exactly the same.

Table 4.2. Cone Index Statistics of 10 points within the muddy experimental field

Statistics	Cone Index (kg/cm^2)
Maximum	3.1
Minimum	0.8
Average	1.55
Variance	0.45

For paved asphalt condition, the surface material is relatively standardized, so it is considered to be sufficient as an experimental environment reference. According to our testing experience, the model parameters for the non-linear model and linear model for asphalt roads are set as: $(\alpha_{f0} = 5°, k_f = 0.15, \alpha_{r0} = 5°, k_r = 0.2)$ and $(k_f = 0.15,\ k_r = 0.2)$, respectively. However, muddy field environment is more complex and it's difficult to provide an accurate definition. Thus, we evenly picked up 10 points near the desired path in the field, and measured the Cone Index, which is used as the measure of soil strength in the traction equations (Goodin and Priddy, 2016), as mentioned in Chapter 3. The measured statistical results of the 10 points within the muddy experimental field are shown in Table 4.2, which could be regarded as a reference of the muddy field condition tested in this research. Regarding the model parameters for this muddy field condition, based on testing experience, both α_0 and k should be greatly reduced to simulate the weak lateral force from muddy soil. Therefore, the model parameters for the non-linear model are set as: $(\alpha_{f0} = 2°, k_f = 0.03, \alpha_{r0} = 2°, k_r = 0.04)$. Considering that the lateral force of the linear model can continue to increase as the side-slip angle becoming large, with same slope parameter k, the side-slip amount of linear model must be smaller than that of the nonlinear model, which will weaken the significance of the comparative experiment. For a more objective comparison, the slope k of the linear model is set to be slightly smaller than that of the nonlinear model, and the parameters of linear model are set as: $(k_f = 0.0225,\ k_r = 0.03)$.

The navigation error statistics of both asphalt road and muddy field validation experiments are shown in Table 4.3. The average lateral errors of real asphalt experiment, non-linear model and linear model are 0.107 m, 0.106 m and 0.101 m, respectively, while the average heading errors are 7.86°, 7.87° and 7.82°, respectively. It is obvious that during the validation experiments on the asphalt road, both lateral errors and heading errors of real experiment, non-linear model and linear model are very similar. For the validation experiments of muddy field, however, the non-linear model and linear model perform great difference. The average lateral errors of real experiment and the non-linear model are 0.167

m, and 0.163 m, respectively, which are significantly different from that of linear model. In terms of heading error, although the maximum and average values of the non-linear model are slightly larger than those of the real muddy field experiment, but still closer to the actual tractor's data than the linear model. In conclusion, from Table 4.3, both non-linear model and linear model can accurately estimate the maximum and average error level of a real tractor for asphalt condition. However, under muddy field environment as tested in this research, the simulation accuracy of the non-linear model has significant advantages over that of the linear model.

Table 4.3. Navigation error statistics of asphalt road and muddy field validation experiments

Error type			Real Experiment	Non-linear Model	Linear Model
Asphalt Road	Lateral Error	Maximum	0.207 m	0.203 m	0.201 m
		Average	0.107 m	0.106 m	0.101 m
	Heading Error	Maximum	15.68°	15.67°	15.44°
		Average	7.86°	7.87°	7.82°
Muddy Field	Lateral Error	Maximum	0.372 m	0.369 m	0.271 m
		Average	0.167 m	0.163 m	0.122 m
	Heading Error	Maximum	22.3°	23.5°	20.2°
		Average	9.12°	9.70°	8.38°

To further evaluate the detailed performance of the proposed non-linear model and the linear model, navigation errors change during both validation experiments are collected and shown in Fig. 4.10. For the validation experiments of asphalt road, both linear model and the proposed non-linear model perform very close to the real tractor. The changing trends of lateral error and heading error of the two models can accurately simulate the states of the real tractor, with almost no time phase difference. This proves that both non-linear model and linear model can be used to accurately estimate the real-time state of the real tractor, which is moving on asphalt road.

However, for the validations experiments of muddy field, there is a big difference in the performance of the non-linear model and the linear model, which is consistent with the result of Table 4.3. The linear model is not capable to well estimate the maximum and average error of the real tractor under muddy environment, and there is also a very obvious phase difference. In contrast, the proposed non-linear model can not only approximate the maximum error more precisely, but also keep pace with the error state changes of the real tractor. This indicates that the side-slip simulation mechanism of the non-linear model is closer to the real situation. One point worth noting is that the estimation of the non-linear model may sometimes be minor different from states of the real tractor, such as the downward trough shown in Fig. 4.10 (c) around the beginning stage. One possible reason it that the model parameters of the non-linear model are static, while the soil parameters in reality have sufficient temporal and spatial differences. To achieve better comprehensive simulation results, we recommend to tune the non-linear model parameters based on the average soil status of the field. Another possible reason is that the steering system of the real tractor is asymmetric, while in simulation the virtual steering system is perfectly symmetrical.

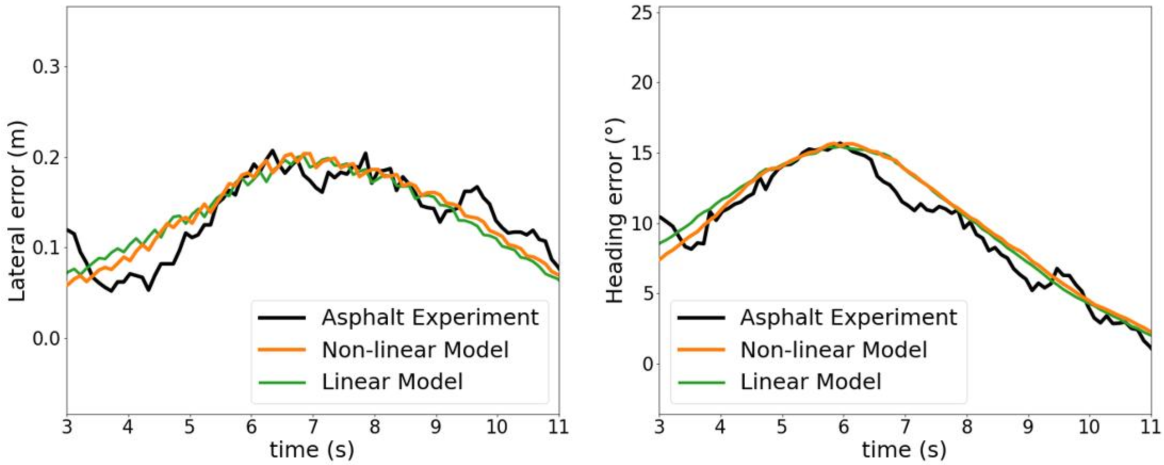

(a) Lateral error change of asphalt road test (b) Heading error change of asphalt road test

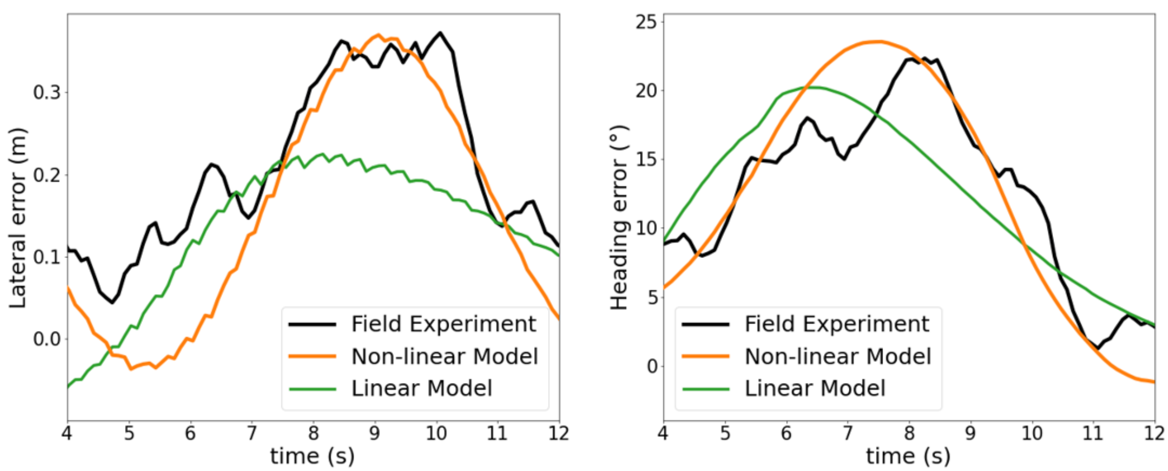

(c) Lateral error change of muddy field test (d) Heading error change of muddy field test

Fig. 4.10. Navigation errors change during real-experiments validation

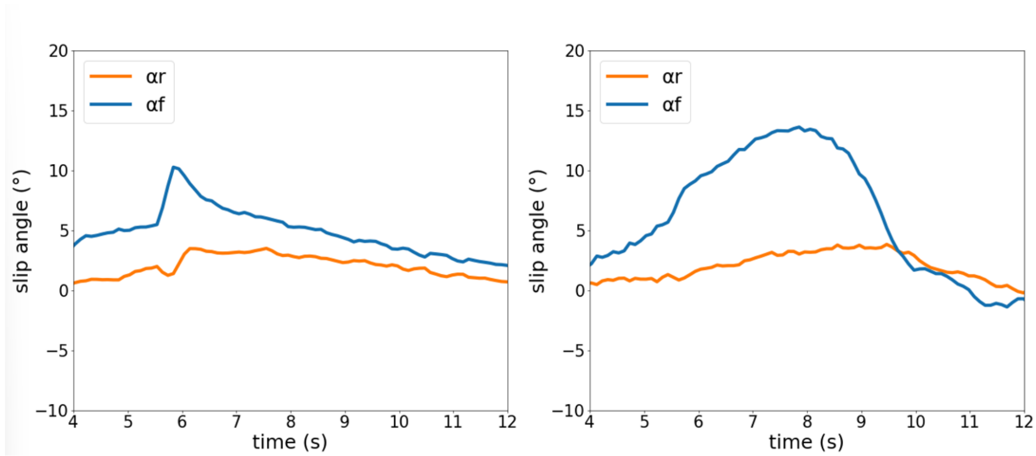

(a) Linear model **(b) Non-linear model**

Fig. 4.11. Side-slip angle change during the validation experiment for muddy field

Finally, in order to further reveal the reason of the superiority of the non-linear model over the linear model in muddy environments, the side-slip angle change during validation experiments, as shown in Fig. 4.11, is analyzed. The side-slip angle change patterns of the non-linear model and the linear model are clearly different. When the time is approaching 6s, there is a slip angle increase of the front wheel that maybe caused by a suddenly increased steering angle as the desired path curvature also increased. Obviously, for the linear model, the high value of the front wheel slip angle can only be maintained for a short time, and then it quickly falls back and always remains at a position close to the rear wheel slip angle. This suggests that the vehicle posture of the linear model is relatively stable, explaining the smaller average heading error, as shown in Table 4.3. In contrast, the front wheel slip angle of the non-linear model will slowly but continuously increase until it reaches the maximum value and then quickly falls back. This slip angle change process will last for a longer time than that of linear model. This characteristic of the non-linear model is due to the limitation of the maximum lateral force in the model. When the slip angle is greater than 2°, the lateral force will no longer increase, resulting in a large difference between front slip angle and rear slip angle and thereby cause a larger vehicle posture change than linear model. The vehicle body can only return to a stable state naturally as the steering input changes.

According to the validation results from real-world experiments, the proposed non-linear model can accurately simulate the tractor state for both asphalt condition and muddy field condition, performing a wider range of environmental adaptability than traditional linear model. The validation tests also prove that by simply adjusting the parameters of the proposed non-linear model, different working scenarios can be matched, which is a big advantage in coping with the changing agricultural environments.

4.5. Conclusions

This chapter proposed a non-linear dynamic model for simulating side-slip of agricultural vehicles in cyber space. According to the validation tests in the constructed cyber space and real-world experiments on two extreme grounds, it has been proved that the model can be successfully used to simulate the performance of agricultural vehicles under various conditions. The conclusions for the proposed non-linear model abilities are as follows:

(1) The proposed non-linear model is accurate. Even though the proposed non-linear tire model parameters are simplified compared with the traditional magic formula of non-linear tire model, still, the proposed model is validated by real experiments to be capable of simulating the vehicle states of a real tractor with acceptable accuracy.

(2) The proposed model can be adapted to different environments. Compared with traditional linear model, the proposed non-linear model has a wider range of environmental applicability. It can more accurately simulate the states of agricultural vehicle under various agricultural environments, including those soil conditions that may cause large side-slips.

(3) The proposed non-linear model has a solid practicality. It can be applied to different working environments just by adjusting simple model parameters, which is a big advantage in coping with the changing agricultural environments.

Based on the advantages of the above abilities, the proposed non-linear model can assist in improving the accuracy of the proposed DT system in extreme ground conditions.

CHAPTER 5. DEVELOPMENT OF ONLINE COMMUNICATION SYSTEMS FOR CYBER-PHYSICAL SYNCHRONIZATION

5.1. Introduction

According to the limitations verified in Chapter 3, during the offline operation of the proposed DT system, trajectory errors between cyber space and physical space may continue to accumulate. These errors are mainly caused by two following reasons: (1) tractor model difference between cyber and physical. (2) dynamic environment changes such as soil wetness and soil deformation. In fact, trajectory error is a kind of lateral control error, ignoring the longitudinal differences. Therefore, in most cases, the closed-loop steering controller can eliminate this error and keep it within an acceptable range. However, even with a closed-loop steering controller, short-term open-loop control may still occur in some extreme cases. For example, when the steering angle has reached its maximum value and maintained for a period of time, the closed-loop steering controller is actually presented in the form of open-loop control. If there is an initial trajectory error when entering open-loop control, this error will continue to accumulate over the time of open-loop control.

Besides, the closed-loop velocity controller only reduces the velocity error compared with target velocity, but cannot reduce the distance error between the virtual tractor and real tractor. Thus, longitudinal errors also accumulate over time. For the pre-verification of agricultural machinery operations for a real farm and the optimization of steering control strategies, a certain degree of error is acceptable. However, if we want to use the DT system for applications that require higher real-time performance, the accumulated errors will become a major obstacle. An existing solution to reduce errors between DT system and real system is to transmission real-world data in real time to cyber space (Angin et al., 2020; Skobelev et al., 2020). Therefore, this chapter introduces how to develop an online communication system, to synchronize cyber space and physical space without error accumulating.

5.2. Online Communication Methodolgoy

5.2.1. Development tool of communication system

To develop this communication system, WebSocket is utilized as a tool for data transmission. WebSocket is a computer communications protocol, providing a simultaneous two-way communication channel over a single Transmission Control Protocol (TCP) connection. Generally, compared with other communication systems or protocols, WebSocket has the following advantages:

(1) Real-time communication:

WebSocket provides a full-duplex, bi-directional connection, allowing the server to push data to the client without waiting for requests, and vice versa.

(2) Low latency:

WebSocket maintains a persistent connection, and minimizes the overhead of establishing a new connection for each data transfer, to achieve lower latency and fast response.

(3) Flexibility and scalability:

WebSocket supports a variety of data formats, including binary data, and can handle multiple simultaneous connections. This makes them suitable for a wide range of applications, including real-time media streaming.

Based on the above-mentioned advantages, a real-time communication system is constructed between virtual tractor and real tractor using WebSocket.

5.2.2. Communication system construction

The communication system is used to establish a data exchange bridge between the virtual tractor and the real tractor. As mentioned in Section 5.1, the communication system is an important support for realizing functions of both remote monitoring and remote controlling. Therefore, two types of communication framework are proposed for monitoring and controlling respectively, as shown in Fig. 5.1.

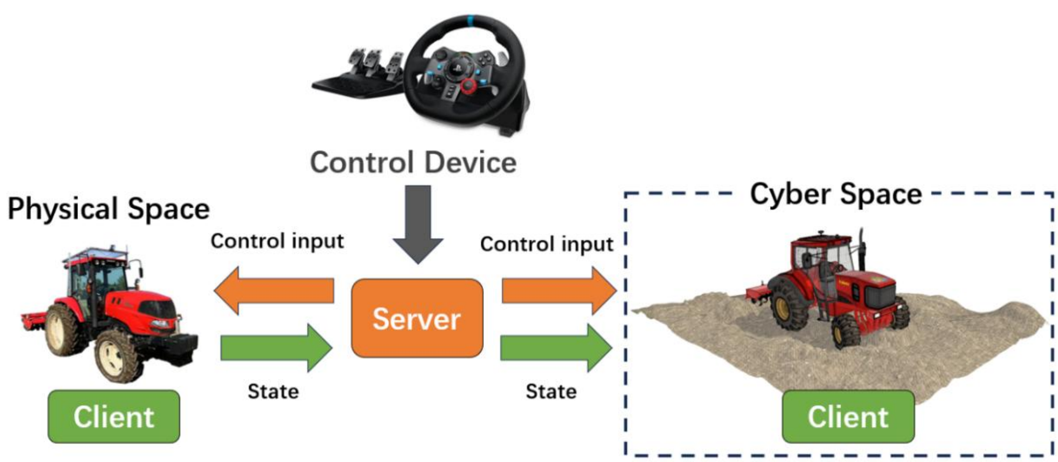

(a) remote controlling system

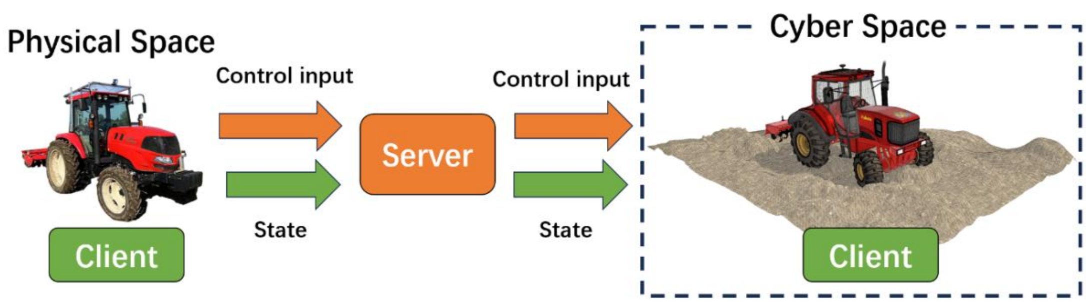

(b) remote monitoring system

Fig. 5.1. Framework of two types of systems using online communication

In the remote controlling system, there are two clients, representing the real tractor in physical space and the virtual tractor in cyber space. Logi G29 Gamepad is used as a control device for receiving manually steering inputs, and then transfer the steering inputs to the server. Through server, manually entered steering inputs are sent to both clients simultaneously. Besides, to synchronize physical space and cyber space, the server will obtain the real tractor state from the client in physical space, and send this data to the client in cyber space for state error correction. This synchronization direction is for safety reasons. The state of the virtual tractor in the cyber space is corrected to follow the real tractor to ensure that the real tractor moves in a more stable state.

In the remote monitoring system, since no human operation is involved, control input device is removed. Steering inputs are transmitted directly between the two clients, without the need for external input. Similarly, for safety reasons, the synchronization direction is that the virtual tractor state is corrected to follow state of the real tractor. Under this mode, server is more like an information transfer station between clients.

After the communication system structure is designed, the detailed data content transferred between server and clients should be decided. In this study, the data frame structure is defined as follows:

```
public class Cyber_Physical_Data
    {
        public string client_type;
        public float outputEasting;
        public float outputNorthing;
```

```
    public float outputHeading;
    public float outputVelocity;
    public float inputVelocity;
    public float inputSteering;
    public int inputShuttle;
    public bool start;
}
```

In the defined data frame, the string variable client_type is used to represent the client identification. Based on the string value of client_type, the server can recognize whether the connecting client is from physical space or cyber space. The float variables outputEasting and outputNorthing are the Universal Transverse Mercator (UTM) coordinate of the real tractor. Since the 3D model of terrain in cyber space has already been calibrated with GNSS information, through the conversion between UTM and GNSS coordinates, the real-time coordinate of the real tractor can be directly located in cyber space. The float variable outputHeading is the heading angle of the real tractor, which is used to correct the virtual tractor's heading direction. The float variables outputVelocity and inputVelocity are velocity command and real velocity of the real tractor, respectively. When the difference between outVelocity and inputVelocity is consistently higher than 0.5 km/h, the physical velocity controller of the real tractor may not be able to control the tractor to the input velocity command, and then the value of outputVelocity will be used as the input velocity command of the virtual tractor directly. The float variable inputSteering is the steering command from control device or output from the real tractor. The int variable inputShuttle is the shuttle of the real tractor. When the value of this variable changes from 0 to 1, the virtual tractor will start to turn on the PID velocity controller to calculate torque. The bool variable start is a switch to determine when to start both the real tractor and the virtual tractor.

Based on the above-mentioned communication system structure and data frame definition, remote controlling system and remote monitoring system are constructed.

5.2.3. State error correction

When the real tractor and the virtual tractor are moving at the same time, the state error between them will continue to accumulate. The purpose of constructing communication systems is to eliminate state errors on a regular basis. In this study, the frequency of data frame obtained by the client of cyber space is around 10 Hz, while the state correction frequency is 1 Hz. The technical architecture of the state error correction is shown in Fig. 5.2.

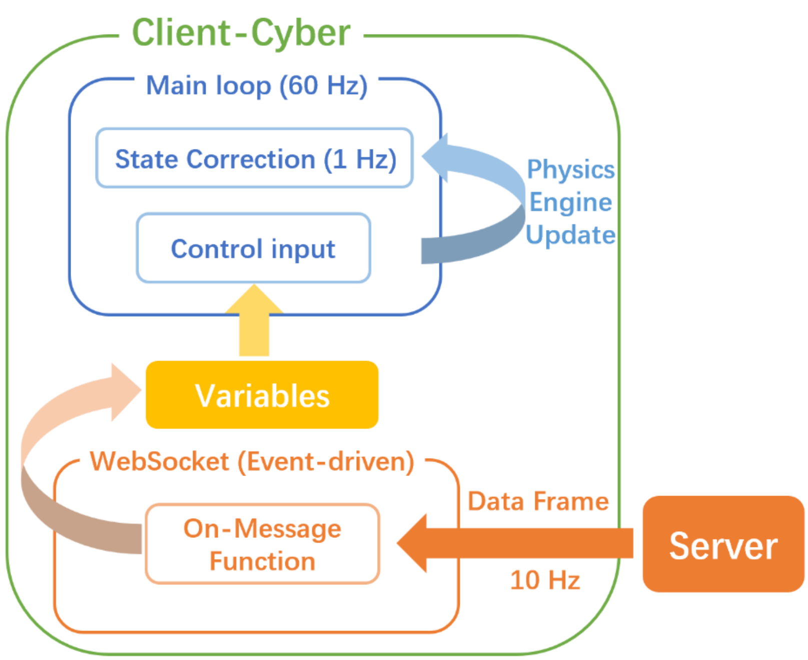

Fig. 5.2. Technical architecture of state error correction

In the program architecture of the client representing cyber space, the main loop is always updating with a fixed frequency of 60 Hz. Once the control input is decided at the end of the main loop, the cyber space state, including the virtual tractor state, will be updated through physics engine. Unlike main loop, WebSocket communication is event-driven. When the server sends a data frame, an event is generated, which corresponds to the On-Message function in WebSocket communication. Therefore, every time the client receives a data frame, the On-Message function will be called to modify the corresponding variable value in its own program according to the content of the data communication. At the same time, in the main loop, the value of control input is updated based on these variables.

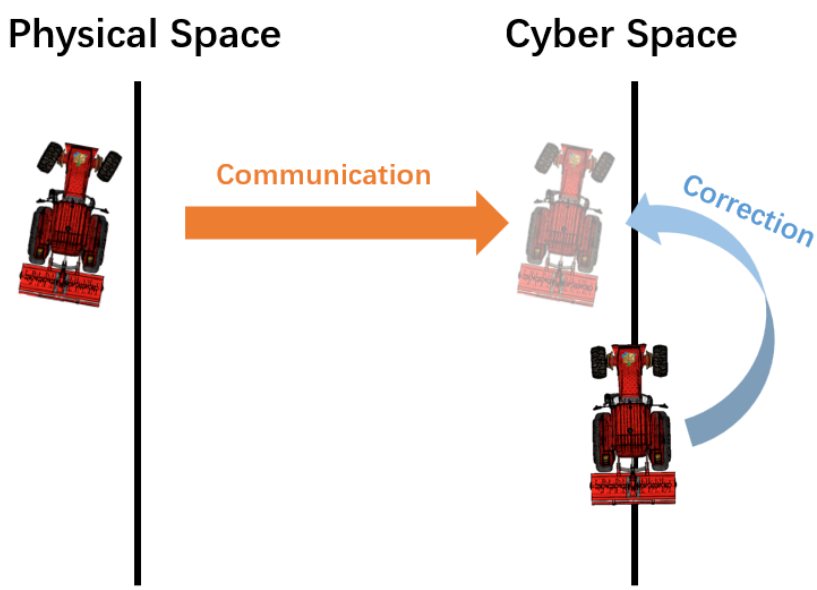

Fig. 5.3. State error correction

The state error correction is a part of the main loop with a lower frequency of 1 Hz, and the process of state error correction is shown in Fig. 5.3. The state error between the real tractor and the virtual tractor will accumulate for around 1s and then the state of real tractor will be transferred into cyber space. Based on the coordinate position and heading angle of the real tractor, the virtual tractor would be smoothly adjusted to the same position and heading using interpolation function provided by Unity.

5.3. Validations for Online Communication Systems

5.3.1. Pre-validation between two DT systems

For safety and convenience reasons, the developed communication systems will first be verified using the DT system. This is also one of the important advantages of the proposed DT system, which is used for pre-verification of field tests and is absolutely safe and low-cost. Since remote controlling system rely on manual control input through gamepad, it is not conducive to unifying control standards and objectively evaluating the effectiveness of communication systems. Therefore, the pre-validation tests were conducted using the developed remote monitoring system, as explained in Section 5.2.2. In this pre-validation test, two DT systems are set up as two clients with same field terrain and basic simulation logic. The DT system which is sending tractor state to server is defined as client master, while another DT system is called client slave.

Since the 3D terrain model and simulation logic of the two DT systems are exactly the same, the error between two systems only comes from a tiny communication latency, which is not conducive to fully verifying the remote monitoring system. Thus, for client slave, the tractor model is revised to make a difference with that of client master. In this way, the state error would be magnified to better validate the correction ability of communication system. Specifically, for client master, the relationship between the steering input from physical space and the steering input conducted in cyber space is expressed in Eq. (2.10), while for client slave, this relationship is expressed as:

$$\delta_{d\_slave} = \begin{cases} (0.6527535 * \delta_{p\_slave}{}^{1.040})^{1.04058} & \delta_{p\_slave} \geq 0 \\ -(0.7555497 * \left|\delta_{p\_slave}\right|^{1.006})^{1.04058} & \delta_{p\_slave} < 0 \end{cases} \quad (5.1)$$

This steering correction relationship was calibrated for Kubota MR1000A Wheeled-type Tractor, which is also the tractor utilized for field validation tests in this chapter. Besides, the target velocity for this experiment is 4km/h.

Fig. 5.4. Experimental path for pre-validation test between two DT systems

Fig. 5.4 shows the experimental path for the pre-validation test of remote monitoring system between two DT systems. From the starting point, the tractor will move along a long straight path, and then make a corner turning to enter the second long straight path. The trajectories of the two virtual tractors are shown in Fig. 5.5. According to the experimental result, the client slave could successfully follow the client master and their trajectories are very close, which validates the feasibility of the developed communication system. To better evaluate the accuracy of the remote monitoring system and the state error correction method, the trajectories of the turning part are zoomed in, as shown in Fig. 5.5. (b). According to Eq. (2.10) and Eq. (5.1), the tractor of client slave has a better steering ability compared with that of client master. Therefore, under same steering input, the turning radius of client slave is smaller, which explains why the trajectory of the client slave tends to be on the inside of the curve. Every 1s, the tractor state of client slave would be adjusted to that of client master, which explains the reason of why the trajectory of client slave is shaped like waves.

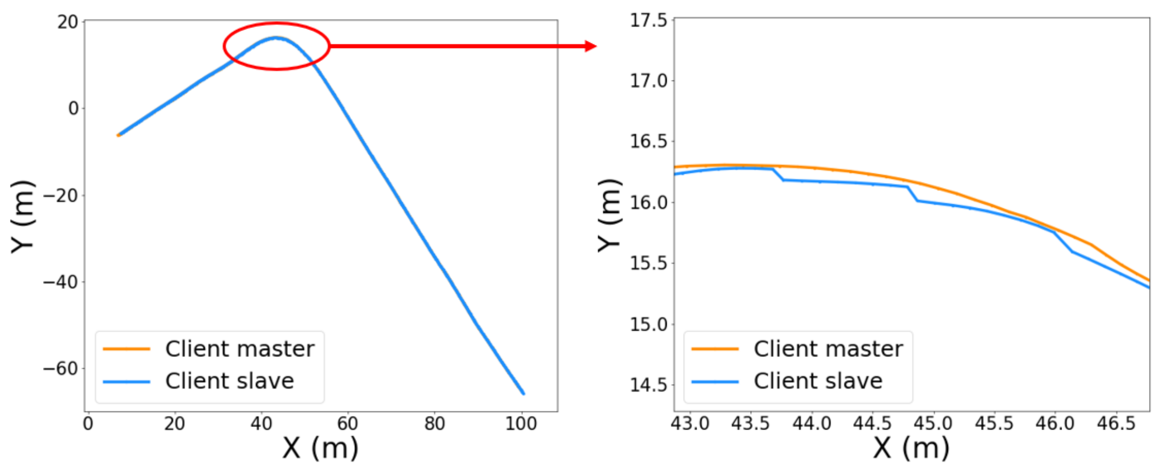

(a) overall trajectory **(b) corner turning trajectory**

Fig. 5.5. Trajectory results of the remote monitoring system validation test

Then, quantitative analysis is made and the trajectory difference between client master and client slave is shown in Fig. 5.6. From this figure it can be seen that under most cases the trajectory difference would not be higher than 5 cm. This result has achieved the trajectory accuracy verified in Chapter 3 using two independent closed-loop steering controllers for physical space and cyber space respectively. At the same time, it can be proved that this trajectory accuracy can meet the needs of real agricultural production.

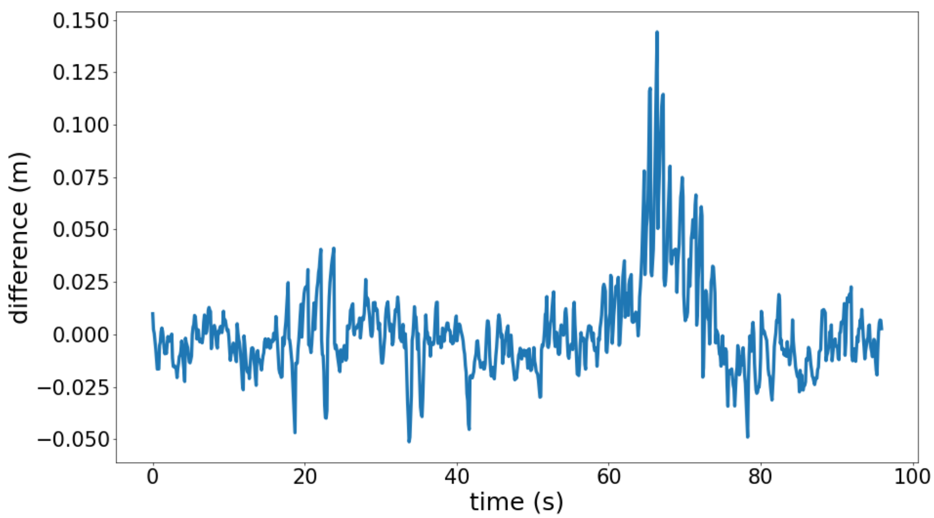

Fig. 5.6. Trajectory difference between client master and client slave

However, between 60s - 80s, the trajectory difference increased significantly, reaching 14.5 cm. In order to explore the reasons for the increased trajectory difference, the time series of steering input for both clients are investigated and shown in Fig. 5.7. According to the change of the steering input, a left turning is made also between 60s – 80s. This phenomenon suggests that the trajectory difference between the two clients increases with the increase of steering input, which is caused by the difference in steering ability of tractor models.

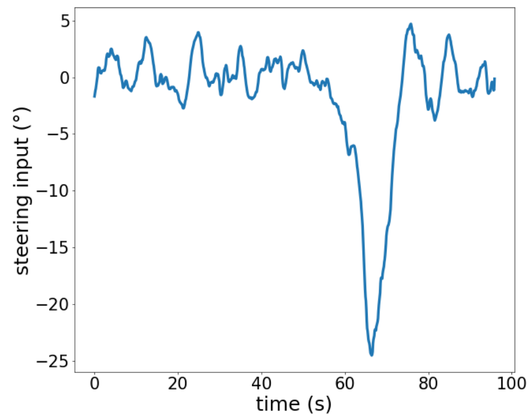

Fig. 5.7. Time series of steering input for both clients

5.3.2. Field validation experiment between DT system and the real tractor

After validating the online communication system between two DT systems in cyber space, the feasibility of the communication system using WebSocket has been validated. On the premise of effective communication, the next step is to verify the online communication system through the proposed DT system and the real tractor. The experimental path for the field validation is completely same with that of pre-validation tests mentioned in Section 5.3.1. Different from previous chapters, the real tractor utilized in this test is Kubota MR1000A Wheeled-type. This real tractor serves as the client master, sending state information and control command to the DT system, which serves as the client slave. The steering correction relationship of the client slave is also following Eq. (5.1). Fig. 5.8 shows the online communication systems between the real tractor and the DT system. Besides, for safety consideration, the target velocity is set to be 3.2 km/h, lower than that of pre-validation test between two DT systems. It is worth noting that in the real tractor's navigation program, the thread that controls sending the tractor status to the server is limited to only 3 Hz due to resource restrictions.

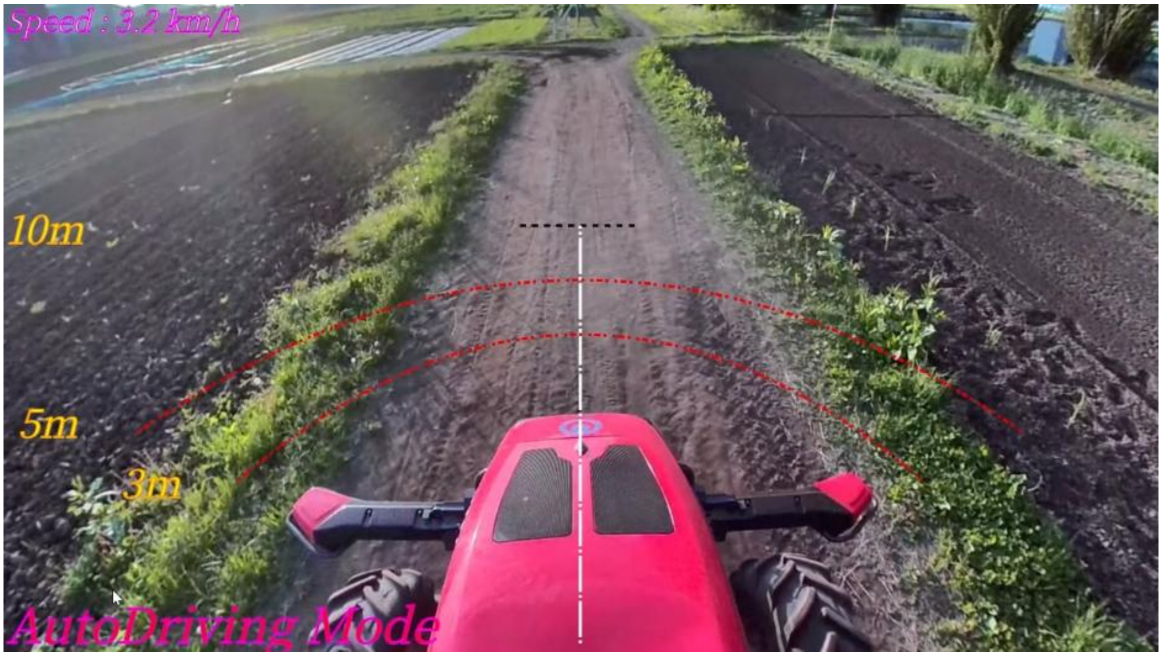

(a) Camera view from the real tractor

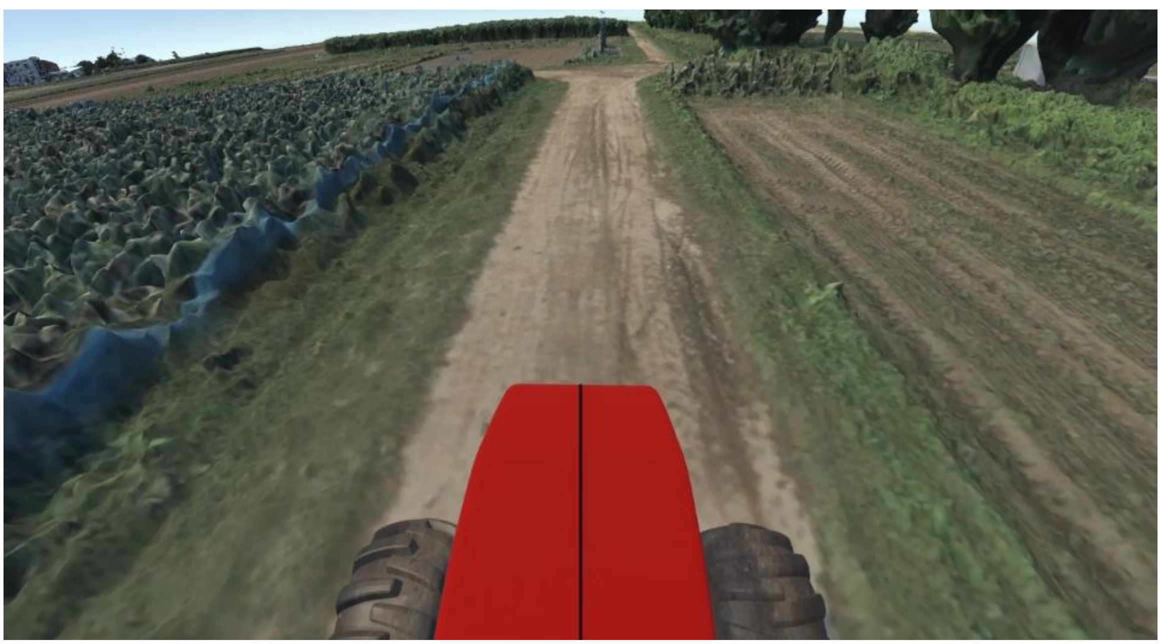

(b) Camera view from the DT system

Fig. 5.8. Online communication systems between the real tractor and the DT system

Similar as in the pre-verification experiment in cyber space, the developed online communication system enables the virtual tractor in the DT system to follow the real tractor to safely complete the desired path without collision. In order to more comprehensively analyze the state error and correction effect, the real tractor state and virtual tractor state were recorded at each state correction. The position distance and heading angle difference between the real tractor and the virtual tractor at each state correction are calculated and shown in Figure 5.9.

Compared with trajectory difference, the position difference is more comprehensive since not only the lateral error, but also the longitudinal error is included. According to Fig. 5.9 (a), during most of the time, the position error is fluctuating between 0.5m-1m. This result is significantly much larger than the trajectory difference verified in Section 5.3.1. One potential reason is that the communication frequency of tractor status from real tractor is only 3 Hz, which is too sparse for the virtual tractor to tightly follow the real tractor's condition. For example, even if the real-time error between the virtual tractor and the real tractor is very small, due to communication delays and too sparse state communication frequency, the virtual tractor will be updated to the state of 0.3s ago. Besides, longitudinal error is included in position error, which explains a higher error value of position error as well. Fig 5.9 (b) shows the heading angle difference change during the experiment. The fluctuation range is about 6°, which is acceptable for remote monitoring or operating system. Additionally, the maximum error occurs at around 10-11s, mainly due to a large steering angle input.

Although the effect and accuracy of the current online communication system is limited by the frequency communication of the tractor status, all errors are limited to a certain range without accumulation. This result demonstrates the effectiveness of the scheme developed in this chapter.

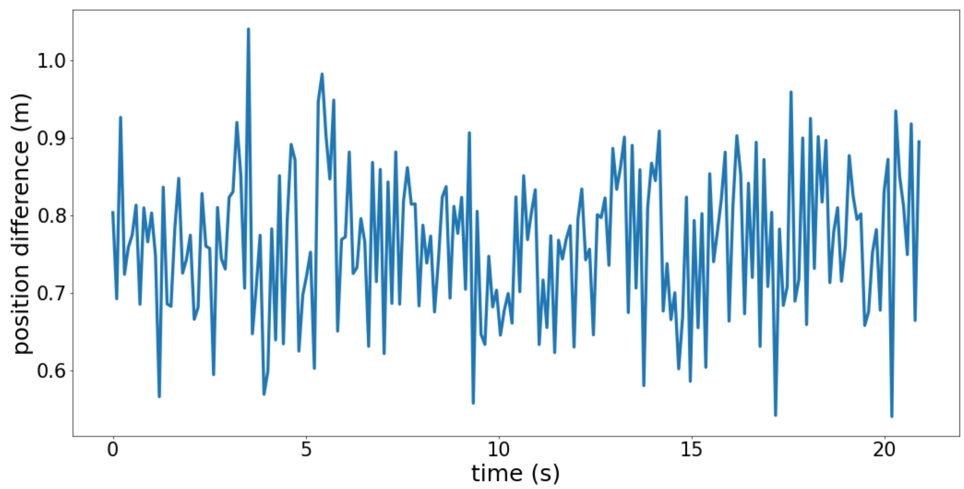

(a) position difference change

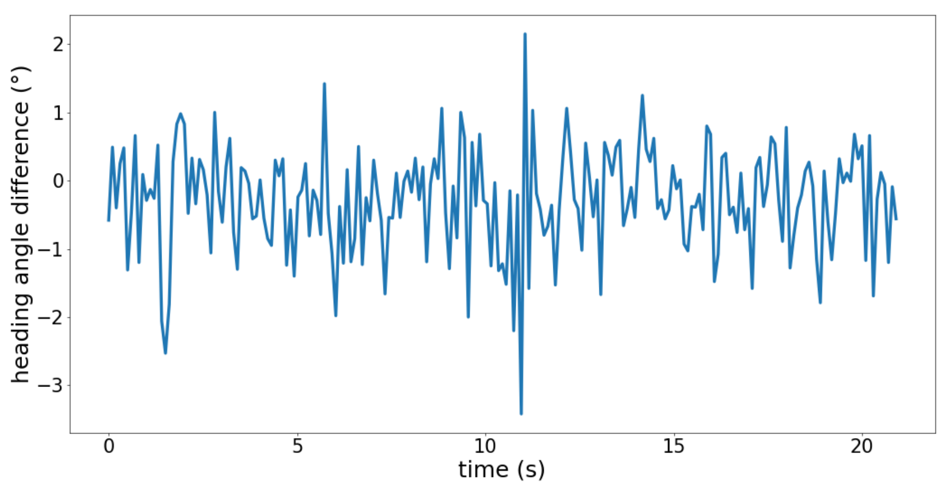

(b) heading angle difference change

Fig. 5.9. Experimental results of the online communication systems between the real tractor and the DT system

Finally, the developed remote controlling system was also validated by field test and the system is shown in Fig. 5.10. The laptop on the left is running the program of the proposed DT system, while the monitor on the right is showing the image from the real tractor’s onboard camera. The viewing angle displayed in the DT system is very close to the camera image from the real tractor. Therefore, the driver can complete remote driving by controlling the steering angle simply through the DT system's screen.

Fig. 5.10. Display image of remote controlling system

5.4. Conclusion

To deal with accumulated errors between the proposed DT system and real tractor during a long time period of agricultural operation, an online communication system is proposed in this chapter. For development of this communication system, WebSocket is utilized as a tool for data transmission, and two types of communication framework are constructed for remote monitoring and controlling respectively. During data communications between cyber space and physical space, the tractor state error of virtual tractor would be corrected every 1 Hz. Finally, validation experiments were conducted and the following conclusions are made:

(1) The constructed online communication system utilizing WebSocket tool is proved to be feasible based on both pre-validation experiments and field validation experiments.

(2) The current online communication system can limit the state error between the virtual tractor and the real tractor to a certain range without accumulation.

(3) The current system can basically meet the safety requirements of remote driving and monitoring without collision.

CHAPTER 6. POTENTIAL APPLICATIONS OF THE PROPOSED DIGITAL TWIN SOLUTION

6.1. Introduction

As mentioned in the previous chapters, the proposed DT solution can be applied in the applications of agricultural machinery feasibility pre-validation and work schedule optimization. This section will validate and discuss the potential applications of the proposed DT system in cyber space. In general, the applications of the proposed DT system can be divided into two categories: (1) Robot tractor side (2) Agricultural operation side.

For robot tractor side, the proposed DT system could support developing or selecting robot tractor. For example, testing the developed tractor in cyber space will improve development efficiency with very low cost. Once the robot tractor has been decided, for agricultural operation side, the proposed DT system can help optimize the navigation path planning, work schedule and control strategies (Kolator and Białobrzewski, 2011). For example, before real operation, simulation can be conducted first to optimize the operation plan in terms of time and energy consumption. Specifically, in this study, simulation for design and development of new agricultural vehicles (Robot tractor side) and simulation for agricultural work schedule optimization (Agricultural operation side) are pre-validated in the constructed cyber space based on the proposed DT system.

6.2. Simulation for Design and Development of New Agricultural Vehicles

Unstable vehicle conditions such as oversteer can be simulated based on the non-linear theoretical vehicle model, and thus some extreme testing scenarios that are very difficult to conduct or very dangerous in physical space can be carried out in the cyber space by using the proposed non-linear model in DT system. In addition, considering that the proposed non-linear vehicle model accounts for many vehicle properties such as the ability of the tires to provide cornering force or the position of the center of mass (CoM), different vehicle structures and vehicle parts can be validated in cyber space by using the proposed model, thus providing guidance and a reference for new agricultural vehicle development. Specifically, simulation validation tests for the selection of tire parts and for the design of a vehicle's CoM position were conducted herein as shown by application cases in Fig. 6.1.

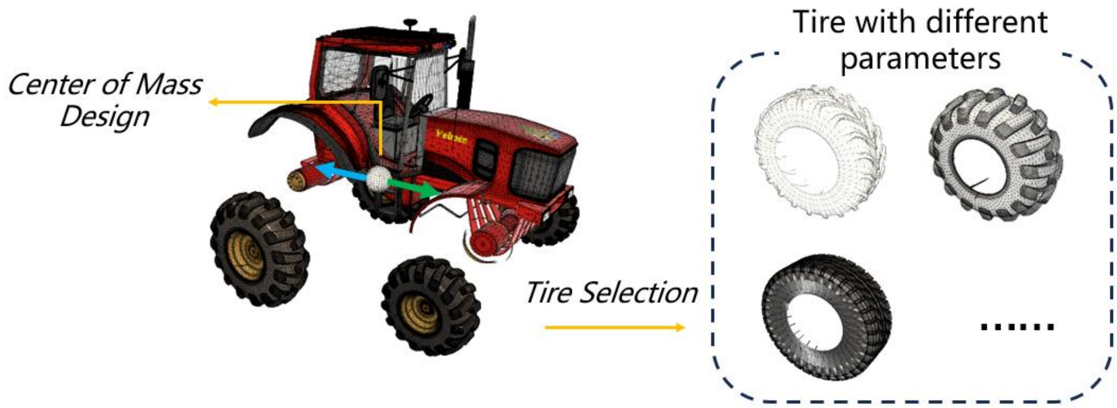

Fig. 6.1. New agricultural vehicle development cases using the proposed DT system

6.2.1. Front and rear tire parts selection guide

Different types of front and rear tires will affect the cornering force of an agricultural vehicle and thereby influence the vehicle's stability. Selecting or designing suitable tires for a particular agricultural vehicle to keep it stable is important for new agricultural vehicle development. Certainly, under the premise of ensuring that the basic properties of the tires remain stable, such as service life, brand, etc., the more expensive the tire is, the better its performance and ability to provide cornering force and keep the vehicle stable can be expected to be. Costs are also a very important consideration for vehicle manufacturers, who strive to reduce the cost of tires as much as possible while ensuring the stability of the agricultural vehicle. It is therefore very important to explore the boundary parameters of tire lateral stiffness that can maintain vehicle stability.

The lateral stiffness that a tire can provide is illustrated as part of the non-linear tire model used in this study, as mentioned above in Chapter 4. It should also be noted that the present discussion of different tire models is based on the premise of identical tire specifications. That is, all of the different tire models being tested are assumed to have the same size and nearly the same weight; only the tire lateral force curve and parameters are different, and these do not affect the vehicle structure. For example, the same agricultural vehicle could be equipped with special snow tires or ordinary tires. The specifications and sizes of these two types of tires are the same, but the lateral forces they can provide are different.

However, it is very labor-intensive and costly to manufacture or buy different types of front and rear tires and install them on agricultural vehicles for testing in real space. In addition, extreme working conditions often arise when stability tests are being conducted in real space, increasing the risk of accidents and posing safety risks to technicians. Using the proposed simulation platform to test different front and rear tire models in cyber space is a safer alternative that can save significant amounts of time and money. Test results obtained in the cyber space can provide guidance for real-world agricultural production concerning how to select the optimal tires for the vehicle.

In this experiment, in order to control variables, the front tire models were fixed when we investigated the parameter boundaries of the rear tire models, and vice versa. According to the proposed tire model as expressed by Eq. (2.3) and (2.4), two parameters, i.e., k_f (or k_r) and α_{f0} (or α_{r0}), can completely determine the tire model. The model parameters of the fixed front and rear tires are $(\alpha_{f0} = 5°, k_f = 0.005)$ and ($\alpha_{r0} = 5°, k_r = 0.01$), respectively.

In order to explore the parameter boundaries of the tire under examination within a reasonable parameter range, we set the two parameter ranges of the tire as $\alpha_{f0}(\alpha_{r0}) \in [1°, 10°]$ and $k_f(k_r) \in [0.001,0.02]$ based on published tire model research (Albinsson et al., 2019; Li et al., 2019). In the case of $\alpha_{f0}(\alpha_{r0})$, discrete values would be tested every 1°, while for $k_f(k_r)$ they would be tested every 0.001. Additionally, considering that (i) the maximum steering angle of the vehicle constructed in cyber space is 35°, and (ii) the vehicle speed during most agricultural operations, including tillage and transplanting, is 4–6 km/h, all of the tests described in this section were conducted at a fixed steering angle of 35° and a fixed speed of 5 km/h.

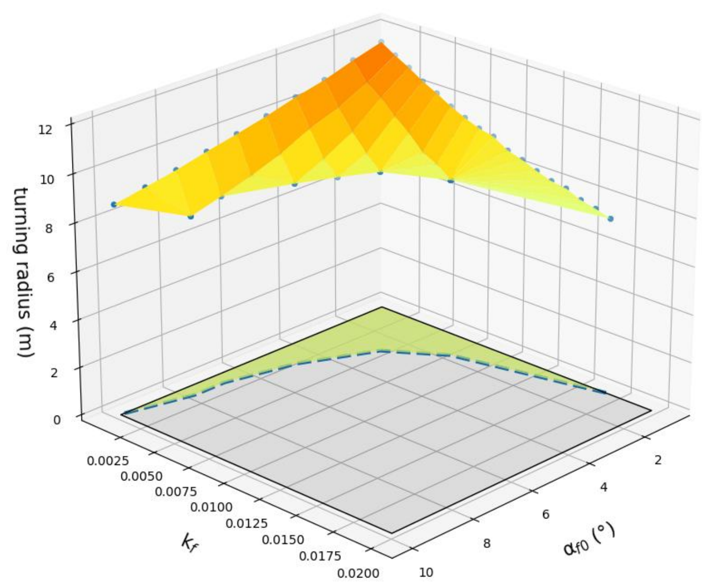

(a) The parameter boundaries of the front tire model under a fixed rear-tire condition

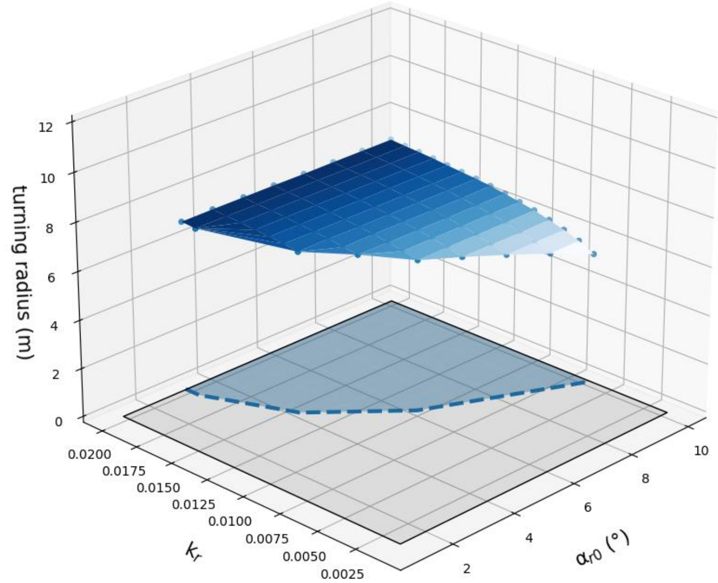

(b) The parameter boundaries of the rear tire model under a fixed front-tire condition

Fig. 6.2. Tire parameter boundaries to maintain vehicle stability. Gray rectangle: the set of test ranges of the two parameters. Light yellow and light blue parts of the bottom rectangle: the effective parameter ranges of the front and rear tires that can keep the vehicle stable without any oversteer. Floating surface: the turning radius value under a 35° steering angle of the effective parameter ranges.

Figure 6.2 illustrates the tire parameter boundary experimental results. As shown in Figure 6.2 (a), when the value of k_f is fixed, the turning radius is inversely proportional to α_{f0}, and similarly when the value of α_{f0} is fixed, the turning radius is also inversely proportional to k_f. This implies that when the rear tire model is determined, the vehicle will be increasingly stable with a decreasing ability of the front tire to provide lateral force. It is also clear that as the parameters change, the height of the floating surface will also change. This means that different front tire models can significantly affect the vehicle's steering ability. As shown in Figure 6.2 (b), it seems that when k_r is fixed, the change of α_{r0} cannot influence the turning radius; in addition, when α_{r0} is fixed, the change of k_r within the effective parameter range can influence the turning radius only slightly. Compared to the front tire parameter boundary, the rear tire has a very limited impact on the vehicle's steering ability. Additionally, unlike the front tire model, the effective parameter range that can keep the vehicle stable is located in the parameter area that enables the rear tires to provide stronger lateral force. This means the stability of the whole vehicle is consistent with the grip and stability of the rear tires.

Based on the above-described results, it can be concluded that: (1) The stability of the rear tire model is in proportion to the steering stability of the vehicle, but it has a limited correlation with the steering ability. (2) Once the rear tire model is decided, the front tire model needs to provide a relatively low grip in order to keep the vehicle stable. Moreover, the stability of the front tires can affect the steering ability of the whole vehicle.

It is therefore recommended that for new agricultural vehicle development, rear tires with a strong grip should be used to ensure the stability of the vehicle's steering. After the rear tire model is determined, the stability parameter boundary area of the front tire model can be explored based on extreme steering tests in cyber space. Finally, according to the vehicle's steering ability requirements, a suitable front tire model within the stability parameter boundary area should be determined in order to adjust the vehicle's steering performance.

6.2.2. The center of mass position design guide

According to Eq. (2.1) and (2.2), the position of the vehicle's CoM is essential for the formation of side-slip angle. The forward and rearward movements of the CoM design will directly affect the side-slip angle of the front and rear wheels, thereby affecting the stability of the agricultural vehicle when it turns. However, the concept of the CoM is somewhat abstract for vehicle manufacturers. For investigations of the impact of the CoM position on a vehicle's stability, it is very difficult, expensive, and time-consuming for companies to manufacture agricultural vehicles with different CoM positions and conduct field stability tests to compare them. However, based on the proposed non-linear vehicle model, it is very easy to conduct such tests in cyber space.

To preserve the symmetry of an agricultural vehicle when it turns left or right, the CoM is usually designed to be positioned on the central axis of the vehicle, and only the distance between the center of mass and the front and rear wheels (l_f and l_r) changes. In tests described in Section 6.2, the position of the center of mass was fixed at $l_f = 1.3\ m$, $l_r = 1.1\ m$. In the present test, the center of mass position was moved forward and rearward to test the impacts of different center of mass positions on vehicle stability. The non-linear model tested for different center of mass positions was $(\alpha_{f0} = 5°, k_f = 0.005, \alpha_{r0} = 5°, k_r = 0.01)$, with a fixed velocity of 5 km/h.

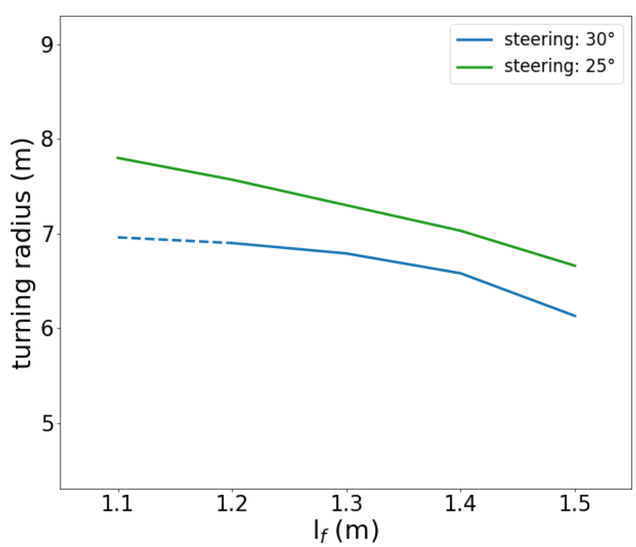

(a) Turning radius with different CoM positions

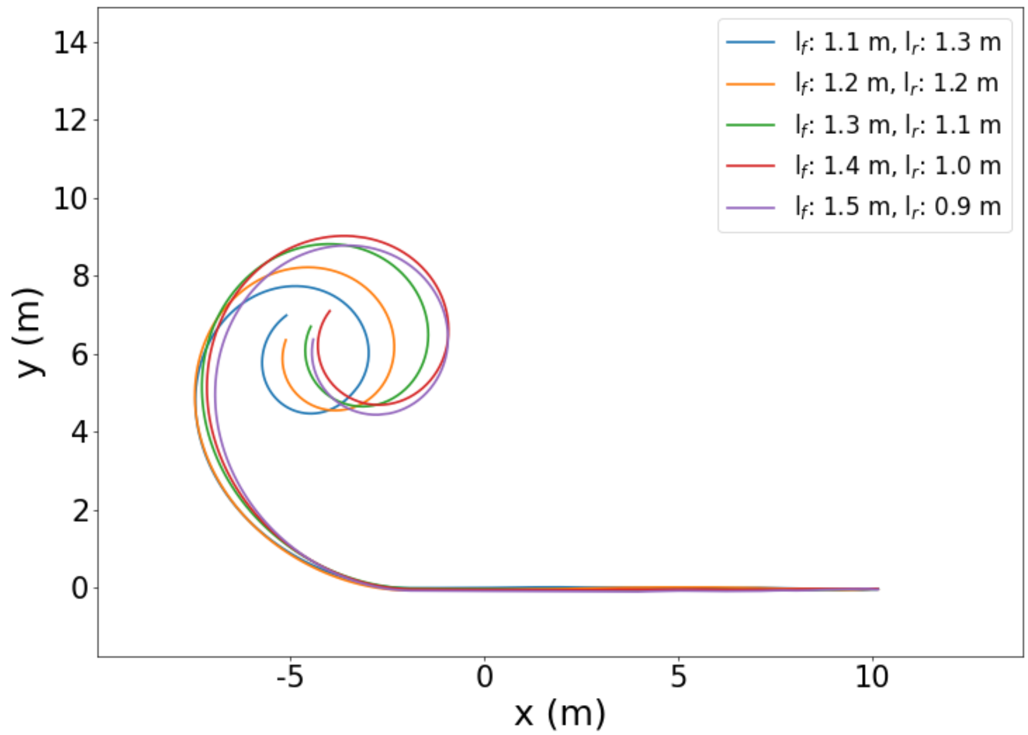

(b) Trajectories of different CoM positions under 35° steering input

Fig. 6.3. The results obtained with different center of mass (CoM) positions

The results for different center of mass positions are shown in Fig. 6.3. The dashed line in the figure indicates that the vehicle cannot steer stably at the corresponding CoM position. When the steering angle input is 25°, the vehicle can finish turning stably under all of the different CoM positions, but the turning radius decreases as the CoM moves backward. However, when the steering angle input is 30°, the vehicle will oversteer and becomes unstable if the CoM is far forward on the vehicle. If the steering angle input is further increased to 35°, the vehicle will oversteer at all CoM positions, as shown by the trajectories in Figure 6.3 (b).

From the trajectories it can be observed that the real-time curvature radius of the steering is changeable. When the CoM is forward on the vehicle, the real-time curvature radius of steering changes from large to small, and as the CoM position moves backward, the range of changes in the real-time curvature radius becomes smaller, which means the vehicle is prone to be more and more stable. These results demonstrate that placing the CoM position at the rear part of the vehicle will help stabilize the vehicle during turning, and the CoM position will also influence the turning radius.

As noted above in Section 6.2, the rear tire is usually used to maintain the stability of the vehicle. However, when the CoM is placed at the front part of the vehicle body, l_r becomes quite large and will enhance the linear velocity of the rear tire rotating around the CoM. This will undermine the stability of the rear wheel when turning. This result means that if the CoM is at the front of the agricultural vehicle, it will affect the stability of the vehicle steering. Similarly, when the CoM is placed at the rear part of the vehicle body, l_f becomes quite large and will enhance the linear velocity of the front tire rotating around the center of mass. This will exaggerate the side-slip of the front wheels, causing a tendency to oversteer; nonetheless, the rear wheels will ensure the stability of the vehicle, so finally the vehicle will be able to turn stably and the turning radius will become small.

6.3. Simulation for Agricultural Work Schedule Optimization

After fully determining the type of robot tractor to be used, how to optimize the agricultural operation plan is an important issue in practical farming. Typically, evaluating the feasibility of an agricultural operation plan involves factors such as time spent and economic costs. The time spent refers to the time required to complete all agricultural operations under the operation plan. The economic cost usually means two things: the first is the number of robot tractors used, and the second is the total fuel consumption during the operation of the robot tractors. The number of robot tractors is very easy to understand. Using more robot tractors generally means higher efficiency, but also more costs for purchasing or renting tractors. However, even for the same number of robot tractors, different operation strategies will result in different time spent and fuel consumption. Therefore, in this section, there are two issues that will be verified in cyber space: optimization of the number of tractors, and optimization of the operation strategy for tractors, to provide examples for potential applications of the proposed DT system. Considering that this is an application scenario for real agricultural operations, the 3D terrain of Iwamizawa field was used for verification in cyber space.

6.3.1. Optimization of the number of tractors

In order to conduct agricultural operation tests, the constructed virtual robot tractor was equipped with cultivator implements. The operation width of the cultivator is $3\ m$. The size of the operation field (Iwamizawa field) is $270m \times 70m$. Multiple robot tractors will work together in a triangle formation, ensuring that there are no gaps between the working areas of two adjacent tractors. In this section, the number of robot tractors being tested are 1, 3, 5, 7, 9,11, respectively. The illustration of the tractor formation and the number of tractors is shown in Fig 6.4. The numbers on the right represent the number of tractors ending at that row. For example, when 5 robot tractors are used for operation, the robot formation is only 3 rows. The distance between two adjacent rows will be controlled at about $10\ m$. The target velocity of the first-row tractor for operation is assumed to be 5 km/h. However, to control the distance between two adjacent tractors, a simple velocity control strategy is defined for the following tractors as:

$$v_{row} = \begin{cases} 0 \\ v_{row-1} - 0.5 * (10 - d_{row}) \\ v_{row-1} \end{cases} \tag{6.1}$$

Where v_{row-1} represents the velocity of the tractor in the previous row adjacent to the current tractor, d_{row} represents the distance between the current tractor and the adjacent tractor in the previous row. When multiple robot tractors perform agricultural operations inside the field, they will track straight navigation paths according to the above formation and target velocity control method.

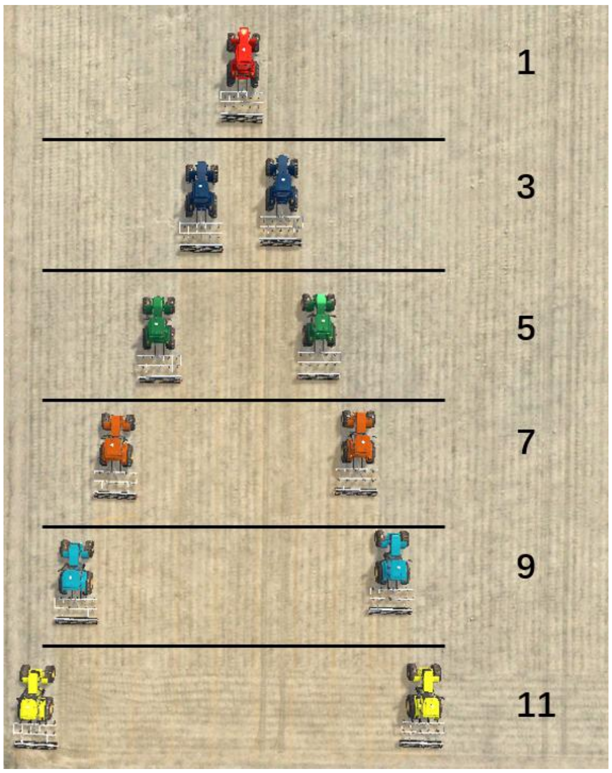

Fig. 6.4. Illustration of the tractor formation and the number of tractors

When multiple robot tractors enter the field and perform headland turning at the edge of the field, a waiting queue would be established based on the row number. For example, when the only tractor in the first row entering the field, the following tractors will just stop and wait. Once that tractor reaches the designated formation location, the two tractors in the second row will start simultaneously and move toward their designated formation locations. And so on, until all the tractors reach the designated formation position, and then all the tractors will start at the same time and perform straight-path operations in a fixed formation.

Table 6.1. Time spent of different number of tractors for same operation field

Number of tractors	Time spent
1	74min 35s
3	25min 30s
5	20 min 53s
7	17 min 25s
9	12 min 30s
11	13 min 10s

According to the above operation plan, simulations of different number of robot tractors were conducted using the proposed DT system and the experimental result is shown in Table 6.1. From the results, it can be seen that as the number of tractors increases, the time spent will continue to decrease. However, when the number of tractors increases to 11, the time spent also increases compared with that of 9. This is because when 9 robot tractors are used, it takes 3 straight navigation paths to traverse the entire field, while when 11 robot tractors are used, although the lateral operation width is increased, it still takes 3 times to traverse the entire field. And compared with using 9 tractors, a formation of 11 tractors will take more time for entering the field and headland turning, so the total time spent is longer. This result suggests that for a specific field, the number of tractors is not always positively correlated with operating efficiency, and detailed operation planning is needed, which is the potential application of the proposed DT system.

In addition, it can be found from the results that, assuming that each tractor in the tractor formation has the same cost of utilization, the cost-effectiveness of using a single tractor is the highest. As the number of tractors utilized increases, the operating efficiency per unit price decreases. This is because when a multi-robot system is introduced, the tractors will inevitably have to wait for each other in order to work together, which will drag down the overall operation efficiency. Therefore, from an economic point of view alone, using a single robot tractor seems to be the most appropriate solution. However, when farmers are very time-sensitive, for example, they have to complete a specific agricultural operation before a heavy rain, they can choose a multi-robot tractor solution that meets the time requirement based on the simulation results. This simulation results verifies that the proposed DT system can help guide the preliminary planning of agricultural operation plans by optimizing the number of robot tractors.

6.3.2. Optimization of the operation strategy for tractors

In addition to the optimization of the number of tractors to be used, the proposed DT system can also be used for more detailed planning such as optimization for operation strategy. As mentioned above, the multi-robot tractor formation operates according to a defined headland turning strategy, which means the robot tractors will do headland turning 'row by row'. This is just one kind of operation strategy, and in addition to this method, other strategies also exist. For example, instead of using a formation, we can have multiple robot tractors responsible for different areas of field operation at the same time separately.

Table 6.2. Time spent of different strategies when using 3 robot tractors

Strategy	Time spent
Operation in formation	20 min 53s
Operation separately	21 min 30s

Here we take the solution of using 3 robot tractors as an example. In addition to the triangle formation operation plan described above, the field can be divided into 3 parts and each tractor would be responsible for one part separately. The advantage of operation separately is that the tractors do not need to wait for each other, nor do they need to control the target velocity during the operation, thus breaking free from the constraints of formation. The disadvantage of operation separately is that, since there is no formation, when each tractor is doing headland turning at the end of the field, the interval between the current navigation path and the next navigation path becomes smaller, so normal U-turning cannot be used. In this condition, robot tractors must use switch-back turning to transition to next navigation path, which consumed much more time than U-turning. It is difficult to accurately know which strategy is better through qualitative analysis alone, so simulation for operation separately is also conducted, and the time spent result of these two strategies when using 3 robot tractors is shown in Table 6.2. According to the simulation result, operation separately consumed much more time than operation in formation.

Additionally, even a solution plan of formation operation is adopted, there are still different strategies. Here we take the formation of 5 robot tractors as an example. Multi-robot tractors can also do headland turning ‘col by col’. Similar to ‘row by row’, the only tractor in the first row completes the headland turning first, then the tractors on the right side of the second and third rows complete the headland turning one after another, and finally the tractors on the left side of the second and third rows complete the headland turning one after another. Not only that, even when utilizing formation strategy of ‘row by row’, the waiting time between tractors in different rows can also be optimized. For example, under the premise that no collision occurs, the tractors in the third row can be started ahead of time before the tractors in the second row reach the designated formation location.

Table 6.3. Time spent of different strategies when using 5 robot tractors

Strategy	Time spent
Row by row	20 min 53s
Row by row (waiting time optimized)	17 min 18s
Col by col	21 min 30s

According to the simulation result, the time spent difference between strategies of ‘row by row’ and ‘col by col’ is very small, less than 1 min. But when the waiting time of the strategy of ‘row by row’ is optimized, the time spent is significantly reduced. Therefore, under this situation, the proposed DT system can provide a strategy optimization guidance for actual agricultural operation plans through simulation easily.

6.4. Conclusions

In this chapter, the potential applications utilizing the proposed DT system have been discussed and validated in cyber space. The potential applications of the proposed DT system can be divided into two aspects: (1) Robot tractor side, and (2) Agricultural operation side.

For robot tractor side, based on the test results, the following conclusions and suggestions for the development of new agricultural vehicles that rely only on front wheel steering can be drawn: (1) The CoM should be positioned at the rear part of the vehicle body in order to keep the vehicle stable when turning, and (2) the turning radius of an agricultural vehicle can be adjusted by changing the position of the CoM. Appropriately moving the CoM rearward can improve the vehicle's steering performance.

For agricultural operation side, it is demonstrated that the proposed DT system can be used to optimize operation plans, including both determining the number of robot tractors to be used and optimizing operation strategies. Specific suggestions include: (1) Economy-sensitive farmers are advised to use formations of smaller number of tractors for operations, while time-sensitive farmers are advised to select the number of tractors with the lowest cost based on the simulation results while meeting the time requirements. (2) For formation operation plans with a fixed number of tractors, optimizing the waiting time for headland turning can significantly improve operation efficiency.

CHAPTER 7. CONCLUSIONS

7.1. Research Summary

This study proposes a Digital Twin (DT) solution for agricultural machinery systems that could accurately replicate the motion state of a real tractor during planed operations in cyber space. The proposed DT system includes a detailed tractor model with side-slip simulation and online communication functions, which could support potential applications such as tractor design pre-validation or work schedule optimization. The summaries of main contributions in this study are as follows:

(1) Framework of the proposed DT system

A preliminary digitization was conducted to import the real terrain and real tractor into cyber space, which was created by Unity software. Then, subsystems reflecting detailed tractor motion characteristics were developed to implement the proposed DT solution. These subsystems include a global navigation satellite system (GNSS) error simulator, a steering system simulator, and a tire interaction simulator, designed to accurately replicate the dynamic motion of the target tractor. Finally, experimental results from both small-scale steering trajectory validation (step response test) and large-scale work schedule validation (real navigation test) demonstrate the feasibility and effectiveness of the proposed DT solution on both asphalt and dry soil.

(2) Non-linear improvement on the tractor model for side-slip simulation

To make the DT solution more practical to be applied under extreme agricultural environments, such as muddy field that are prone to cause large side-slips, a non-linear tractor model was proposed. First, a simplified non-linear tire model and side-slip angle estimation method were combined to make a lateral force-estimation method. Then the lateral force estimation was applied to the tractor model in DT system, to construct a non-linear dynamic model for agricultural vehicles in cyber space. The validation tests of both cyber space and real-world experiments prove that, the proposed non-linear model has strong practicality and can maintain higher accuracy compared with traditional linear vehicle model especially under extreme agricultural environments.

(3) Development of online communication systems for cyber-physical synchronization

To ensure the accuracy of the DT system during a long period of operation, online communication subsystem was developed using WebSocket programming. Two types of communication framework are constructed for remote monitoring and controlling respectively. During data communications between cyber space and physical space, the tractor state error of virtual tractor would be corrected every 1 Hz. Validation tests prove the feasibility of the developed online communication system to solve accumulated errors between virtual tractor and real tractor. This communication system also shows potential ability to support remote monitoring and controlling safely.

(4) Potential applications of the proposed DT system

The potential applications of the proposed DT system can be divided into two categories: one is for robot tractor, and another is for agricultural operation. For robot tractor, the proposed DT system was utilized to explore the optimal design of different combinations of tire parameters and center of mass positions. For agricultural operation, pre-validation examples are given to show the potential of the proposed DT system in work schedule optimizations for both tractor numbers and operation strategies.

7.2. Future Plans

In this study, currently the collected 3D terrain model is static, without any change over time. However, the agricultural environment is highly time-variable. The shape, hardness and humidity of the soil and the growth of roadside weeds are constantly changing and may affect the tractor's movement along the road. To solve this problem, the 3D terrain model could to be collected and updated more frequently to reflect the shape change of the real terrain, and a database needs to be established to collect tractor steering data sets on soils of different humidity and hardness. According to the current different terrain conditions, the corresponding steering correction parameters and non-linear tire parameters are matched for accurate simulation.

Next, for the online communication system, a new hardware system architecture should be proposed based on the current methodology, to achieve higher tractor state transmission frequency. In this way, the error between cyber space and physical space would be controlled in a smaller range, which is better for remote driving by humans. Additionally, the tractor needs to be equipped with an all-round obstacle perception system and synchronize obstacle information to the cyber space through the developed online communication system, to achieve remote driving. Current remote controlling system cannot get enough safety information. When the operator performs tractor operations only through cyber space, he may not be able to cope with dynamic obstacles which are suddenly appeared such as animals or farmers.

Finally, based on the online communication system, the proposed DT system can be upgraded to a tractor management control center. Multiple tractors are connected and communicated with the DT system at the same time, receiving real-time control instructions and feeding back status information to correct errors. In this way, for multiple robot tractor systems, it is not necessary to develop individual programs for the onboard controller for each tractor. Instead, all the control logics and strategies are realized in the DT systems and can easily performed by tractors in physical space.

REFERENCES

Alves, R. G., et al. (2019). A digital twin for smart farming. 2019 IEEE Global Humanitarian Technology Conference (GHTC). 2019, 17-20th, Oct.

Aliev., et al. (2018). Modeling of mechanical and technological processes of the agricultural industry. *CABI Databases*. **54**(1):95-104.

Angin, P., et al. (2020). AgriLoRa: A Digital Twin Framework for Smart Agriculture. *J. Wirel. Mob. Networks Ubiquitous Comput*. **11**: 77-96.

Arulmozhi, E., et al. (2024). From Reality to Virtuality: Revolutionizing Livestock Farming Through Digital Twins. *Agriculture*. **14**(12).

Cazan, A. C. et al. (2023). Contemporary manufacturing techniques used in agricultural engineering. Proceedings of the 49th International Symposium, Actual Tasks on Agricultural Engineering. 409-417. Opatija, Croatia, 2023.

Cutini, M. et al. (2023). A Co-Simulation Virtual Reality Machinery Simulator for Advanced Precision Agriculture Applications. *Agriculture*, **13**(8):1603.

Escribà-Gelonch, M., et al. (2024). Digital Twins in Agriculture: Orchestration and Applications. *Journal of Agricultural and Food Chemistry*. **72**(19): 10737-10752.

REFERENCES

Geng, G. et al. (2017). Research and application of digital design and manufacturing technology of agricultural machinery. *Agro Food Industry Hi Tech*. **28**(1): 2891-2894.

Goodin, C., and Priddy, J. (2016). Comparison of SPH simulations and cone index tests for cohesive soils. *Journal of Terramechanics*. **66**: 49-57.

Guo, D., et al. (2024). Online optimization of adjustable settings for agricultural machinery assisted by digital twin. *Computers and Electronics in Agriculture*. **227**: 109504.

Han, B., et al. 2023. Research on interaction law of longitudinal/lateral slip of mountain tractor based on tire-soil model. *Proceedings of the Institution of Mechanical Engineers Part D-Journal of Automobile Engineering.*

Iqbal, J., et al. (2020). Simulation of an Autonomous Mobile Robot for LiDAR-Based In-Field Phenotyping and Navigation. *Robotics*. **9**(2): 46.

Iwasaki, K., et al. 2020. Application of Ground-Penetrating Radar and a Combined Penetrometer-Moisture Probe for Evaluating Spatial Distribution of Soil Moisture and Soil Hardness in Coastal and Inland Windbreaks. *Geosciences.* **10**(6): 238.

Jeong, D. Y., et al. (2023). Digital Twin Application: Making a Virtual Pig House Toward Digital Livestock Farming. *IEEE Access*. **11**: 121592-121602.

Jo, S. K., et al. (2019). Energy Planning of Pigsty Using Digital Twin. International Conference on Information and Communication Technology Convergence (ICTC). 2019, 17-20th, Oct.

REFERENCES

Kim., et al. (2022). Development of DEM-MBD coupling model for draft force prediction of agricultural tractor with plowing depth. *Computers and Electronics in Agriculture*. **202**: 107405.

Kise, M., et al. (2001). Development of the Agricultural Autonomous Tractor with an RTK-GPS and a Fog. *IFAC Proceedings Volumes.* **34**(19): 99-104.

Kolator, B., Białobrzewski, I. 2011. A simulation model of 2WD tractor performance. *Computers and Electronics in Agriculture.* **76**(2): 231-239.

Krid, M., et al. 2017. A New Explicit Dynamic Path Tracking Controller Using Generalized Predictive Control. *International Journal of Control Automation and Systems.* **15**(1): 303-314.

Li, S., et al. (2020). Predictive lateral control to stabilise highly automated vehicles at tire-road friction limits. *Vehicle System Dynamics.* **58**(5): 768-786.

Li, S., et al. (2021). Agricultural machinery GNSS/IMU-integrated navigation based on fuzzy adaptive finite impulse response Kalman filtering algorithm. *Computers and Electronics in Agriculture*. **191**: 106524.

Lin, J. et al. (2024). Application of digital design technology in the design of intelligent agricultural machinery and equipment. *Applied Mathematics and Nonlinear Sciences*. **9**(1):1-13.

López-Castñneda, A., et al. 2022. Digital Mapping of Soil Profile Properties for Precision Agriculture in Developing Countries. *Agronomy-Basel.* **12**(2): 353.

Mouratiadou, I., et al. 2023. The Digital Agricultural Knowledge and Information System

REFERENCES

(DAKIS): Employing digitalisation to encourage diversified and multifunctional agricultural systems. *Environmental Science and Ecotechnology.* **16**: 100274.

Mitsanis, C., et al. (2024). A 3D functional plant modelling framework for agricultural digital twins. *Computers and Electronics in Agriculture*. **218**: 108733.

Natsis, A., et al. 2008. Influence of local soil conditions on mouldboard ploughshare abrasive wear. *Tribology International.* **41**(3): 151-157.

Nie, J., et al. (2022). Artificial intelligence and digital twins in sustainable agriculture and forestry: a survey. *Turkish Journal of Agriculture and Forestry*. **46**(5): 642-661.

Ospina, R. and N. Noguchi. 2016. Determination of tire dynamic properties application to an agricultural vehicle. *Engineering in Agriculture, Environment and Food.* **9**(1): 123-130.

Ospina, R. and N. Noguchi. 2018. Alternative method to model an agricultural vehicle's tire parameters. *Engineering in Agriculture, Environment and Food.* **11**(1): 9-18.

Pacejka, H. B. and E. Bakker. 1992. The magic formular tyre model. *Vehicle System Dynamics.* **21**(sup001): 1-18.

Purcell, W., and Neubauer, T. (2023). Digital Twins in Agriculture: A State-of-the-art review. *Smart Agricultural Technology*. **3**: 100094.

Pylianidis, C., et al. (2021). Introducing digital twins to agriculture. *Computers and Electronics in Agriculture*. **184**: 105942.

Singh, K. B. 2019. Vehicle Sideslip Angle Estimation Based on Tire Model Adaptation. *Electronics.* **8**(2): 199.

REFERENCES

Skobelev, P., et al. (2020). Multi-agent approach for developing a digital twin of wheat. IEEE International Conference on Smart Computing (SMARTCOMP). 2020, 14-17th, Sept.

Snider, J. M. 2011. Automatic Steering Methods for Autonomous Automobile Path Tracking. *Robotics Institute.*

Tao, F., et al. (2019). Digital Twin in Industry: State-of-the-Art. IEEE Transactions on Industrial Informatics. **15**(4): 2405-2415.

Turner, A. P. et al. (2019). A discrete event simulation model for analysis of farm scale grain transportation systems. *Computers and Electronics in Agriculture*. **167**: 105040.

Wang, L. (2024). Digital Twins in Agriculture: A Review of Recent Progress and Open Issues. *Electronics*, **13**(11).

Watanabe, M. and K. Sakai. 2020. Numerical analysis of steering instability in an agricultural tractor induced by bouncing and sliding. *Biosystems Engineering.* **192**: 108-116.

Xu, D., et al. (2022). A Model Predictive Control Method for Vehicle Drifting Motions with Measurable Errors. *World Electric Vehicle Journal.* **13**(3).

Xu, L., et al. (2024). Digital Twin for Aquaponics Factory: Analysis, Opportunities, and Research Challenges. *IEEE Transactions on Industrial Informatics*. **20**(4): 5060-5073.

Xu, S., et al. (2021). Preview Path Tracking Control With Delay Compensation for Autonomous Vehicles. *IEEE Transactions on Intelligent Transportation Systems*. **22**(5):

2979-2989.

Yin, Y., et al. (2024). Construction method and case study of digital twin system for combine harvester. *Computers and Electronics in Agriculture*. **226**: 109395.

Yu, Y., et al. (2023). Obstacle avoidance method based on double DQN for agricultural robots. *Computers and Electronics in Agriculture.* **204**: 107546.

Zardin, B., et al. (2018). Modelling and Simulation of a Hydrostatic Steering System for Agricultural Tractors. *Energies*. **11**(1).

Zhang, L., et al. 2022. Research on virtual Ackerman steering model based navigation system for tracked vehicles. *Computers and Electronics in Agriculture.* **192**: 106615.

Zhou, K., et al. (2015). Simulation model for the sequential in-field machinery operations in a potato production system. *Computers and Electronics in Agriculture.* **116**: 173-186.

Zhang, L. et al. (2019). Modeling and simulation in intelligent manufacturing. *Computers in Industry*. **112**:103123.

Zhang, Z., et al. (2023). Design and research of digital twin system for multi-environmental variable mapping in plant factory. *Computers and Electronics in Agriculture*. **213**: 108243.

Zohdi, T. I. (2024). A machine-learning enabled digital-twin framework for next generation precision agriculture and forestry. *Computer Methods in Applied Mechanics and Engineering*. **431**: 117250.